STRUCTURAL CONTROL BY INDUCED STRESS BASED STIFFNESS MODIFICATION

By

Katie Patricia Whipp

Thesis

Submitted to the Faculty of the

Graduate School of Vanderbilt University

in partial fulfillment of the requirements

for the degree of

MASTER OF SCIENCE

in

Civil Engineering

August, 2005

Nashville, Tennessee

Approved by:

Dr. P.K. Basu

Dr. Sankaran Mahadevan

ACKNOWLEDGEMENTS

First and foremost I would like to thank Dr. P.K Basu because without his kindness and patience I would never have been able to accomplish any of my work. In addition, I would like to thank the faculty and staff at Vanderbilt University for their financial and intellectual support, specifically Dr. Alan Bowers for taking his time to help video tape and record my experiments and Dr. Sankaran Mahadaven for his additional input on my paper. Finally, Dr. David Kosson and Dr. Sanjiv Gokhale for giving me the chance to help other students in the classroom through teaching.

If nothing else can be gained from this paper, I hope that I can show others that no matter your lack of experience or knowledge in a field, the desire to learn is the foundation for accomplishing your goals.

TABLE OF CONTENTS

Page

LIST OF TABLES

LIST OF FIGURES

CHAPTER I

INTRODUCTION

Natural disasters, such as earthquakes and hurricanes, can strike without warning, resulting in a range of destruction from structural damage to loss of life. For this reason, research on structural control, which provides the basis for the design of structural systems where dynamic loads such as winds, earthquakes, waves, and traffic, are the governing design considerations, have become of interest in civil engineering. One recent example of a major natural disaster is the Northridge earthquake that struck Los Angeles area on January 17, 1994. The 6.7 magnitude earthquake resulted in 44 billion dollars of property damage, fifty-one deaths, scores of inhabitable buildings, and a number of collapsed bridges. Natural disasters such as the earthquakes remind us of the challenge for structural engineers to design safer structures to better withstand such dangerous environmental effects.

Structural Design and Control

Numerous attempts have been made to find the optimal solution to alleviate the effects of dynamic loadings. However, uncertainty is induced in the design process due to variability of nature and magnitude of external excitation resulting, say, from natural and man-made disasters, and variability of structural attributes such as stiffness and cost-benefit ratio. Theoretically, a structure with close to infinite stiffness would resist all environmental effects; however, this does not offer an economical solution.

Normal design of buildings involves proportioning the elements of the structure such that the constraints on strength and serviceability limit states are satisfied. The conventional approach is to proportion the components to satisfy the strength limit states and then follow it up with serviceability checks. In the case of tall structures, however, where sensitivity to structural motion caused by environmental effects, like wind and earthquake, is an important element of serviceability limit state, the structure is first proportioned to satisfy the serviceability limit state and then followed up with strength limit state checks.

As the building height increases and it becomes more slender, the influence of lateral loads becomes more significant. For an economical solution of the problem supplemental control techniques need to be applied to attenuate such motion. Three methods of structural control are commonly considered: passive control, active control, and semi-active or hybrid control. The devices used in these methods provide supplemental means to enhance energy dissipation or absorption capabilities of a building structure (Teng 2002).

Passive Control

Passive devices involve control exclusively attained by altering the energy or stiffness within the system. As these devices possess fixed, non-controllable properties, they do not require an external source of energy, therefore are independent from the input of earthquakes. Passive control is commonly achieved in our daily activity, such as when suddenly applying the brakes in an automobile, the seatbelt prevents the body from moving forward out of the seat. This restraint is an example of passive motion control.

The methodology for passive devices is to initially design the structural system to meet necessary strength and stiffness requirements. The added stiffness reduces the dynamic response of the structures by absorbing and dissipating vibration energy, which when combined with the change in initial frequency, helps the structure avoid resonance. If correctly applied, passive devices provide many advantages in regions where small to moderate earthquakes are common. Passive devices are the most frequently type of system control implemented because they involve no external power and such devices are inherently stable. Passive devices have a low cost of maintenance and installation in both design and construction practice because the system only entails providing additional stiffness. However, the adaptability of passive devices is of concern. Because passive systems cannot be modified instantaneously, an accurate model of the physical system and reliable estimate of the design loading is critical to the effectiveness for any passive control system. The design may also be over conservative due to the inability of a passive system to compensate for an unexpected loading. Even if a passive device is ideally designed, these devices are meant to protect a structure from a particular dynamic loading; therefore the device may reduce responses in the first mode, but may not reduce responses in second or higher modes (Agrawal 2002). Some of these disadvantages can be overcome by using different types of passive devices depending on the necessary type of control desired for the structure.

Viscous Dampers

Passive devices can be categorized into damping mechanisms such as viscous dampers, friction dampers, passive tuned mass dampers, and base isolation systems.

Viscous damping, or called material damping, dissipates energy due to the viscosity of the material which reduces acceleration and displacement for most of the desired frequency range. A common example of viscous dampers is the ones mounted on building doors to prevent the door from slamming shut. The schematic diagram for a viscous damper is shown in figure 1 below. Fluid is forced through the orifices located in the piston head. As the piston rod position is changed a resisting force is developed that depends on the velocity of the rod (Connor 2003). Viscous dampers are most useful in areas where engineers wish to reduce displacement without increasing frequency. However, for medium to strong earthquakes, the damping effect is small since "the energy absorption due to yielding is much greater than that due to damping" (Soda 1996).

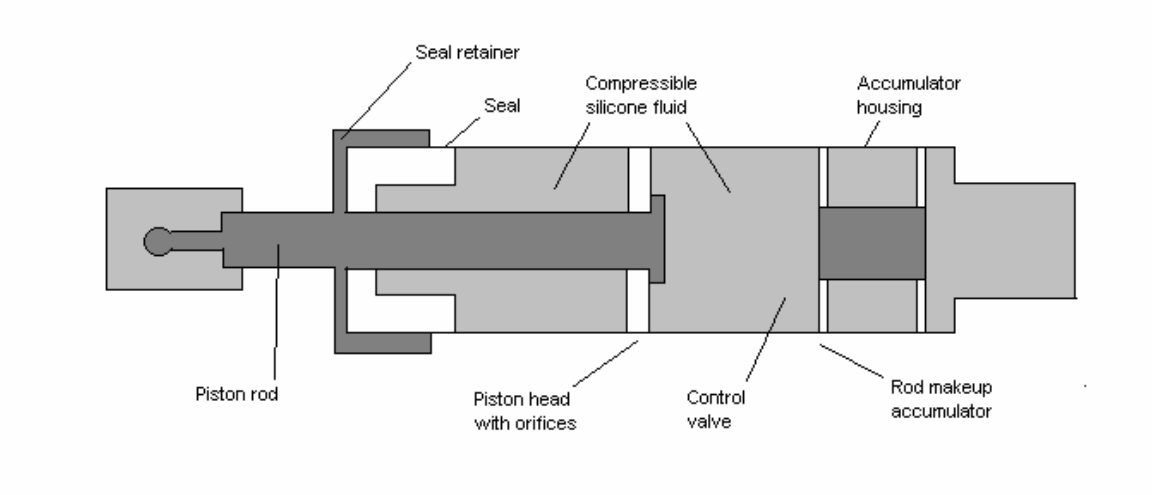

Figure 1: Viscous Damper

Frictional Dampers

Frictional damping dissipates energy due to the heat caused by friction between moving bodies in contact. A frictional damper consists of the friction surface clamped together by high strength bolts with slotted holes. Frictional pads are inserted at the bolt-plate connections as shown in the figure 2 (Connor 2003). The slip force is designed

large enough so that no sliding is caused by wind forces. The beneficial approach to passive damping is that because energy is removed the response cannot become unstable. However frictional damping looses effectiveness during large seismic excitation (Miyamoto 2004).

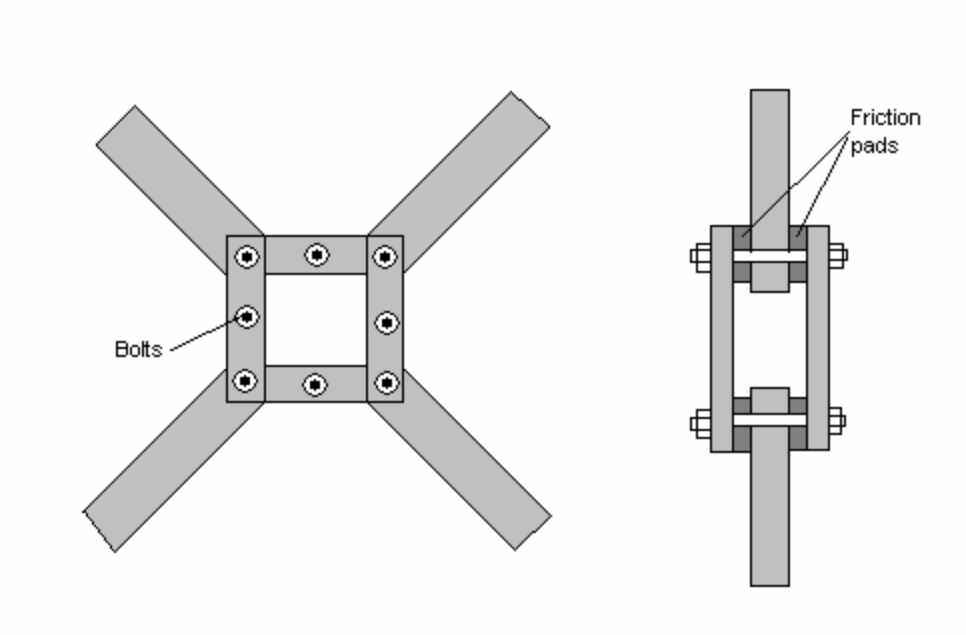

Figure 2: Frictional Damper

Passive Tuned Mass Dampers

Passive tuned mass damper systems, shown in the figure 3 (Connor 2003), consist of an auxiliary mass, a spring, and a damper, which are attached to a structure in order to reduce the dynamic response of the structure, particularly under wind excitation. The auxiliary mass limits the motion of the structure when it is subjected to a particular excitation causing the damper to resonate 90° out of phase with the motion of the structure. The difference in the phase produces energy dissipation by the damper inertia force acting on the structure. The advantage to tuned mass dampers is that since no mechanical parts are involved, little or no maintenance is required. However, because

additional mass is introduced, a tuned mass damper added to an existing structure increases the overall mass of the system, which may violate design constraints imposed on the initial self-weight design. In addition, tuned mass dampers are relatively ineffective during earthquakes due to their inability to reach a resonant condition and therefore dissipate energy under random excitation (Kwok 1995). In recent years, tuned mass dampers have been installed in a number of buildings worldwide to reduce building vibration. For instance, the John Hancock Tower in Boston, Massachusetts has been successfully equipped with tuned mass dampers. The building experienced large wind gusts that not only caused discomfort to occupants but also caused glass window panes to fail and fall to the ground. To counteract sway and twisting motion, tuned mass dampers were successfully placed at opposite ends of the 58^{th} floor (Christenson 2002). It uses a big block of concrete floating in a bed of oil; computer-controlled hydraulics push it around to counter the building's sway. A more recent example is the world's tallest building Taipei 101 in Taipeh, Taiwan (Fig. 4), which has been successfully equipped with a tuned mass damper. To control the excessive sway of the building under large wind gusts a massive pendulum with dampers has been installed. It features the world's largest passive tuned mass damper, an 800-ton sphere 18 feet across (Fig. 5) that swings like a pendulum from the 92nd floor in the view of restaurant-goers.

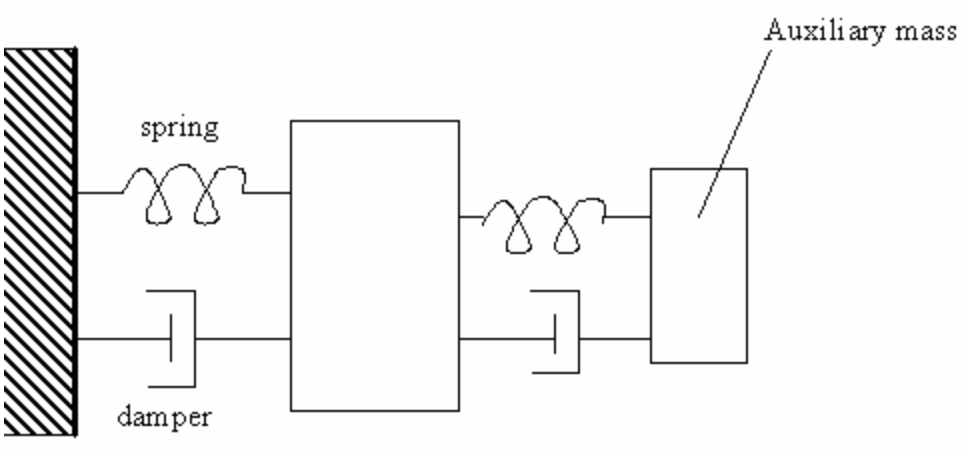

Figure 3: Passive Tuned Mass Damper

Figure 4. World's Tallest Building (1661 ft tall with101 stories)

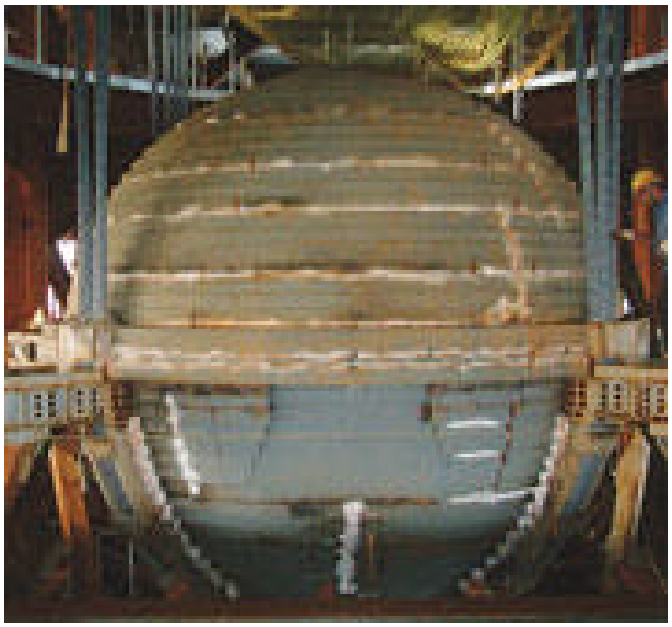

Figure 5. 800 ton steel sphere used in the passive mass damper

Base Isolation Systems

Base isolation systems allow a structure to sit on top of rubber bearings to isolate the structure at the base to attenuate the effect of ground motion experienced by the structure. A base isolation system, shown in the figure 6, consists of a set of flexible support elements, typically rubber bearings that have layers of natural rubber sheets bonded to steel plates, are proportioned such that the natural period of vibration of the isolated structure is much greater than the dominant period of excitation. Although the relative motion between the structure and the support may be large, the absolute structural motion is small (Connor 2003). The concept behind base isolation is similar to that of mounting mechanical equipment where the isolation system acts as a buffer between the equipment and the support. Base isolation is best implemented in locations of high seismicity or if increased building safety and post-earthquake operations are

required, such as a hospital or a nuclear facility. Base isolation may also be necessary if reduced lateral design forces are desired, or if an existing structure needs upgrading to satisfy current safety requirements. For cost effectiveness, base isolation needs to be considered in the planning stages of the building project; if such a device is added after completion of the structural design, complications may arise since construction techniques may have to be altered. The Toushin 24 Ohmori Building in Tokyo required an isolation system to reduce traffic vibrations from two adjacent railways, as well as reduce seismic motion. The building, with one underground parking garage and nine stories above ground, was fitted with a combination of laminated rubber bearings and steel rod dampers.

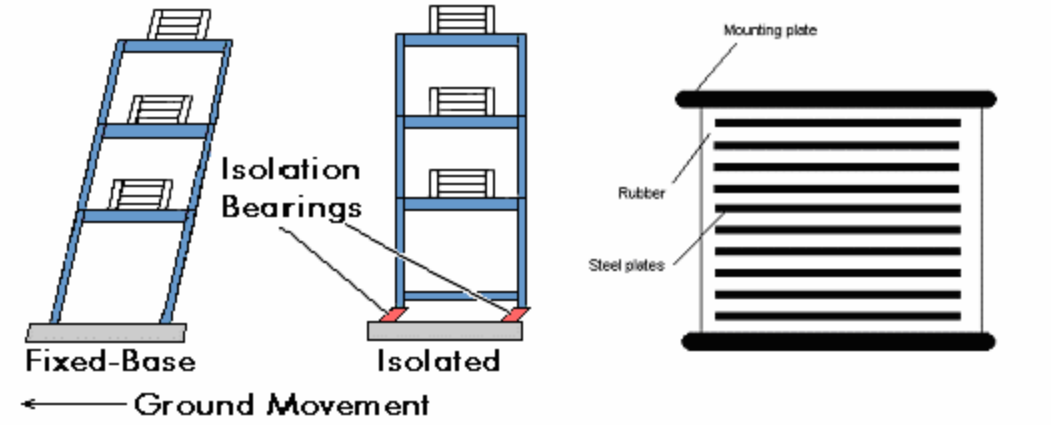

Figure 6. Typical base isolation system

Another example of base isolation system is the renovation and upgrading of a 150 year old historic landmark (Fig. 7), the State House building of South Carolina, to meet

current code requirements for safety, to correct worn components, and to replace failing systems. In addition, for protecting the structure from earthquake damage, a base isolation system was built under the existing foundations of the building, see Fig. 8.

Figure 7. State House, Columbia South Carolina

Figure 8. Base isolation system used under State House, Columbia, South Carolina

Active Control

Active control, opposite to passive control, requires an external source of energy to control the motion of a structure. Active control systems are best employed where weight is a critical issue, such as long span structures. Because active devices measure and estimate the response over the entire building to determine appropriate control forces, these control systems can theoretically accommodate unpredictable environmental changes, meet performance requirements over a wide range of operating conditions, and compensate for the failure of a limited number of structural components. Additionally, unlike passive control systems, active control systems have the ability to control different vibration modes and to accommodate different loading conditions, such as pulse-type loadings. "Properly designed optimal active control systems are highly effective in reducing peak structural vibrations during earthquakes" (Marzbanrad 2004). However, because active control is more complex than passive control due to the control equipment, active devices inherently possess a number of added complications. The cost of capital, maintenance, reliance on external power, system reliability and stability are all concerns that have led to problems in acceptance by the profession (Connor 2003).

Typically, an active control system consists of three main components: (1) a monitor, which is the data acquisition system; (2) a controller, a module that decides on an intelligent course of action; and (3) an actuator, a set of physical devices that execute the instructions from the controller. This algorithm is shown in figure 9. The actuator is an integral component of the control system, which generates and applies the control forces at specific locations on the structure according to instructions from the controller (Connor 2003). Civil structures require actuator systems, such as hydraulic systems, which are capable of generating large forces. For example, the hydraulic systems, shown

in the figure 10, generate the force by applying a pressure on the face of the piston head contained within the cylinder. Fluid is forced in or out of the cylinder through the hydraulic supply and return line to compensate for the piston displacement and maintain a certain pressure (Christenson 2002) . A successful system of this type will have the capability to determine the present state of the structure, decide on a set of actions that will change this current state to a more desirable state, and carry out these actions in a controlled manner in a short period of time.

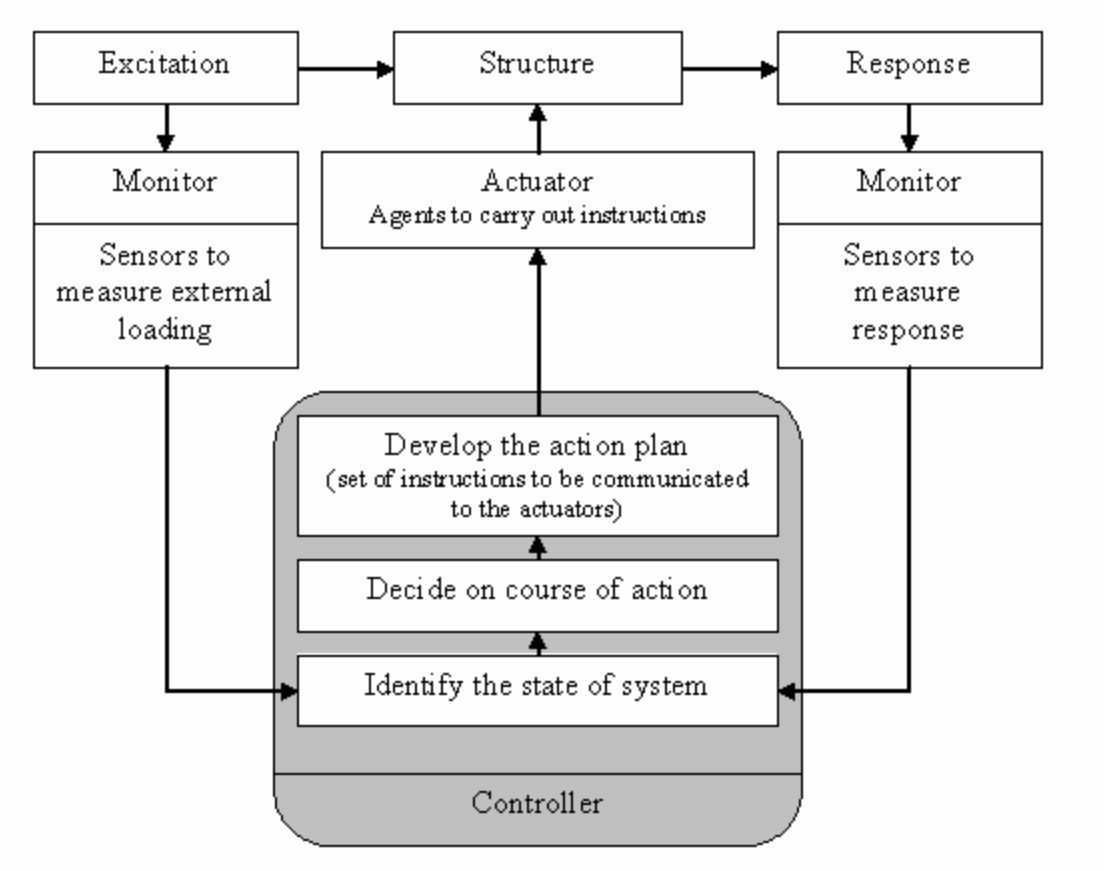

Figure 9: Active Control Algorithm

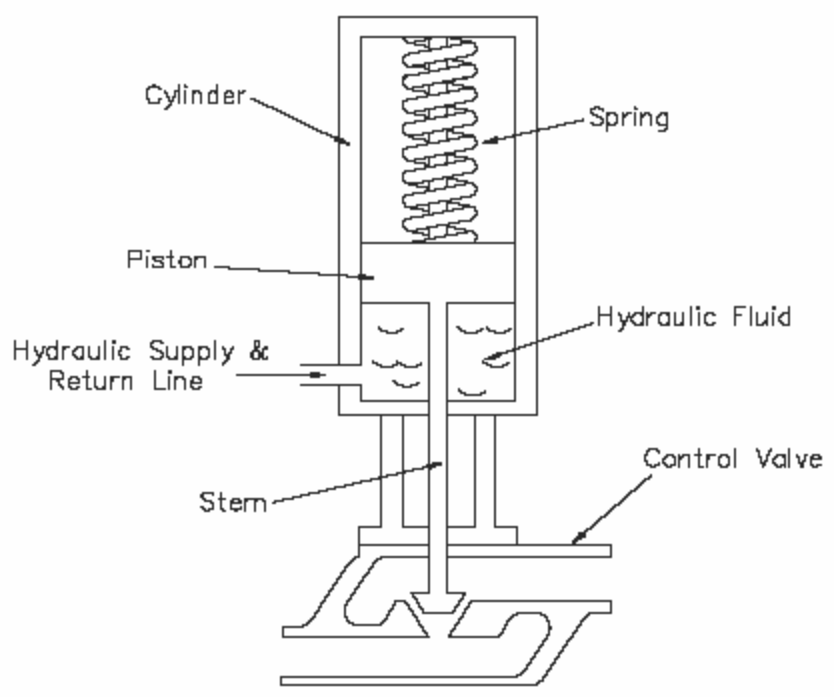

Figure 10: Hydraulic Actuator System

Active Mass Driver

Two common active control devices are the active mass driver and the active variable stiffness. In an active mass driver, an auxiliary mass is attached to the piston and supported by rollers shown in figure 11. The mass moves with respect to the structure with an absolute acceleration. Because force is generated by driving the mass, the actuator is designed to provide the required force at a certain level of acceleration. A successful active mass driver was implemented in the Kyobashi Seiwa Building (Connor 2003). Two active mass drivers were installed on the top floor to reduce the maximum lateral response associated with building vibrations caused from earthquakes and strong winds. Sensors were installed in the building at ground level, midheight, and the roof level to detect seismic motions and tremors. A control computer analyzes each signal and issues a drive order. Actuators then execute the control order and drive the masses

(Connor 2003). Although active mass drivers are relatively simple to operate, research has found an inefficiency due to mechanical or frictional problem effects on movement in the higher frequency range (Yoshida 1995).

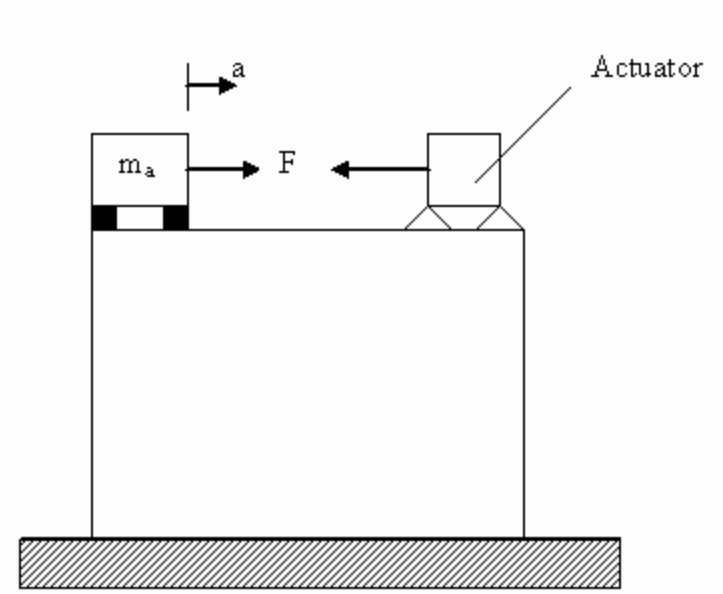

Figure 11: Active Mass Driver

Active Variable Stiffness Control

Active variable stiffness control reduces the energy input to buildings from external excitation by continuously shifting the stiffness of the building based on the nature of the excitation. The resonant state is avoided by changing the stiffness through locking or unlocking certain devices, shown in the figure 12, located between the beams or diagonal braces of the structure. This stand-by stiffness, controlled by oil movements, can be switched on and off at a particular time in accordance with the occurring earthquake. An active variable stiffness system was implemented in the three-story Kajima Technical Research Institute building (Connor 2003). The variable stiffness devices were installed between the steel brace tops and the lateral beams, which can alter the stiffness of the building by shifting from the locked mode to the unlocked mode. The

active variable stiffness devices solve many of the problems encountered with most active control devices. An active variable stiffness system can be activated and driven with a small amount of energy and typical safety concerns are alleviated because this system does not induce forces. However, although an active variable system is effective in controlling interstory drifts, the system may cause significantly increased floor accelerations (Pnevmatikos 2003).

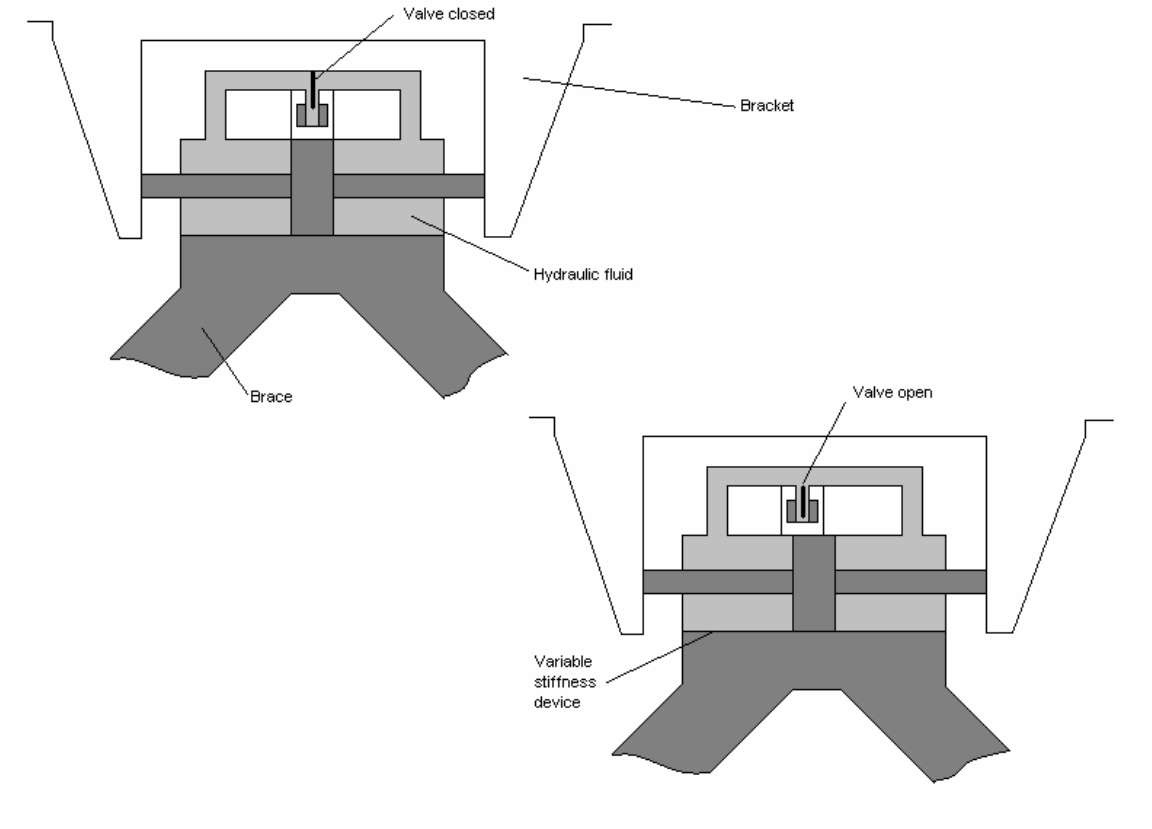

Figure 12: Active Variable Stiffness Control

Semi-active Control

Semi-active or hybrid control devices performance is bounded by passive and active control. Semi-active control strategies are similar to active control strategy, expect the control actuator does not directly apply force to the structure, but instead it is used to

control the properties of a passive energy device, a controllable passive damper (Christenson 2002). Another chief difference between active and semi-active control is that semi-active devices can only produce dissipative forces. Semi-active control devices combine the positive aspects of passive and active devices, these devices are controllable, low-power, and reliable. Some common types of semi-active devices are the hybrid-mass damper and the variable orifice damper.

During its lifetime the earthquake and wind effects experienced by a building vary in strength, size, and frequency and are thus uncertain. So it is necessary to develop control devices which will be adaptive to the characteristics of the external effect experienced by the structure at a particular time. Such control devices should be inexpensive to install and easy to maintain.

This thesis investigates one possible way of eliminating some of the disadvantages of the previously discussed control methods by using a biologically inspired technique. In the subsequent chapters, diagonal-bracing systems implemented on ideal frames will be explored through means of computer simulation and experimental validation. Depending upon the nature and magnitude of external excitation, the stiffness characteristics of the structure will be changed by introducing changes in the stiffness characteristics of the bracing systems.

CHAPTER II

OBJECTIVE AND SCOPE

The magnitude, intensity and frequency of an earthquake to be experienced by a structure at a certain seismically active locality are uncertain. So it is necessary to use structural control devices, which can adjust the attributes of the building to prevent damage and loss of life. The device should effectively perform its function during the whole period of time an earthquake or wind of certain magnitude lasts. The best result would for these devices to have the property of adaptation observed in biologically inspired adaptability of the human body against the forces acting on it. For example, active control is in play when a person is surfing. When the surfer is on the board, the body is constantly adjusting balance and shifting footing to compensate for the changing waves in the water. This concept can be applied to an adaptive control system for modifying the response of buildings subjected to earthquakes. Of the many possibilities, the author chose to study the effect of stress induced bracing systems, because of simplicity and integral nature. The main objective of this study, therefore, is to determine the effectiveness of stress induced bracing systems in controlling the response of framed structures subjected to earthquake excitation. This objective will be realized through the following steps:

1. Identification of representative structural systems including geometry, dimensions, and material; bracing systems; stress inducing mechanisms; the nature of earthquake excitation; and response quantities of interest.

2. Study the effect of induced stress on the stiffness of structural elements.
3. Undertake analytical studies to determine the effect of induced stress in the dynamic response of the selected structures for the following conditions.
    a. Sinusoidal base input (Modal analysis)
    b. El Centro earthquake
    c. Different bracing arrangements.
    d. Different magnitudes of induced stress.
4. Undertake laboratory experiments for some selected cases considered under Item No. 3.
5. Validate the analytical results with experimental findings and discuss the numerical results.
6. Draw conclusions and make recommendations about the efficacy of using stress induced bracing system for adaptive structural control under seismic excitation.

Objective 1 is covered in the present chapter. Objectives 2 and 3 are considered in Chapter III. Work under objectives 4 and 5 are described in Chapter IV. Objective 6 can be found in Chapter V.

Identification of Structural System

In identifying the structural system, the foremost consideration was the capacity of the shake table available for undertaking the experimental investigation. The specifications of the shake table, shown in figure 13 manufactured by Quanser

Consulting, Inc., is given in Table 1. The shake table is designed to subject earthquake excitation to scaled model structures.

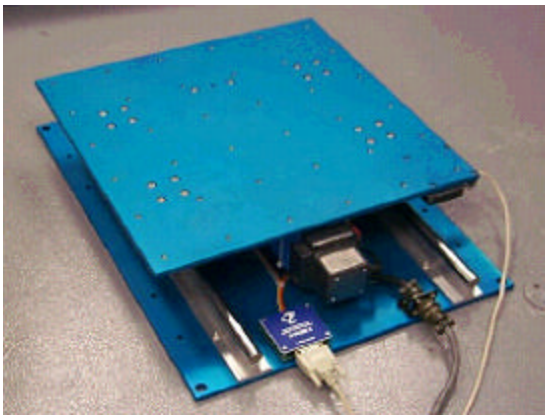

Figure 13. Quanser Shake II Shake Table

Table 1: Specifications of Shake Table

Parameter	Value
Table dimension	18” x 18”
Maximum payload	33 lbs
Operation bandwidth	0 - 20 Hz
Peak Acceleration	7.5g
Peak velocity	33 in/sec
Maximum stroke	± 3 in
Maximum force	157 lbs

In view of the specifications in Table 1, single bay single and double story frames were decided upon. The bay span was limited to 12 in. The story height was typically taken as 19.3 in. Three materials for construction of the test frame were considered – wood (Pine), polycarbonate (Lexan), and aluminum. In trial experiments, wood frame was found to be too stiff. Polycarbonate frame was quite flexible but the decision for a type of bracing coupled with high structural flexibility was found to be difficult. Both steel

wire with turnbuckles and rubber band were tried. The first choice proved to be too stiff; whereas, the second choice failed to provide enough stiffness to the flexible structure. Eventually a combination consisting of polycarbonate beams and aluminum columns was found to be the best choice.

The components for the test model were readily available in the laboratory. The single story test frame is shown in figure 14. The span is 12 in, and frame height is 19.3 in. The aluminum columns are of size 4.25 in X 0.07874 in. The polycarbonate beam is of size 4.25 x 0.25 in. Steel wire was used as cross bracing in which stresses could be induced by tightening the bracing using a system of threaded eye-bolts and wing nuts.

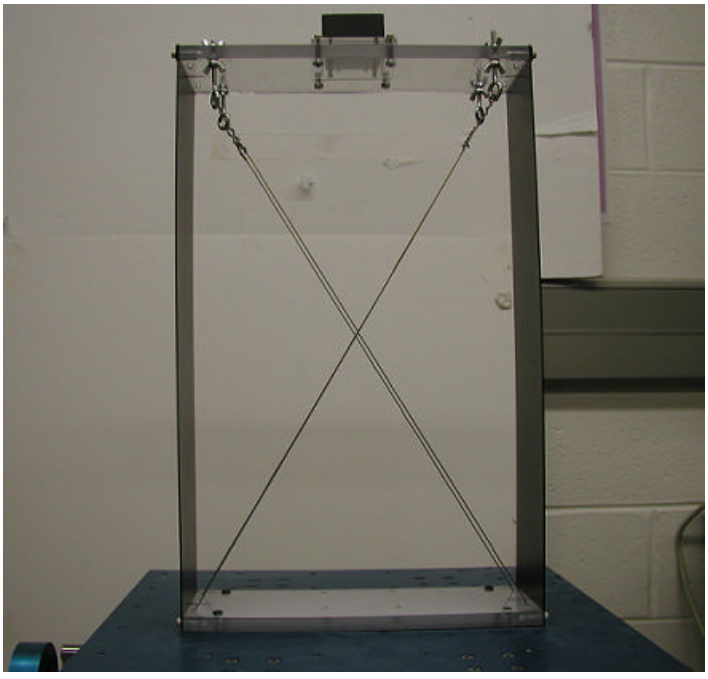

Figure 14: Test Frame

CHAPTER III

ANALYTICAL STUDIES

Effect of Induced Stress on Stiffness

The dominant frequency content of a structure determines the response of a structure to dynamic external excitation like that due to an earthquake. So, modifying its frequency content can alter the response of the structure. In order to modify the natural frequency of a structure either the mass or the stiffness characteristics of the structure need to be altered. For active control during an earthquake, effecting changes in stiffness is the most practical solution. Inducing initial forces or prestress in the structural elements can introduce changes in structural stiffness. This concept is partially based on Lyapunov's dynamic criterion of stability. This criterion states that as the compressive axial load of a structural member approaches the critical buckling load, the natural frequency and stiffness of the member will approach zero. Likewise, as the axial tensile load increases, the natural frequency and stiffness will increase (Jekabosons 2001).

To investigate the effects of prestress on a structural member, consider a straight homogeneous, two-dimensional pinned-pinned column of length L, acted on by an axial force P. The six degrees of freedom are defined as u_1, v_1, $?_1$ for end 1 and u_2, v_2, $?_2$ for end 2, as shown in figure 15.

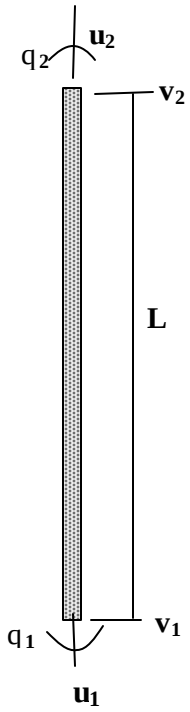

Figure 15: Typical element showing degrees of freedom and directions of local axes

Using Galerkin finite element approach, the matrix equation for deformation takes the following general form.

$$\left(\left[K^{f}\right]+\left[K^{s}\right]\right)\{d\}+[M]\left\{\frac{d^{2}d}{dt^{2}}\right\}=0 \tag{1}$$

$$[d]=[u_1 \quad v_1 \quad q_1 \quad u_2 \quad v_2 \quad q_2]$$

The first and second order stiffness and mass matrices can be shown to be of the forms as shown below.

The first order stiffness matrix is given by:

$$\left[K^{f}\right]=\frac{E}{L^{3}}\begin{bmatrix} AL^{2} & 0 & 0 & -AL^{2} & 0 & 0 \\ 0 & 12I & 6IL & 0 & -12I & 6IL \\ 0 & 6IL & 4IL^{2} & 0 & -6IL & 2IL^{2} \\ -AL^{2} & 0 & 0 & AL^{2} & 0 & 0 \\ 0 & -12I & -6IL & 0 & 12I & -6IL \\ 0 & 6IL & 2IL^{2} & 0 & -6IL & 4IL^{2} \end{bmatrix} \tag{2}$$

Here, E is elastic modulus, A is cross-sectional area of member, and I is the moment of inertia of member for bending in the plane of the plate.

Second order correction to stiffness matrix due to pre-induced force P can be shown to be

$$[K^s] = \frac{P}{30L}\begin{bmatrix} 0 & 0 & 0 & 0 & 0 & 0 \\ 0 & 36 & 3L & 0 & -36 & 3L \\ 0 & 3L & 4L^2 & 0 & -3L & -L^2 \\ 0 & 0 & 0 & 0 & 0 & 0 \\ 0 & -36 & -3L & 0 & 36 & -3L \\ 0 & 3L & -L^2 & 0 & -3L & 4IL^2 \end{bmatrix} \tag{3}$$

The consistent mass matrix with m as mass per unit length of the member will be

$$[M] = \frac{mL}{420}\begin{bmatrix} 140 & 0 & 0 & 70 & 0 & 0 \\ 0 & 156 & 22L & 0 & 54 & -13L \\ 0 & 22L & 4L^2 & 0 & 13L & -3L^2 \\ 70 & 0 & 0 & 140 & 0 & 0 \\ 0 & 54 & 13L & 0 & 156 & -22L \\ 0 & -13L & -3L^2 & 0 & -22L & 4L^2 \end{bmatrix} \tag{4}$$

In order to evaluate the effect of axial force on the natural frequencies of vibration, an 11 in long member with one end pinned and the end on roller was analyzed for induced axial forces in tension and compression. The values of elastic modulus, E = 120574 psi and mass, m = 5.202×10^{-4} lb·sec^2/in. In each case the first three natural frequencies were computed. The induced axial force was normalized with respect to the Euler critical load. Figure 16 shows the plot of the natural frequencies versus the normalized force.

As evident from Figure 16, as the tensile force is increased the natural frequencies of the column are increased and as the compressive force is increased, the natural frequencies of the column are decreased. Therefore, to increase the frequency, induce tensile force and to decrease the frequency, induce compressive force. An increase in

natural frequency signifies corresponding increase in stiffness; whereas, a decrease in natural frequency signifies increased flexibility. If the objective is to reduce drift in the structure under earthquake excitation, an increase in the natural frequency may be necessary.

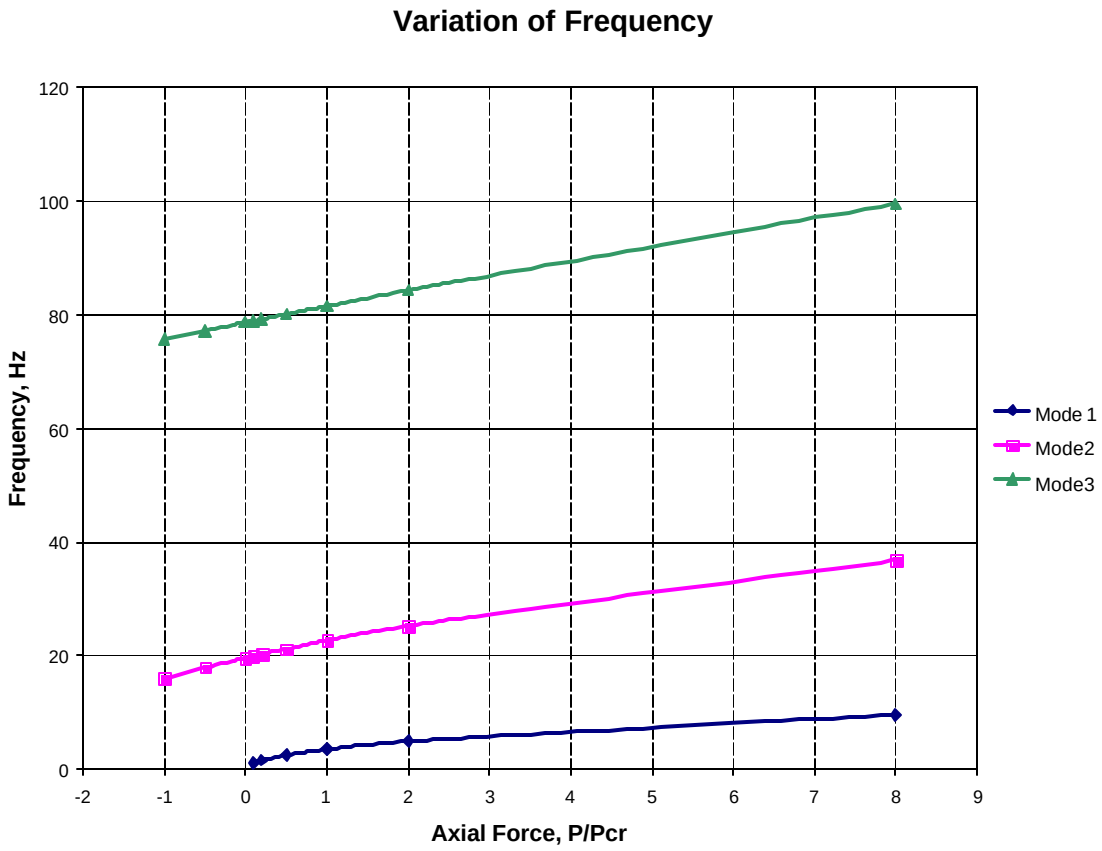

Figure 16: Variation of frequency of a pinned-pinned column with initial axial force (P/P_{cr})

Analytical Solution

A number of frames with different bracing arrangements were studied under free vibration as well as seismic excitation. The finite element software ANSYS (Version 5.3) was used for this purpose. The single and two story frames considered are shown in Fig. 17. It can be noted that in the case of the single story frame, three cases are shown-

SS0, SS1, and SSX. SS0 refers to the unbraced frame. SS1 refers to the frame with single bracing and SSX refers to the frame with cross-bracing. In the case of braced frames, a number of cases arise, namely, braces without induced force and braces with different types and levels of induced force. In the case of the two-story frames, six cases are shown. Only six of the ten possible cases are considered because these combinations are most often used in the field. As before, the last digit (zero) in TS0 signifies an unbraced frame. The characters L1 signify single bracing in the bottom story. On the other had, the characters U1 signify single bracing in the upper story. Therefore, L1U1 in TSL1U1-S and TSL1U1-O signify single bracing in the lower and upper stories with S representing same orientation and O representing opposite orientation. In the case of the two-story frame cross-bracing can be provided in the lower, upper, or both stories. The purpose of considering these cases is to identify the best possible realistic bracing configuration for the two frames considered in this study. An alternative way for this would have been the use of an optimization algorithm to arrive at the best possible configuration for a given situation. In an actual frame, the provision will exist for cross-bracing in each story; depending upon the nature of excitation, a smart structure will activate the appropriate bracing by inducing the correct magnitude of forces in tensile or compressive force as needed. The author of this thesis could not pursue the optimization technique due to the limited availability of such technique in the commercial software readily available to her for undertaking the required type of optimization.

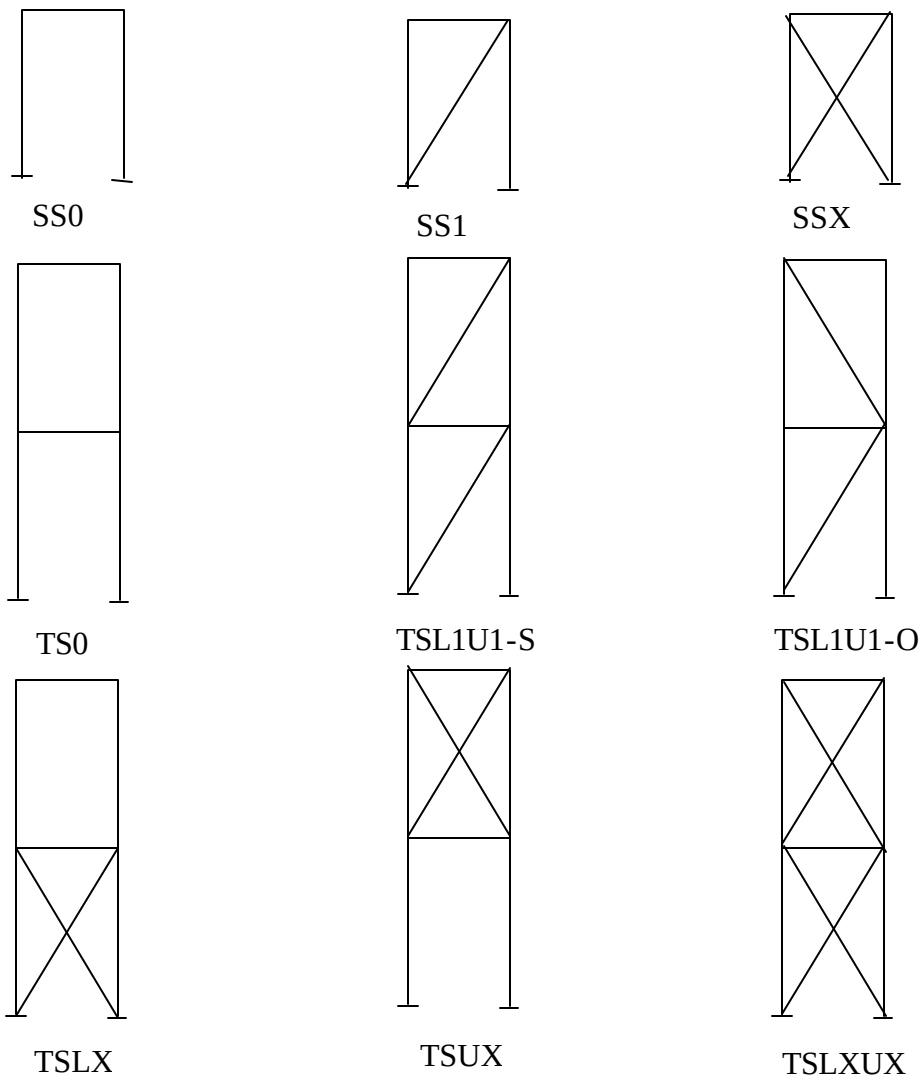

Figure 17. Structural arrangement for single and two story frames

During analysis, for all frames, the base is assumed fixed and the joints are assumed to be rigid. Also, the braces are assumed to act as truss members only. First, the unbraced frame is analyzed. Thereafter, braced frames with no prestress and then with different levels of prestress are considered.

A view of the two story experimental frame mounted on the shake table is shown in figure 18. The material characteristics of the frame were based on those for the

experimental setup discussed earlier. The geometric and material data for the frame are summarized in Table 2 and drawn in figure 19.

Figure 18: Two-story building used for experiments

Table 2: Properties of element types used in ANSYS

Element Number	ANSYS Element Type	Young's Modulus (psi)	Mass Density (lb/in^3)	Mass ($lb \cdot sec^2/in$)	Cross Sectional Area (in^2)	Area Moment of Inertia (in^4)	Total Beam Height (in)	Shear Deflection Constant
1	Beam3	10000000	2.56×10^{-4}	----------	0.265625	0.0000865	0.0625	1
2	Beam3	120572	1.056×10^{-4}	----------	2.125	0.044271	0.5	1
4	Mass21	----------	---------	0.007557	----------	----------	--------	----------
5	Link1	8000000	7.2×10^{-4}	----------	Varied	----------	--------	----------

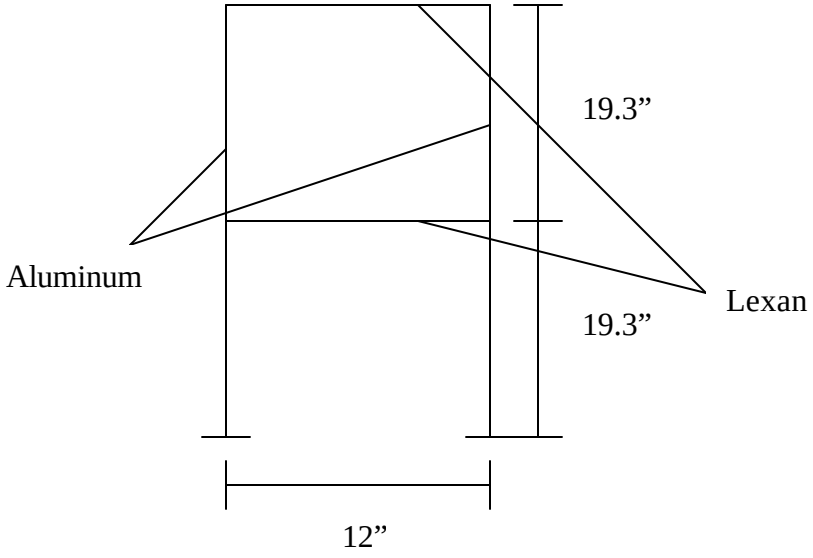

Figure 19: Schematic of two-story frame

One-Story Frame Analysis

The ANSYS models for the single and double-story frames are shown in figures 20-21, respectively. Bold numbers indicate node numbers. Each element type was selected to specifically reflect a particular component of the frame. Elements 1-4 and 8-12, representing the column and beam respectively, are of type Beam3, which is a two-dimensional elastic beam with three degrees of freedom at each node – x - and y-displacements, and rotation about the z-axis. Nodes 4 and 10, representing locations of the mass of the accelerometer on each beam, are represented as element type Mass21, which is a structural mass with all six degrees of freedom. Elements 5-6 and 12-13, representing the bracing, are element type Link1 allowing x- and y-displacements only. After the model was created, two types of analysis were performed, modal and transient analyses, which are discussed in the following sections.

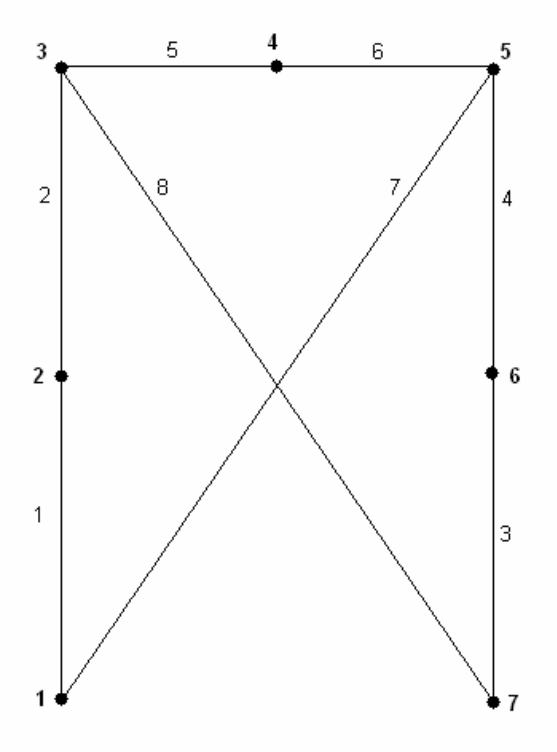

Figure 20: ANSYS model of one-story frame

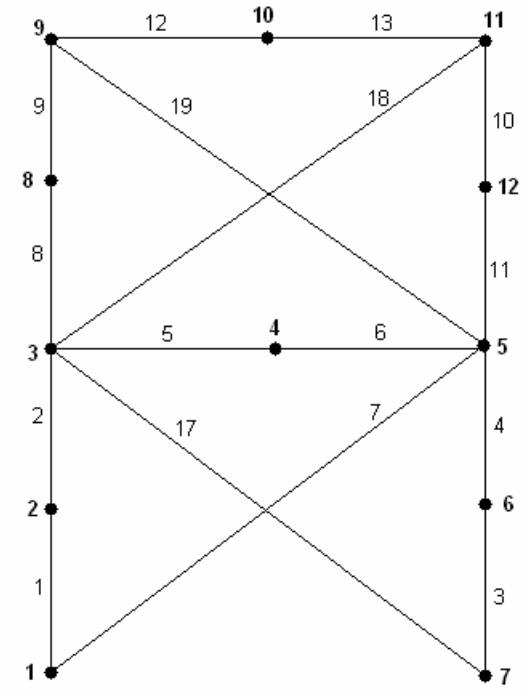

Figure 21: ANSYS model of two-story frame

Modal Analysis

A full modal analysis of a bare frame was undertaken to establish core frequencies and responses. Because no bracing was used, all internal pre-induced forces were shown as zero based on the Static Analysis. Listed in table 3 are the frequencies from Modal Analysis by ANSYS. The corresponding mode shapes are shown in figure 22.

Table 3: Modal frequencies of bare frame

Mode	Frequency
1	4.4795
2	32.001
3	36.900
4	60.500
5	124.44
6	128.15
7	237.38

Figure 22: Seven mode shapes of bare frame

Because the planar ANSYS model used seven degrees of freedom, seven frequencies and mode shapes were generated. However, as seen in figure 22, mode shapes one and five have the same form, but the frequency of mode five is over twenty times the frequency of mode one. This may be attributed to the coarseness of the model used, which failed to capture the mode shapes in needed details.

Transient Analysis

Next, a transient dynamic analysis was conducted to determine the dynamic response of the structure under El Centro. In ANSYS, the full method of a transient analysis was carried out such that all types of nonlinearities are allowed. In the full method, full system matrices, no matrix reduction, are used to calculate the transient response and allows for nonlinearities such as plasticity, large deflections, and large strain. Displacement data for El Centro earthquake shown in table 4 was obtained from Shonkwiler and entered into the Load Step Options in ANSYS.

Table 4: Base displacement data for El Centro Earthquake

Time, sec	Ground Displacement, in
0.47	0.90
0.60	0.70
0.68	0.85
0.82	0.00
0.93	1.10
1.07	-0.60
1.17	0.45
1.28	-0.50
1.42	0.90
1.53	-0.30
1.65	1.10
1.75	0.30
1.87	1.10
1.98	-0.50
2.10	0.70
2.23	-1.20
2.37	0.75
2.47	-0.30
2.58	0.90
2.70	-0.40
2.82	0.70
2.93	-0.50
3.03	0.65
3.15	-0.10
3.27	-0.20
3.38	-0.40

The maximum ground displacement occurred approximately 2.1 seconds after the earthquake was triggered. Therefore, only the first 3.4 seconds of the earthquake during which the maximum response as found occurred are considered, also verified by experimental results. Figure 23 shows the displacement response of the unbraced structure.

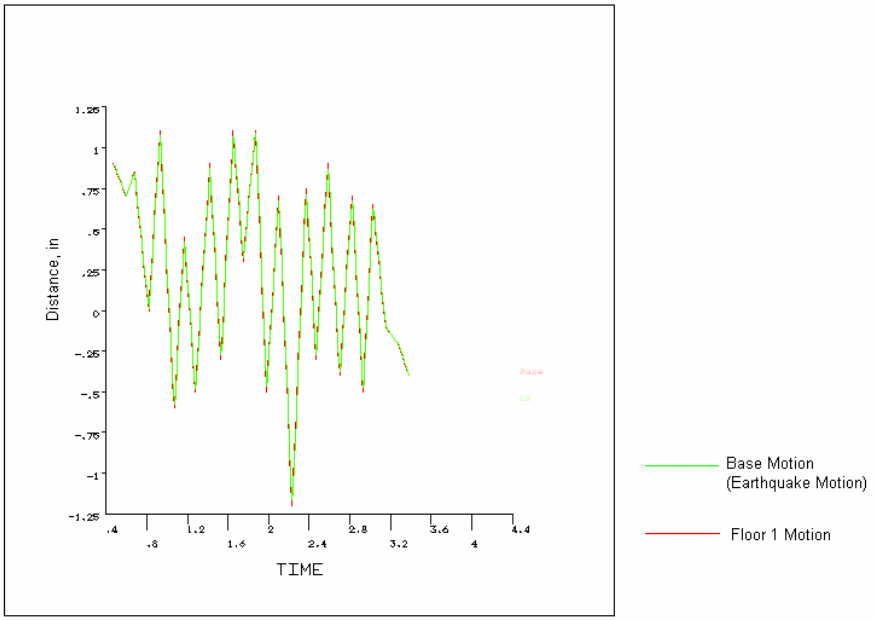

Figure 23: Bare frame earthquake response

From the raw response values, the time history of sway displacement of the structure was determined by subtracting the base displacement from the floor displacement. These results are plotted in figure 24.

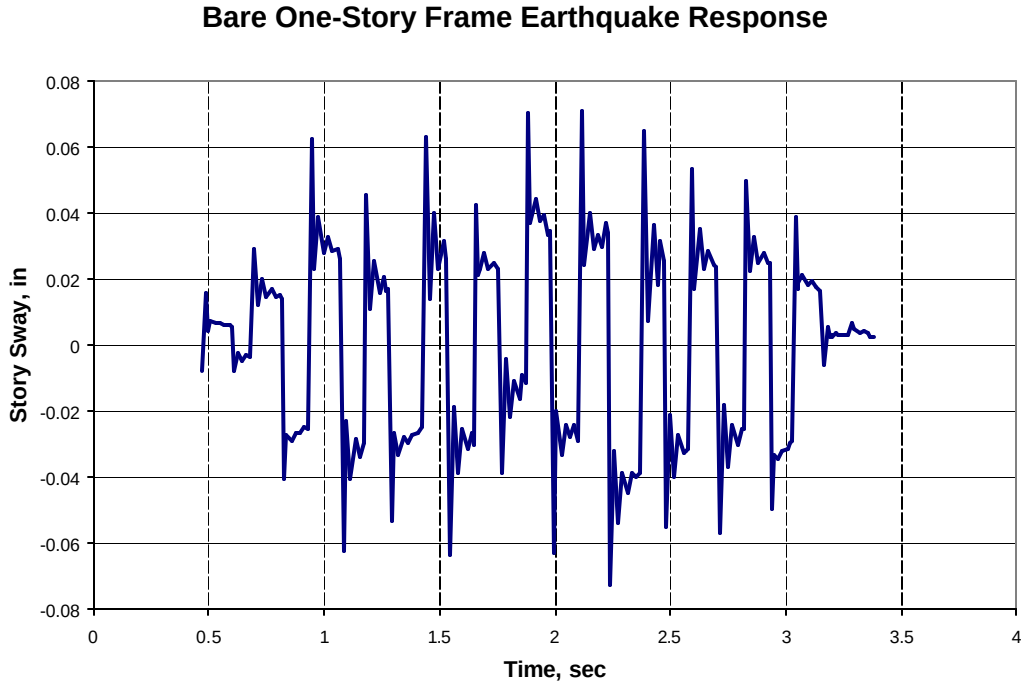

Figure 24: First story sway of bare frame

The absolute maximum sway is noted as -0.073 inches at 2.24 seconds. This result seems to make sense because it occurs shortly after the maximum displacement at 2.1 seconds of the ground motion creating the slight phase difference in the response of the structure.

Figure 25 shows the moment experienced at the base on the columns resulting from the earthquake.

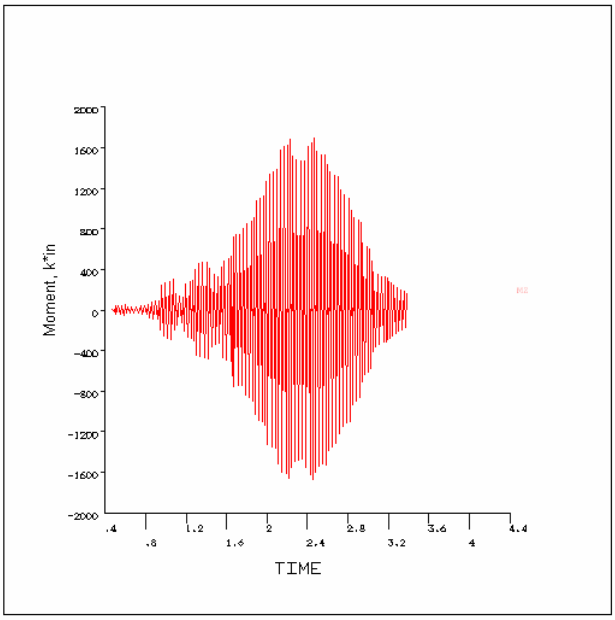

Figure 25: Moment of left column at the base of the bare frame

The moment experienced at column top is shown in figure 26 on the following page.

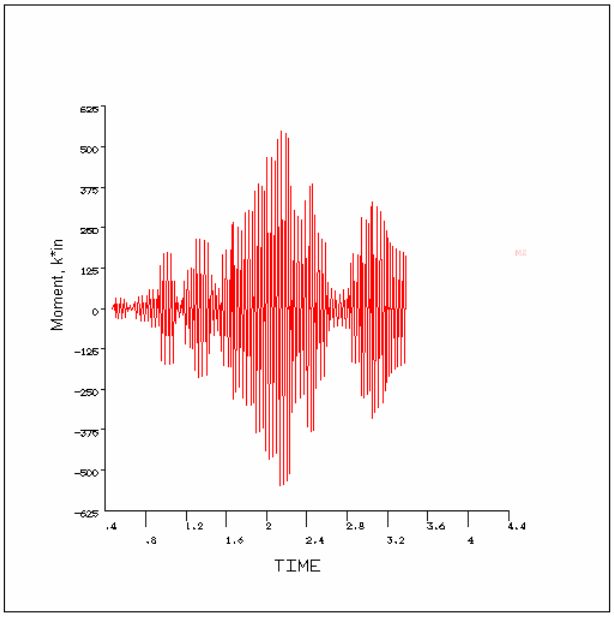

Figure 26: Moment at first floor of bare frame

As seen in figures 25 and 26, both moments have a local maxima occurring around 2 seconds. Although both plots have similar shapes, the moment at the top of column in figure 26 is slightly less than twice the moment at column base. Because only the first 3.4 seconds of the earthquake are considered, the absolute maximum moment was probably not captured within the time period shown in figures 25-26.

Analysis of Braced Frame

After the bare frame analysis, a single diagonal brace with an area of $0.0707 in^2$, unless noted otherwise, was added to the model shown in figure 27.

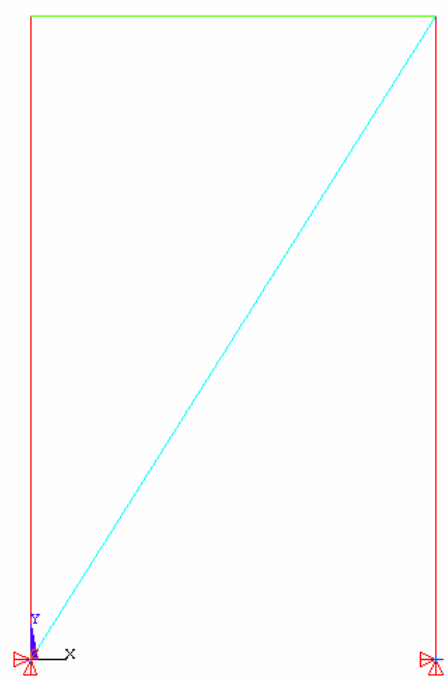

Figure 27: ANSYS model with single brace

This member was first analyzed as one with no pre-strain, and subsequently as a member with induced tension or compression. In ANSYS, the introduction of compressive pre-strain in the brace induces tensile force in the columns. On the other hand, the introduction of tensile pre-strain in the brace induces compressive forces in the columns. During vibratory motion, the brace force may alternate between compression and tension. Moreover, to prevent premature buckling under induced compressive pre-strain, the size of the brace member was so selected that its slenderness ratio, kL/r did not exceed the value 300. Based on this limit, an area of $0.0707 in^2$ and a pre-strain of 0.0000141in/in were arrived at; leading to an induced force of 7.97 lb induced in the brace. Figure 28 also shows the internal forces in pounds by ANSYS with a pre-strain of +0.0000141. The brace force is found to be 3.21 pounds.

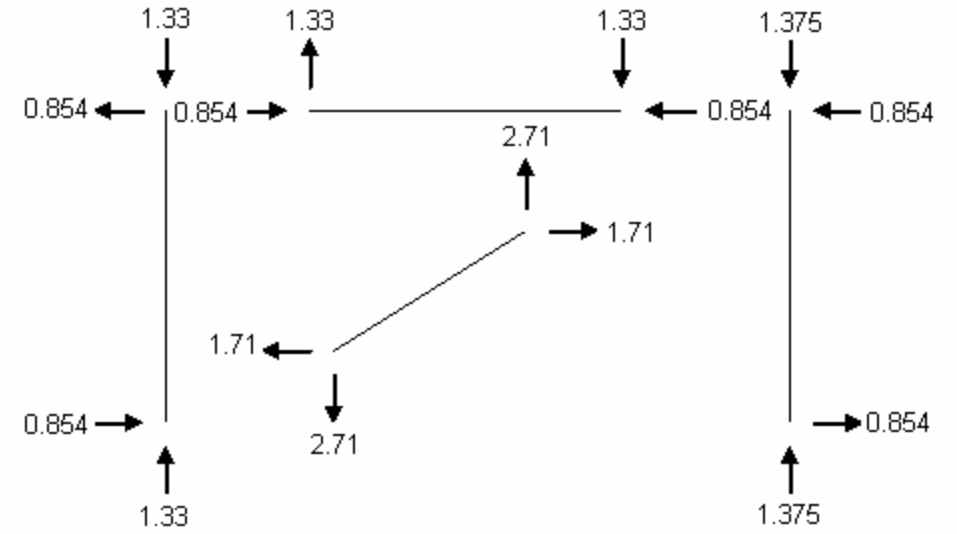

Figure 28: Internal forces in tensioned single brace frame

With tensile and compressive pre-strains of ±0.0000141in/in as well as with zero pre-strain, the results of modal analysis are shown in Table 5. Due to limitations of the student version of ANSYS used in this study, a larger pre-strain could not be used.

Table 5: Frequencies for single braced frame

Frequency	Tension	Zero Force	Compression
1	32.001	32.001	32.002
2	34.500	34.501	34.501
3	60.499	60.500	60.500
4	120.08	120.08	120.08
5	128.15	128.15	128.15
6	210.03	210.03	210.03
7	239.91	239.91	239.91

It may be noted that, as the pre-strain is too small, it has hardly any effect on the natural frequencies of vibration. However, the results for the cross-bracing are more dramatic than the single bracing, as shown in table 6. As expected, compressive pre-

strain in the bracings increased the frequency, signifying stiffening of the structure. The opposite is found to be true with a tensile pre-strain in the brace.

Table 6: Frequencies for cross-braced frame

Frequency	Tension	Zero Force	Compression
1	31.039	32.002	32.933
2	33.554	34.534	35.487
3	60.057	60.503	60.945
4	119.78	120.89	121.99
5	127.07	128.17	129.26
6	234.88	235.33	235.78
7	292.25	292.28	292.32

The results of single story frame analysis for different cases follow hereinafter.

Earthquake Response for SS1 (Pre-strain – Tensile): In this case of a single braced frame, a tensile pre-strain of 0.0000141in/in is induced and response analysis due to El Centro earthquake, as stated earlier, is undertaken. Table 7 shows the frequency values based on modal analysis, and Figure 29 shows the story sway response of the frame. The maximum positive and negative sway values are shown in Table 8.

Table 7: Frequency values from modal analysis

Mode	Frequency
1	32.001
2	34.500
3	60.499
4	120.08
5	128.15
6	210.03
7	239.91

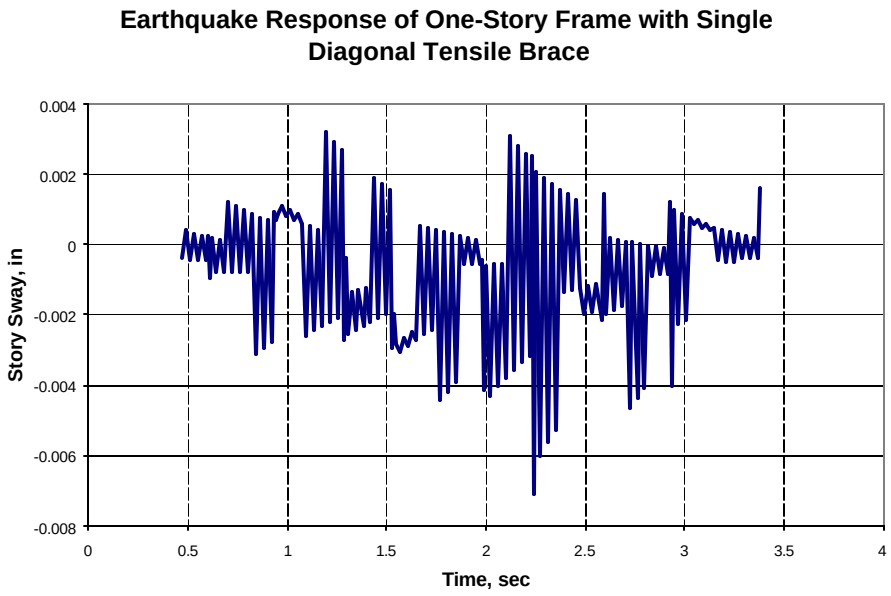

Figure 29: Sway of tensioned induced single braced frame

Table 8: Maximum sway values

	(in)	Time, sec
Positive Sway	0.003189	1.19
Negative Sway	-0.00709	2.24

Earthquake Response for SS1 (Zero Pre-strain): In this case of a single braced frame with no induced pre-strain, the response analysis due to El Centro earthquake, as before, is undertaken. Table 9 shows the frequency values based on modal analysis, and Figure 30 shows the story sway response of the frame. The maximum positive and negative sway values are shown in Table 10.

Table 9: Frequency values based on modal analysis

Mode	Frequency
1	32.001
2	34.501
3	60.500
4	120.08
5	128.15
6	210.03
7	239.91

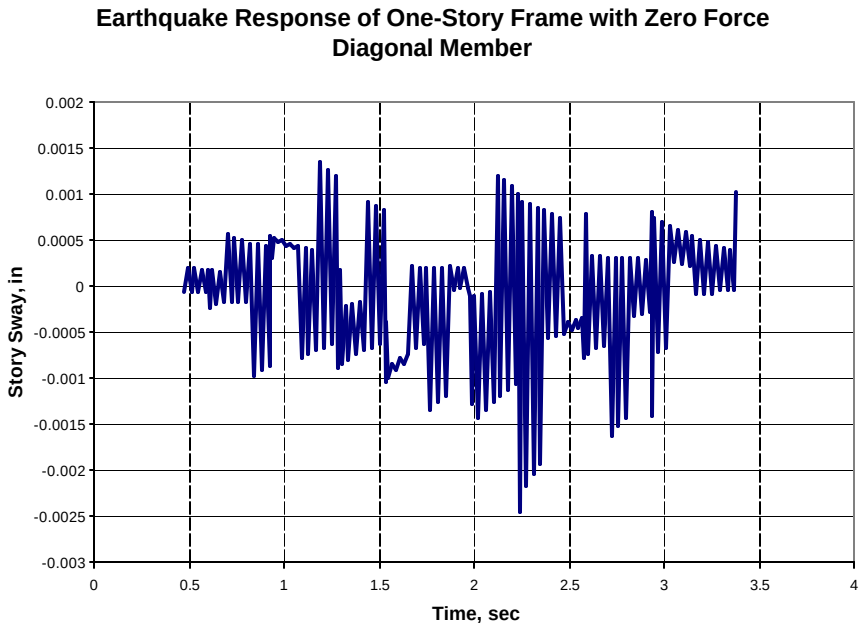

Figure 30: Sway of frame with zero-force brace member

Table 10: Maximum sway values

	(in)	Time, sec
Positive Sway	0.001343	1.19
Negative Sway	-0.00246	2.24

Earthquake Response for SS1 (Pre-strain—Compressive): In this case of a single braced frame with a compressive pre-strain of -0.0000141in/in, the response analysis due to El Centro earthquake, as mentioned earlier, is undertaken. Table 11 shows the frequency values based on modal analysis, and Figure 31 shows the story sway response of the frame. The maximum positive and negative sway values are shown in Table 12.

Table 11: Frequency values based on modal analysis

Mode	Frequency
1	32.002
2	34.501
3	60.500
4	120.08
5	128.15
6	210.03
7	239.91

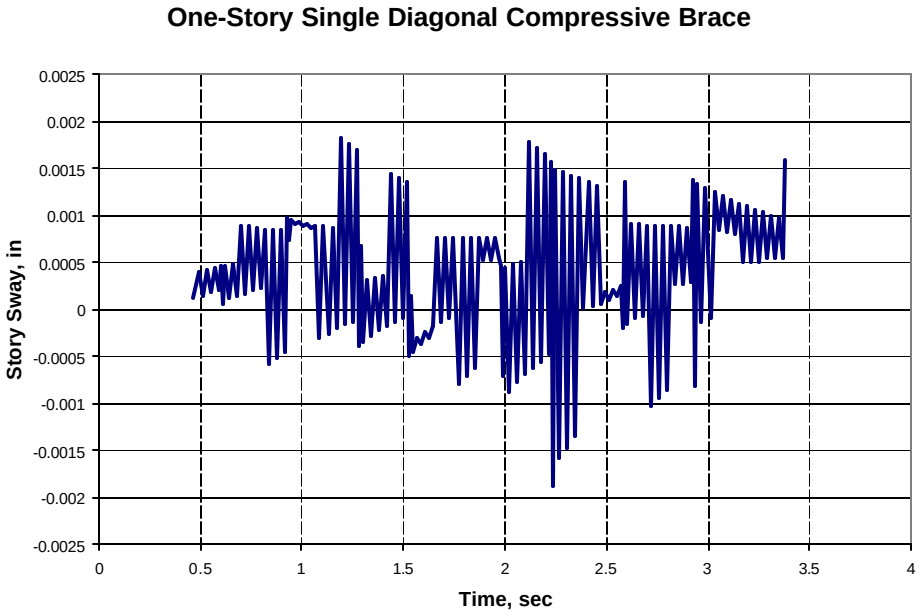

Figure 31: Sway of frame with single compression induced brace

Table 12: Maximum sway values

	(in)	Time, sec
Positive Sway	0.001836	1.19
Negative Sway	-0.00188	2.24

Earthquake Response for SSX (Pre-strain—Tensile): In this case of a cross-braced frame, a tensile pre-strain of 0.0000141in/in is induced in both braces and response analysis due to El Centro earthquake, as discussed earlier, is undertaken. Table 13 shows the frequency values based on modal analysis, and Figure 32 shows the story sway response of the frame. The maximum positive and negative sway values are shown in Table 14.

Table 13: Frequency values based on modal analysis

Mode	Frequency
1	31.039
2	33.554
3	60.057
4	119.78
5	127.07
6	234.88
7	292.25

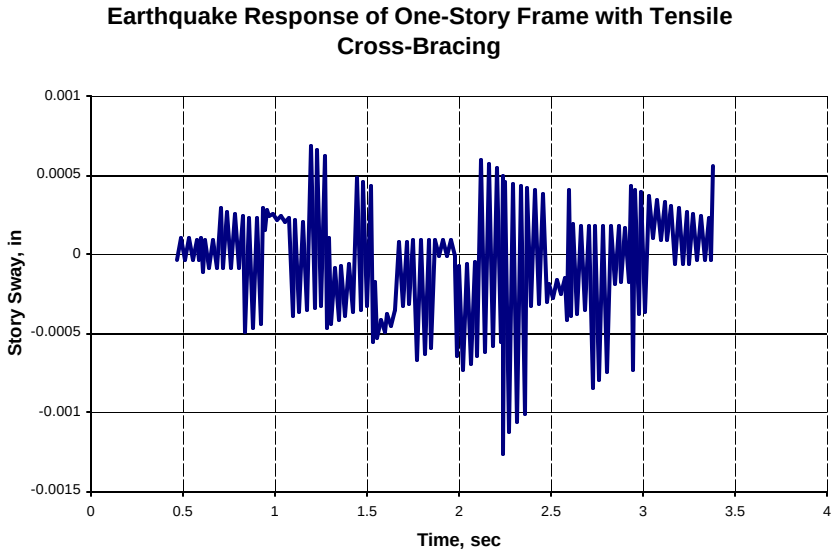

Figure 32: Sway of frame with tensioned cross-bracing

Table 14: Maximum sway values

	(in)	Time, sec
Positive Sway	0.00069	1.19
Negative Sway	-0.00126	2.24

Earthquake Response for SSX (Pre-strain—Tensile): In this case of a cross-braced frame with a brace area of $0.003in^2$, another analysis with tensile pre-strains of 0.0000456in/in induced in both braces and response analysis El Centro earthquake, as discussed earlier, is undertaken. Thus, this analysis can be used for comparing the results between the computer and the experimental results. Table 15 shows the frequency values based on modal analysis, and Figure 33 shows the story sway response of the frame. The maximum positive and negative sway values are shown in Table 16.

Table 15: Frequency values based on modal analysis

Mode	Frequency
1	31.829
2	33.678
3	60.419
4	70.858
5	125.65
6	127.95
7	237.37

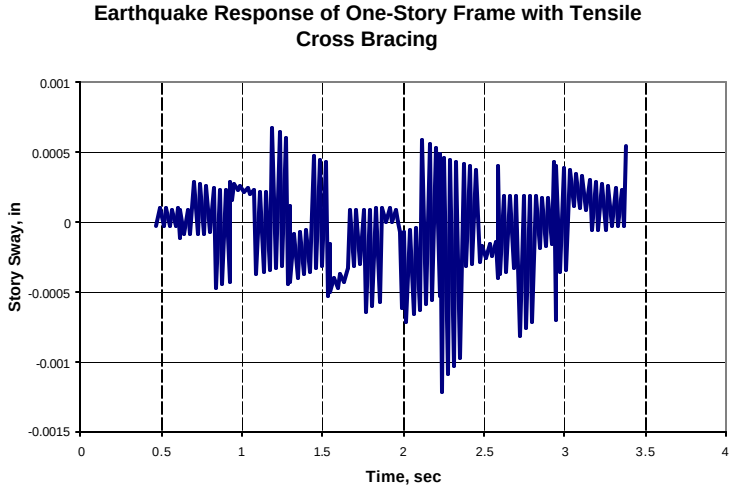

Figure 33: Sway of frame with tensioned cross-bracing

Table 16: Maximum sway values

	(in)	Time, sec
Positive Sway	0.000677	1.19
Negative Sway	-0.00121	2.24

Earthquake Response for SSX (Zero Pre-strain): In this case of a cross-braced frame, no pre-strain is induced and response analysis due to El Centro earthquake, as discussed earlier, is undertaken. Table 17 shows the frequency values based on modal analysis, and Figure 34 shows the story sway response of the frame. The maximum positive and negative sway values are shown in Table 18.

Table 17: Frequency values based on modal analysis

Mode	Frequency
1	32.002
2	34.534
3	60.503
4	120.89
5	128.17
6	235.33
7	292.28

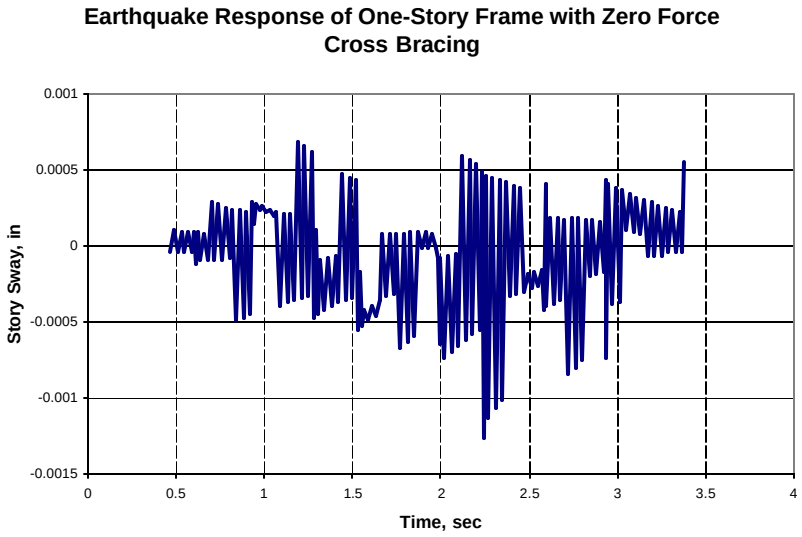

Figure 34: Sway of frame with zero force in cross bracing

Table 18: Maximum sway values

	(in)	Time, sec
Positive Sway	0.000686	1.19
Negative Sway	-0.00126	2.24

Earthquake Response for SSX (Pre-strain—Compressive): In this case of a cross-braced frame, a compressive pre-strain of -0.0000141in/in is induced and response analysis due to El Centro earthquake, as discussed earlier, is undertaken. Table 19 shows the frequency values based on modal analysis, and Figure 35 shows the story sway response of the frame. The maximum positive and negative sway values are shown in Table 20.

Table 19: Frequency values based on modal analysis

Mode	Frequency
1	32.933
2	35.487
3	60.945
4	121.99
5	129.26
6	235.78
7	292.32

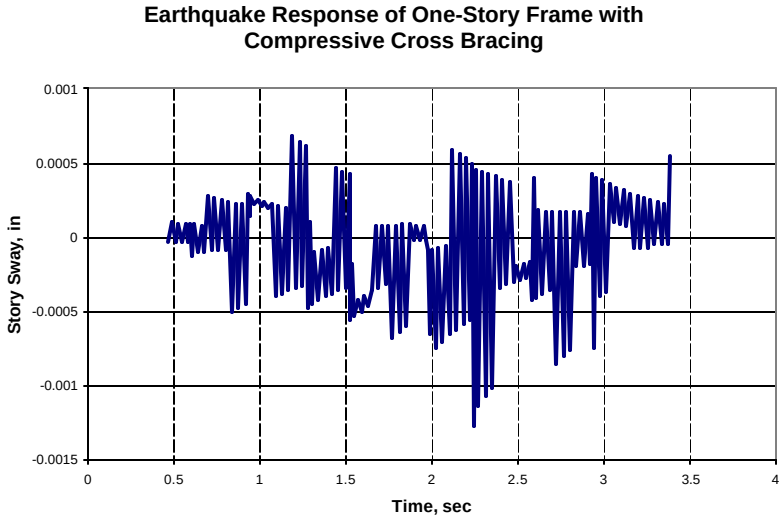

Figure 35: Sway of frame with compression induced cross-bracing

Table 10: Maximum sway values

	(in)	Time, sec
Positive Sway	0.000683	1.19
Negative Sway	-0.00127	2.24

Table 21 summarizes the maximum and minimum sway from the above graphs.

Table 21: Summary of maximum and minimum sway

	Positive Sway	Negative Sway
SS0	0.071369	-0.07258
SS1—Tensile	0.003189	-0.00709
SS1—Zero Force	0.001343	-0.00246
SS1--Compressive	0.001836	-0.00188
SSX—Tensile	0.000677	-0.00121
SSX—Zero Force	0.000686	-0.00126
SSX—Compressive	0.000683	-0.00127

From the above table and plots, the results indicate that induced tensile force does indeed reduce overall response frame sway due to earthquakes.

Two-Story Frame Analysis

For the two-story frame analysis, the procedure followed was the same as described previously for one-story frames. As before, a full modal analysis of a bare two-story frame was undertaken to establish baseline frequencies and responses. The frequencies from Modal Analysis by ANSYS are listed in table 22 on the following page. The corresponding mode shapes are shown in ensuing figure 36.

Table 22: Frequencies for bare two-story frame from modal analysis

Mode	Frequency
1	2.5026
2	6.9539
3	28.643
4	34.224
5	34.281
6	40.330
7	58.152
8	66.758
9	115.01
10	127.53
11	128.54
12	131.82
13	226.65
14	247.91
15	389.36

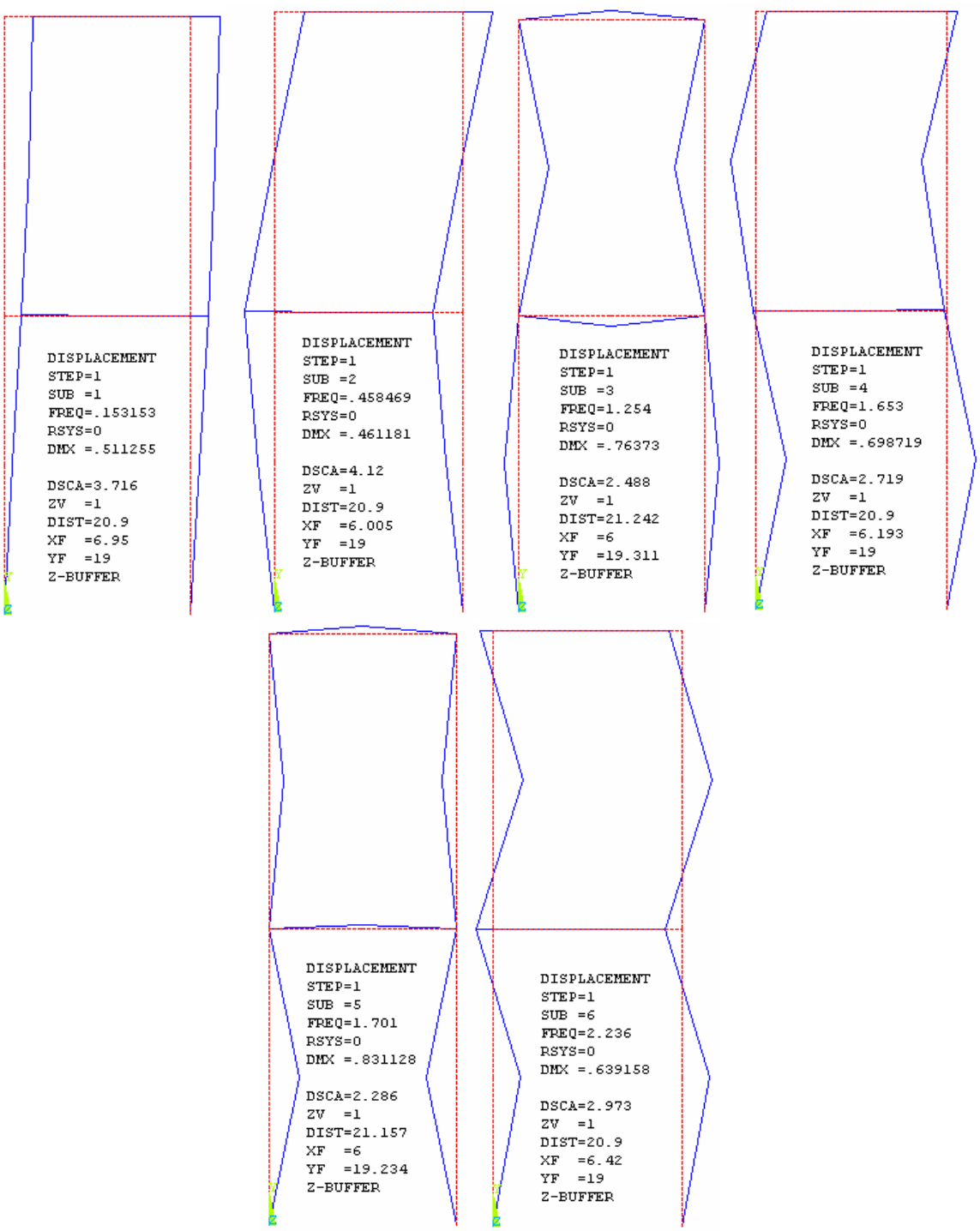

Figure 36: Mode shapes of two-story bare frames

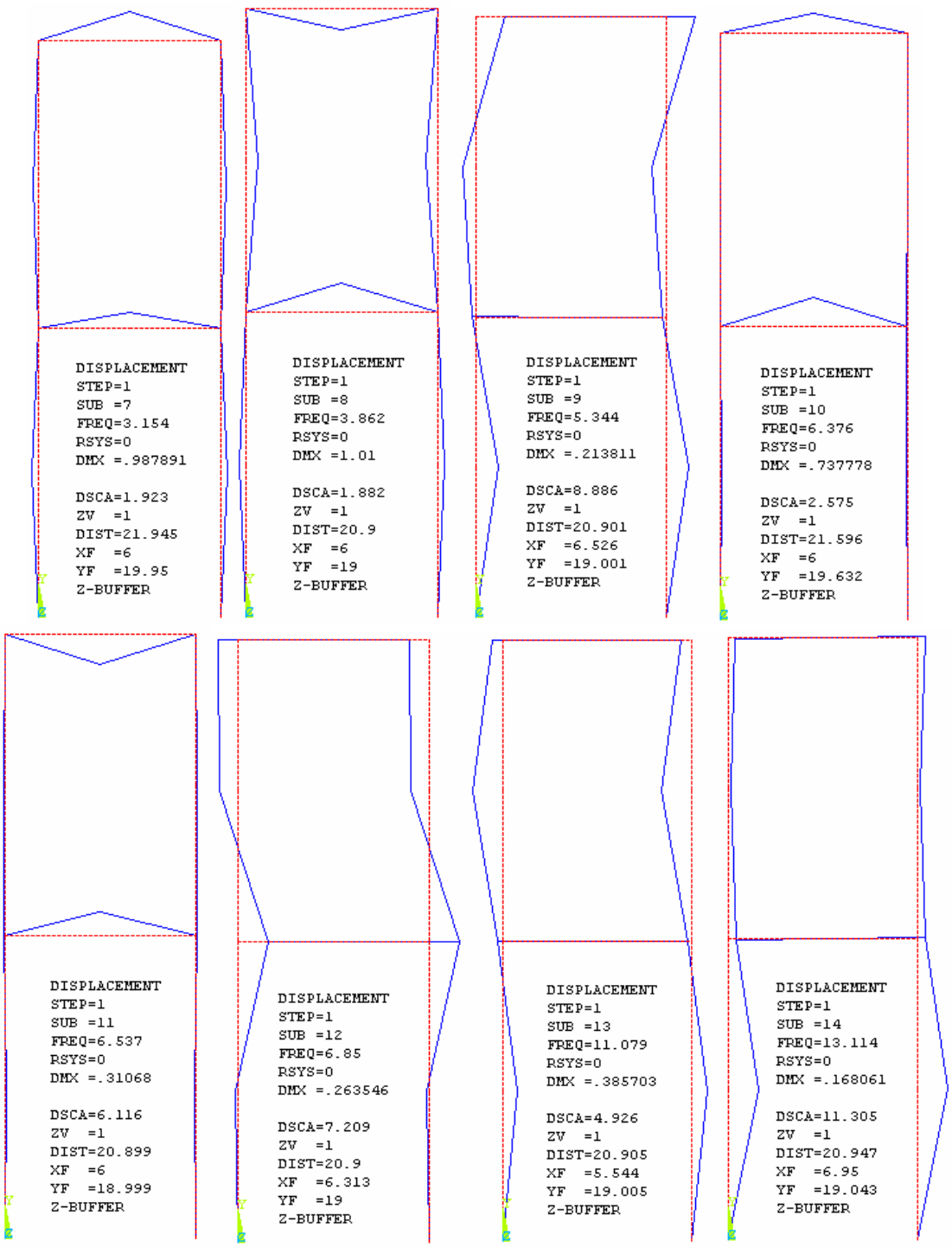

Figure 36—cont'd

Similar to the single-story frames, because the planar ANSYS model used fifteen degrees of freedom, fifteen frequencies and mode shapes were generated using the h-method. Unlike the single story frames, each mode shape is unique. Although some modes have similar shapes, such as mode shapes seven and ten, there are indeed subtle differences.

Two-Story Transient Analysis

As with the single story frames, a transient analysis of the two-story frames was conducted. Figure 37 shows the time earthquake displacement response of the unbraced two-story structure.

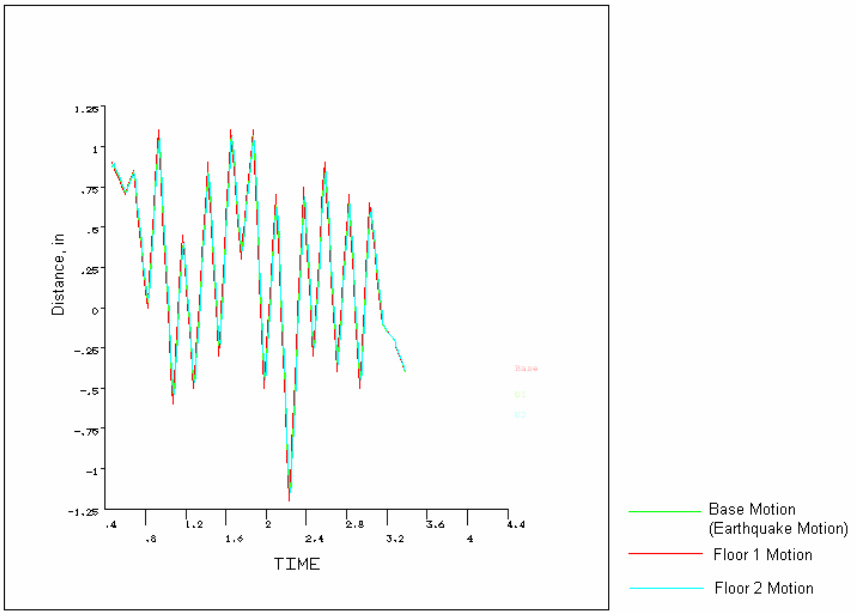

Figure 37: Earthquake displacement of bare two-story frame

From the response of the earthquake, the time history of story sway displacement of the structure was determined by subtracting each floor displacement from the base displacement. The resulting response is plotted in figure 38.

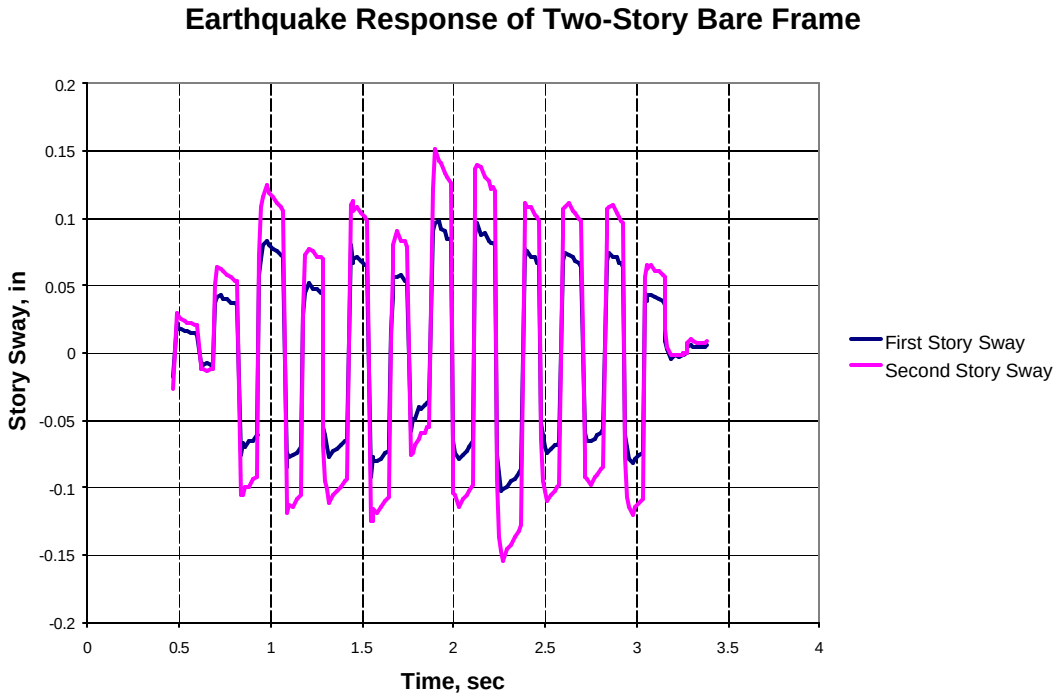

Figure 38: Sway for two-story bare frame

The absolute maximum sway is noted as -0.1546 inches in the top floor at 2.27 seconds. This value of maximum sway occurs 0.03 seconds after the maximum value of the unbraced single story frame.

The results of two-story frame analysis for different cases follow hereinafter.

Earthquake Response for TSUX (Pre-strain—Tensile): In the case of the frame with cross-braced second floor, a tensile pre-strain of 0.0000141 in/in is induced and response analysis due to El Centro earthquake, discussed earlier, is undertaken. Table 23 shows the frequency values based on modal analysis, and Figure 39 shows the first and second story sway response of the frame. Unfortunately, because the story sways are almost the same, the blue line, denoting the sway of the first floor, lies directly underneath the pink line, denoted the second story sway. The maximum positive and negative sway values are shown in Table 24.

Table 23: Frequency values based on modal analysis

Mode	Frequency
1	2.5505
2	27.852
3	33.054
4	34.083
5	38.319
6	57.778
7	66.455
8	112.28
9	125.86
10	126.73
11	128.42
12	225.81
13	247.18
14	344.41
15	389.08

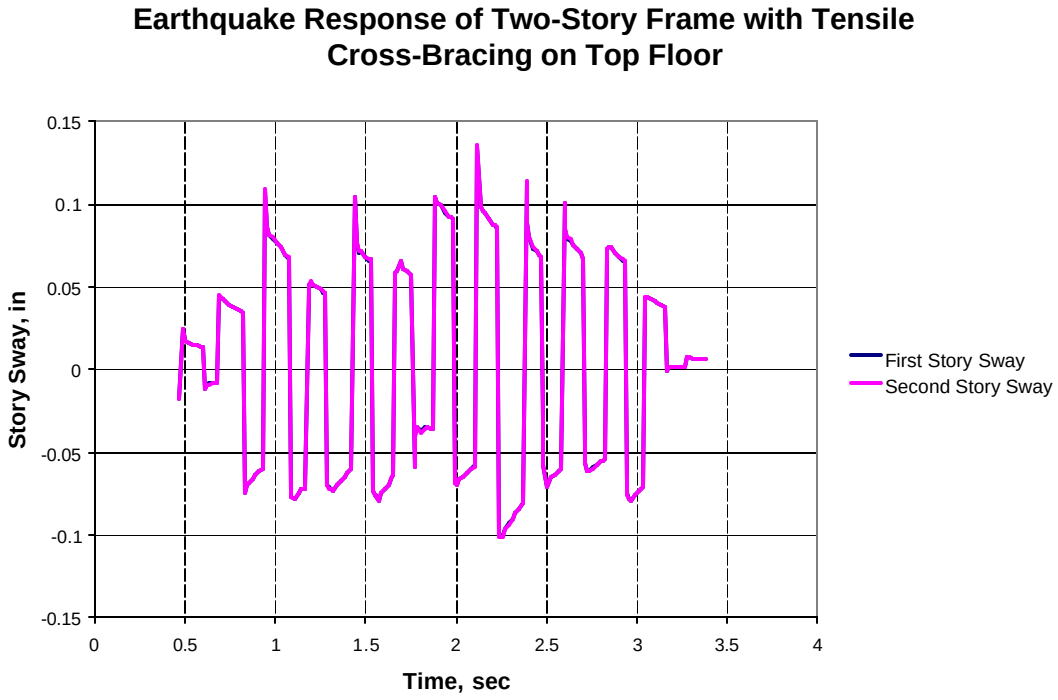

Figure 39: Sway of tensioned TSUX frame

Table 24: Maximum sway values

	First Story Sway, in	Time, sec	Second Story Sway, in	Time, sec
Positive Sway	0.134992	2.12	0.13225	2.12
Negative Sway	-0.100654	2.25	-0.100894	2.25

Earthquake Response for TSUX (Zero Pre-strain): In the case of the second floor cross-braced, no pre-strain and response analysis due to El Centro earthquake, as discussed earlier, is undertaken. Table 25 shows the frequency values based on modal analysis, and Figure 40 shows the story sway response of the frame. Unfortunately, because the story sways are almost the same, the blue line, denoting the sway of the first floor, lies directly underneath the pink line denoting the second story sway. The maximum positive and negative sway values are shown in Table 26.

Table 25: Frequency values based on modal analysis

Mode	Frequency
1	2.5510
2	28.543
3	33.440
4	34.283
5	38.884
6	58.154
7	66.761
8	113.05
9	126.07
10	127.54
11	128.54
12	226.14
13	247.56
14	344.43
15	389.08

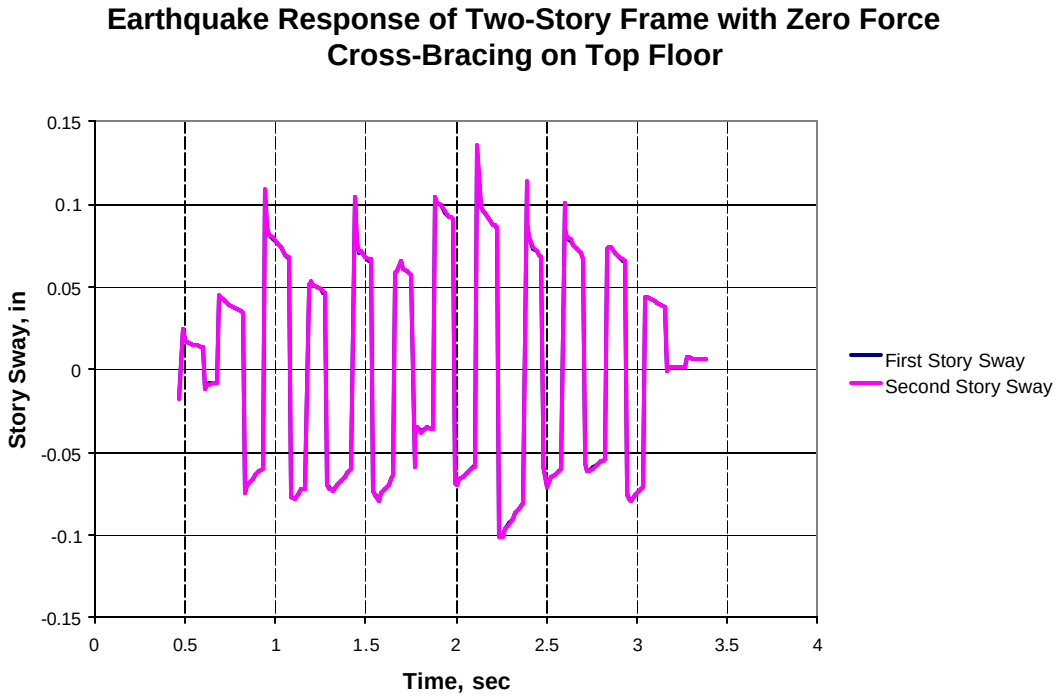

Figure 40: Sway for zero pre-strained TSUX frame

Table 26: Maximum sway values

	First Story Sway, in	Time, sec	Second Story Sway, in	Time, sec
Positive Sway	0.134918	2.12	0.135221	2.12
Negative Sway	-0.100654	2.25	-0.100904	0.47

Earthquake Response for TSUX (Pre-strain—Compressive): In the case of the second floor cross-braced, a compressive pre-strain of -0.0000141 in/in is induced and response analysis due to El Centro earthquake, as discussed earlier, is undertaken. Table 27 shows the frequency values based on modal analysis, and Figure 41 shows the story sway responses of the frame. Unfortunately, because the story sways are almost the same, the blue line, denoting the sway of the first floor, lies directly underneath the pink line, denoting the second story sway. The maximum positive and negative sway values are shown in Table 28.

Table 27: Frequency values based on modal analysis

Mode	Frequency
1	2.5515
2	29.174
3	33.743
4	34.515
5	39.508
6	58.525
7	67.066
8	113.80
9	126.30
10	128.04
11	128.96
12	226.47
13	247.94
14	344.45
15	389.72

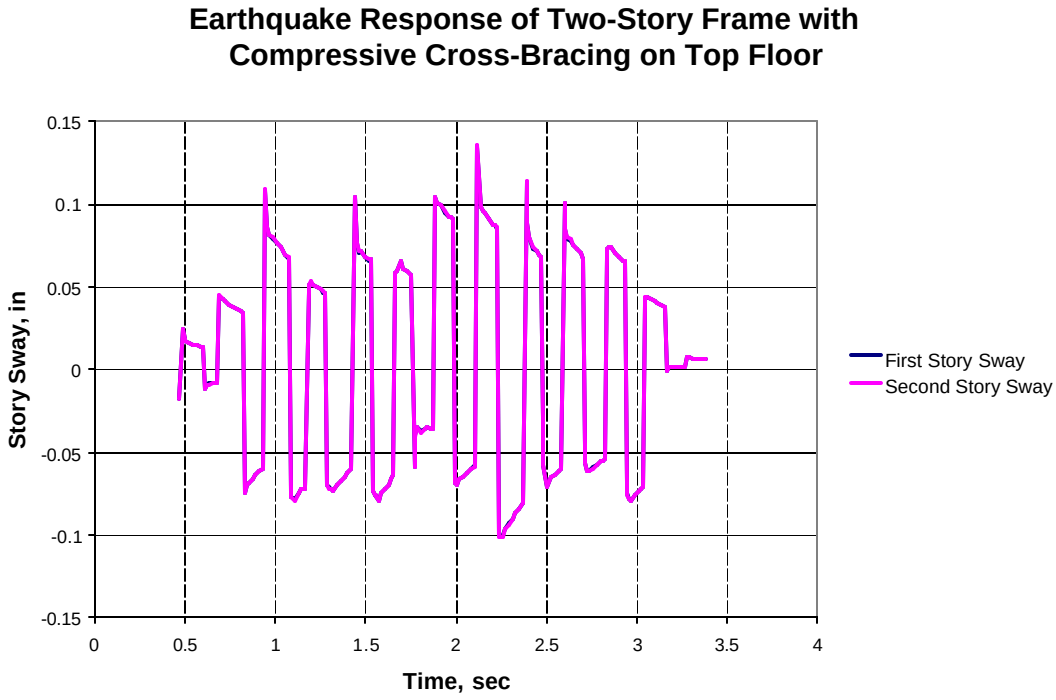

Figure 41: Sway of compressive TSUX frame

Table 28: Maximum sway values

	First Story Sway, in	Time, sec	Second Story Sway, in	Time, sec
Positive Sway	0.134914	2.12	0.135217	2.12
Negative Sway	-0.100654	2.25	-0.100904	2.25

Earthquake Response for TSLX (Pre-strain—Tensile): In the case of the first floor cross-braced, a tensile pre-strain of 0.0000141 in/in is induced and response analysis due to El Centro earthquake, as discussed earlier, is undertaken. Table 29 shows the frequency values based on modal analysis, and Figure 42 shows the story sway responses of the frame. The maximum positive and negative sway values are shown in Table 30.

Table 29: Frequency values based on modal analysis

Mode	Frequency
1	4.3692
2	28.251
3	33.303
4	33.580
5	36.269
6	58.049
7	66.506
8	114.50
9	125.20
10	127.02
11	127.95
12	225.94
13	245.89
14	278.47
15	389.06

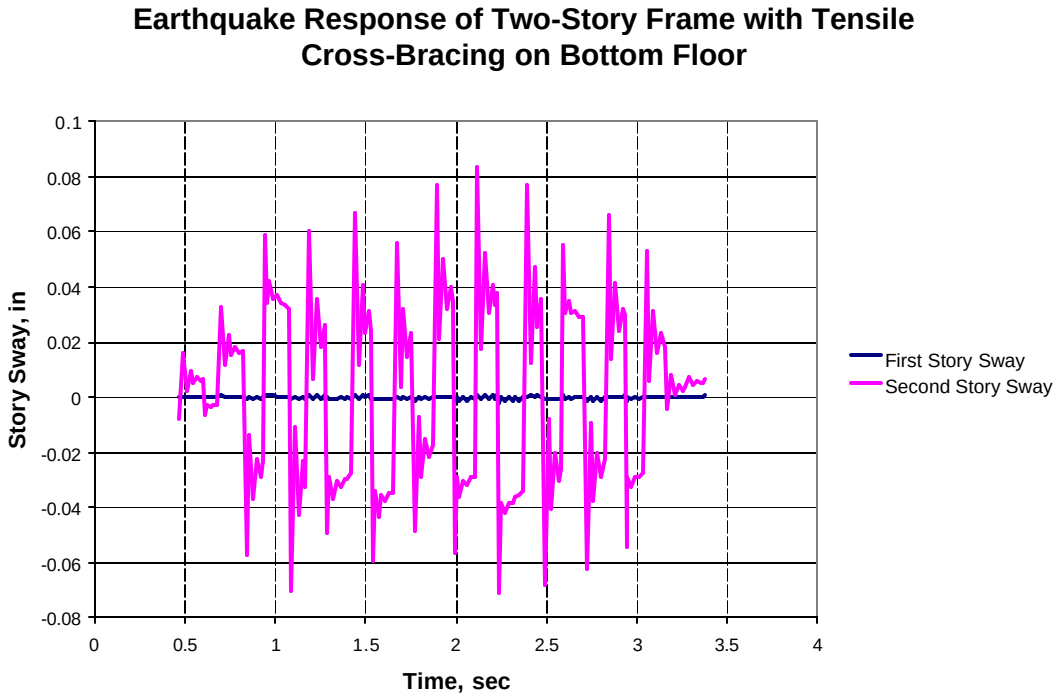

Figure 42: Sway of tensioned TSLX frame

Table 30: Maximum sway values

	First Story Sway, in	Time, sec	Second Story Sway, in	Time, sec
Positive Sway	0.001166	2.12	0.083181	2.12
Negative Sway	-0.0019	2.24	-0.07084	2.24

Earthquake Response for TSLX (Zero Pre-strain): In the case of the cross-braced first floor, no pre-strain is induced and response analysis due to El Centro earthquake, as discussed earlier, is undertaken. Table 31 shows the frequency values based on modal analysis, and Figure 43 shows the story sways response of the frame. The maximum positive and negative sway values are shown in Table 32.

Table 31: Frequency values based on modal analysis

Mode	Frequency
1	4.3698
2	28.543
3	34.108
4	34.282
5	36.449
6	58.159
7	66.759
8	114.93
9	125.91
10	127.53
11	128.55
12	226.11
13	246.10
14	278.49
15	389.36

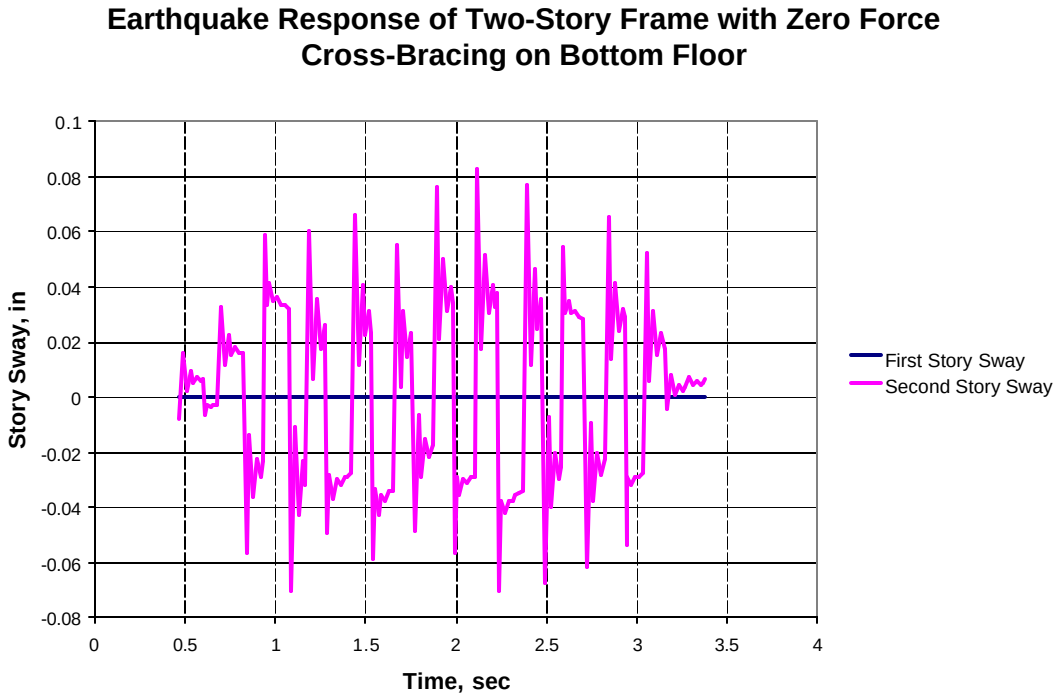

Figure 43: Sway of zero pre-strained TSLX frame

Table 32: Maximum sway values

	First Story Sway, in	Time, sec	Second Story Sway, in	Time, sec
Positive Sway	0.000068	1.19	0.082455	2.12
Negative Sway	-0.00012	2.24	-0.07039	2.24

Earthquake Response for TSLX (Pre-strain—Compressive): In the case of the first floor cross-braced, a compressive pre-strain of -0.0000141 in/in is induced and response analysis due to El Centro earthquake, as discussed earlier, is undertaken. Table 33 shows the frequency values based on modal analysis, and Figure 44 shows the story sway responses of the frame. The maximum positive and negative sway values are shown in Table 34.

Table 33: Frequency values based on modal analysis

Mode	Frequency
1	4.3704
2	28.770
3	34.747
4	35.017
5	36.766
6	58.261
7	67.015
8	115.30
9	126.66
10	127.65
11	129.54
12	226.28
13	246.32
14	278.52
15	389.67

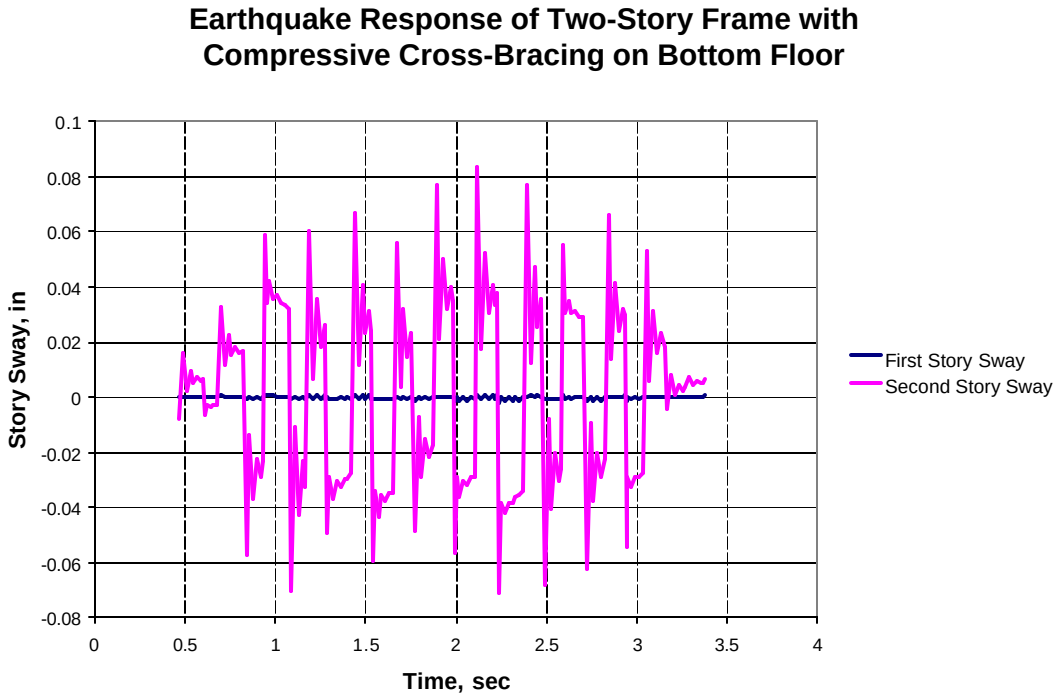

Figure 44: Sway for compressive TSLX frame

Table 34: Maximum sway values

	First Story Sway, in	Time, sec	Second Story Sway, in	Time, sec
Positive Sway	0.001158	2.12	1.578456	2.23
Negative Sway	-0.00191	2.24	-0.07084	2.24

Earthquake Response for TSL1U1-S (Pre-strain—Tensile): In the case of the both floors singly braced in the same orientation, a tensile pre-strain of 0.0000141 in/in is induced and response analysis due to El Centro earthquake, as discussed earlier, is undertaken. Table 35 shows the frequency values based on modal analysis, and Figure 45 shows the story sways response of the frame. The maximum positive and negative sway values are shown in Table 36.

Table 35: Frequency values based on modal analysis

Mode	Frequency
1	28.543
2	29.415
3	33.886
4	34.281
5	49.930
6	58.153
7	66.758
8	98.624
9	116.76
10	127.52
11	128.54
12	141.91
13	226.69
14	247.95
15	389.36

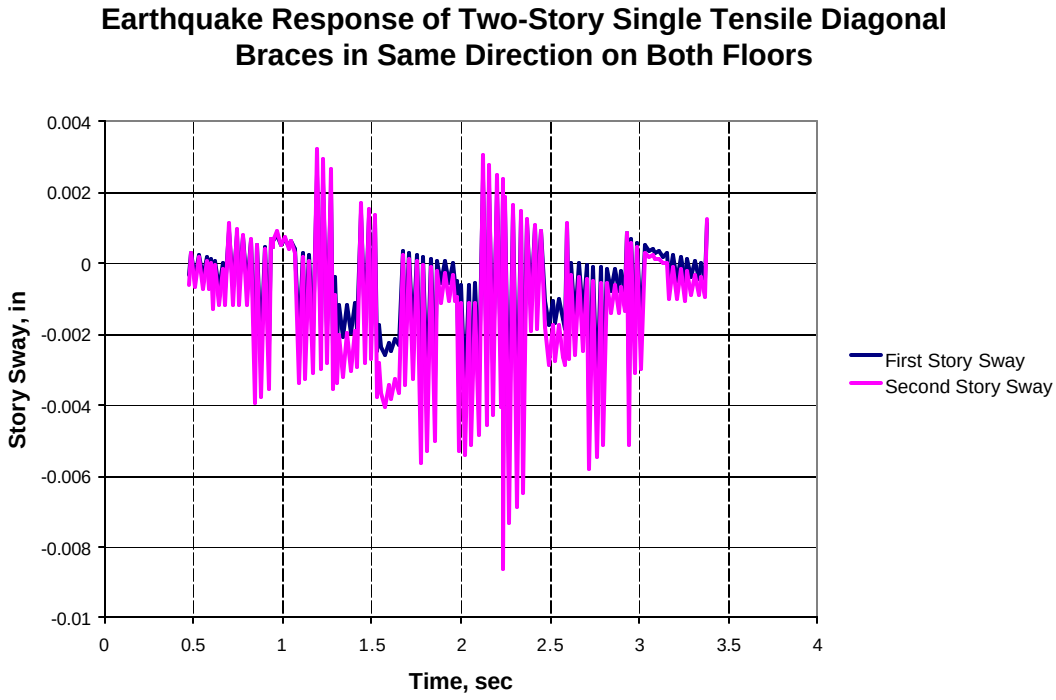

Figure 45: Sway of tensioned TSL1U1 -S frame

Table 36: Maximum sway values

	First Story Sway, in	Time, sec	Second Story Sway, in	Time, sec
Positive Sway	0.00247	1.19	0.003242	1.19
Negative Sway	-0.00583	2.24	-0.00862	2.24

Earthquake Response for TSL1U1-S (Zero Pre-strain): In the case of the both floors singly braced in the same orientation, no pre-strain is induced and response analysis due to El Centro earthquake, as discussed earlier, is undertaken. Table 37 shows the frequency values based on modal analysis, and Figure 46 shows the story sways response of the frame. The maximum positive and negative sway values are shown in Table 38.

Table 37: Frequency values based on modal analysis

Mode	Frequency
1	28.543
2	29.415
3	33.886
4	34.282
5	49.930
6	58.153
7	66.758
8	98.624
9	116.76
10	127.53
11	128.54
12	141.91
13	226.69
14	247.95
15	389.36

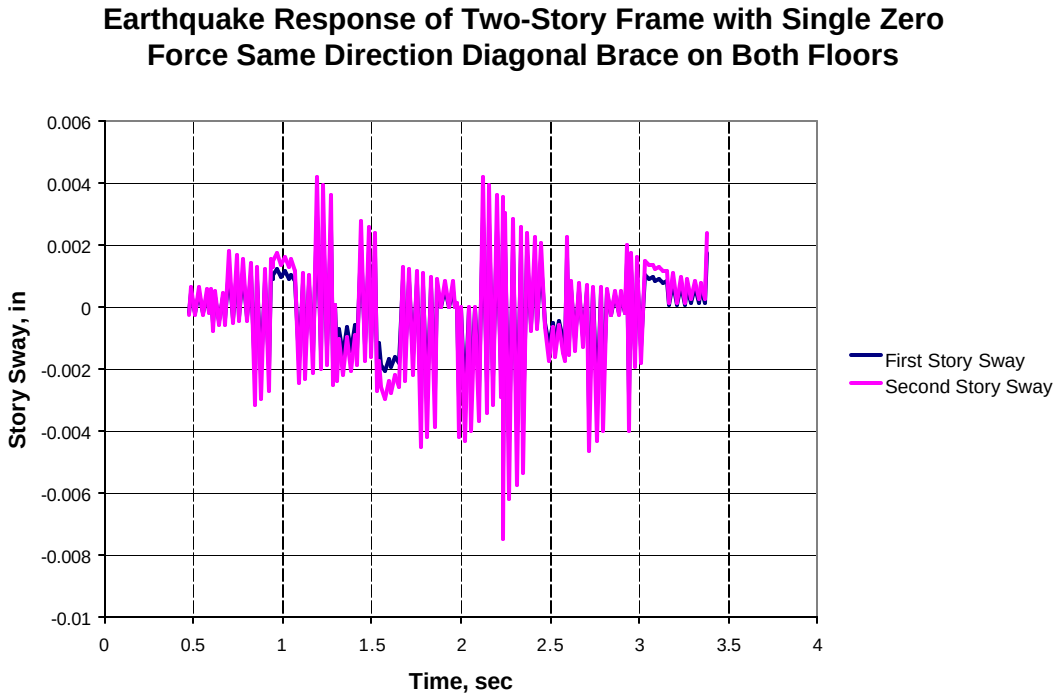

Figure 46: Sway of zero pre-strained TSL1U1 -S frame

Table 38: Maximum sway values

	First Story Sway, in	Time, sec	Second Story Sway, in	Time, sec
Positive Sway	0.002963	1.19	0.004229	1.19
Negative Sway	-0.00525	2.24	-0.00767	2.24

Earthquake Response for TSL1U1-S (Pre-strain—Compressive): In the case of the both floors singly braced in the same orientation, a compressive pre-strain of -0.0000141 in/in is induced and response analysis due to El Centro earthquake, as discussed earlier, is undertaken. Table 39 shows the frequency values based on modal analysis, and Figure 47 shows the story sway responses of the frame. The maximum positive and negative sway values are shown in Table 40.

Table 39: Frequency based on modal analysis

Mode	Frequency
1	28.543
2	29.415
3	33.886
4	34.282
5	49.930
6	58.153
7	66.758
8	98.624
9	116.76
10	127.53
11	128.54
12	141.91
13	226.69
14	247.95
15	389.36

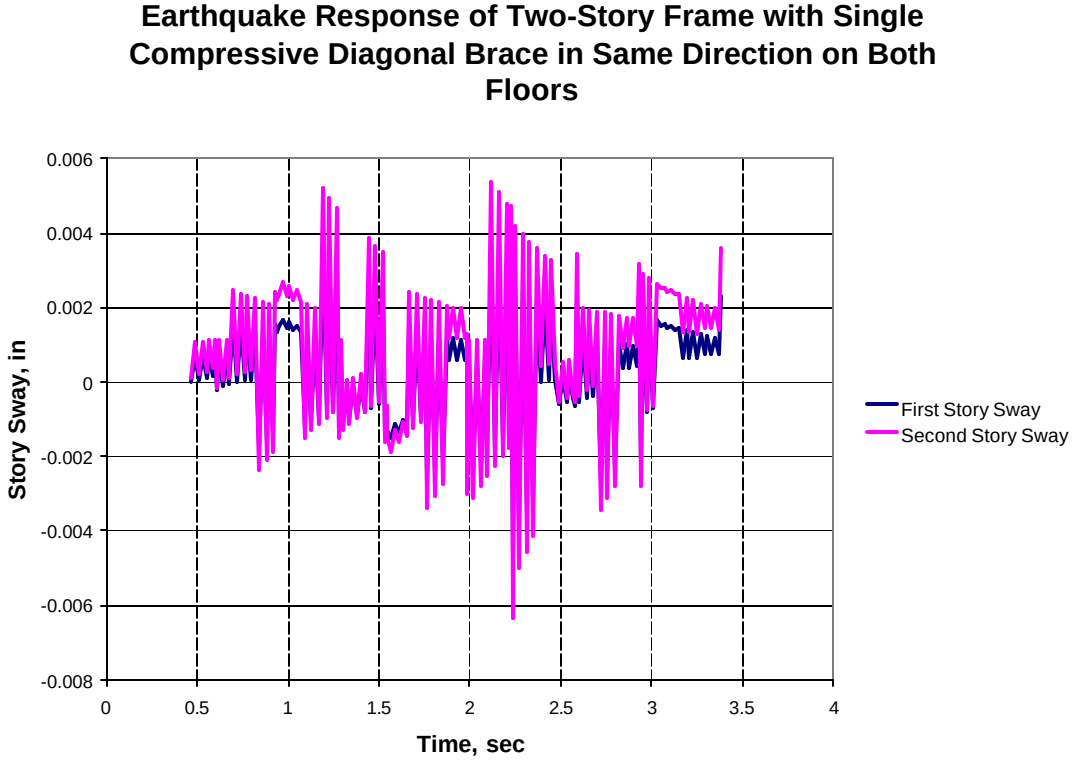

Figure 47: Sway of compressive TSL1U1-S frame

Table 40: Maximum sway values

	First Story Sway, in	Time, sec	Second Story Sway, in	Time, sec
Positive Sway	0.003506	2.12	0.005371	2.12
Negative Sway	-0.00467	2.24	-0.00632	2.24

Earthquake Response for TSL1U1-O (Pre-strain—Tensile): In the case of the both floors singly braced with opposite orientation, a tensile pre-strain of 0.0000141 in/in is induced and response analysis due to El Centro earthquake, as discussed earlier, is undertaken. Table 41 shows the frequency values based on modal analysis, and Figure 48 shows the story sway responses of the frame. The maximum positive and negative sway values are shown in Table 42.

Table 41: Frequency values based on modal analysis

Mode	Frequency
1	28.543
2	29.483
3	33.885
4	34.281
5	50.138
6	58.151
7	66.758
8	98.196
9	116.73
10	127.53
11	128.54
12	141.66
13	226.69
14	247.96
15	389.36

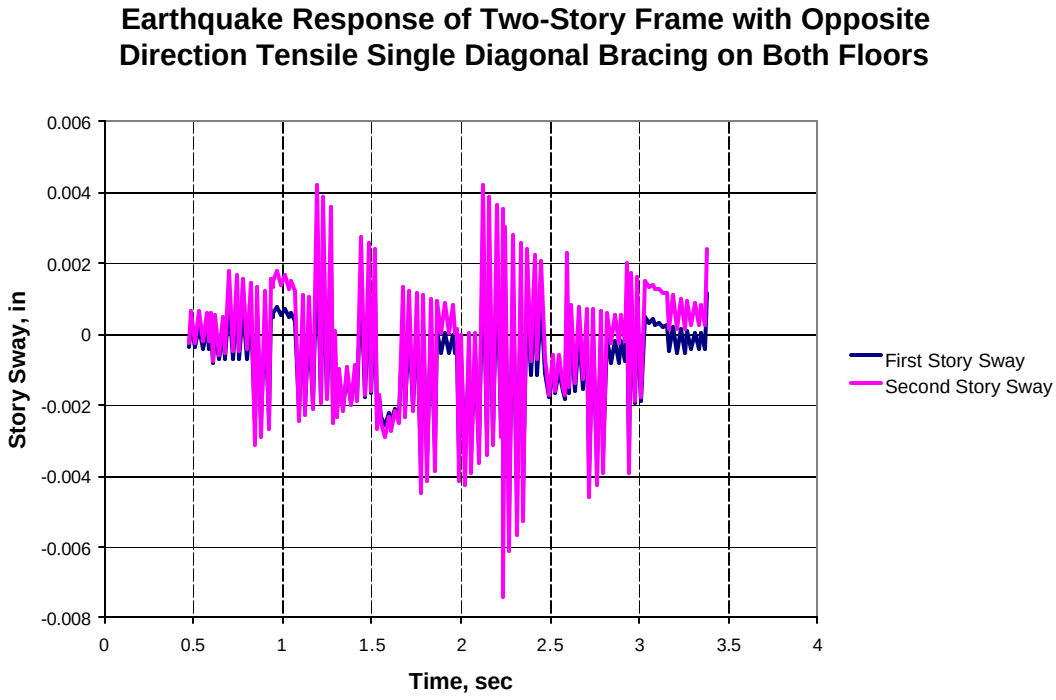

Figure 48: Sway of tensioned TSL1U1 -O frame

Table 42: Maximum sway values

	First Story Sway, in	Time, sec	Second Story Sway, in	Time, sec
Positive Sway	0.002454	1.19	0.004193	1.19
Negative Sway	-0.0058	2.24	-0.00741	2.24

Earthquake Response for TSL1U1-O (Zero Pre-strain): In the case of the both floors singly braced with opposite orientation, no pre-strain is induced and response analysis due to El Centro earthquake, as discussed earlier, is undertaken. Table 43 shows the frequency values based on modal analysis, and Figure 49 shows the story sway responses of the frame. The maximum positive and negative sway values are shown in Table 44.

Table 43: Frequency values based on modal analysis

Mode	Frequency
1	28.543
2	29.483
3	33.886
4	34.281
5	50.138
6	58.152
7	66.758
8	98.196
9	116.73
10	127.53
11	128.54
12	141.66
13	226.69
14	247.96
15	389.36

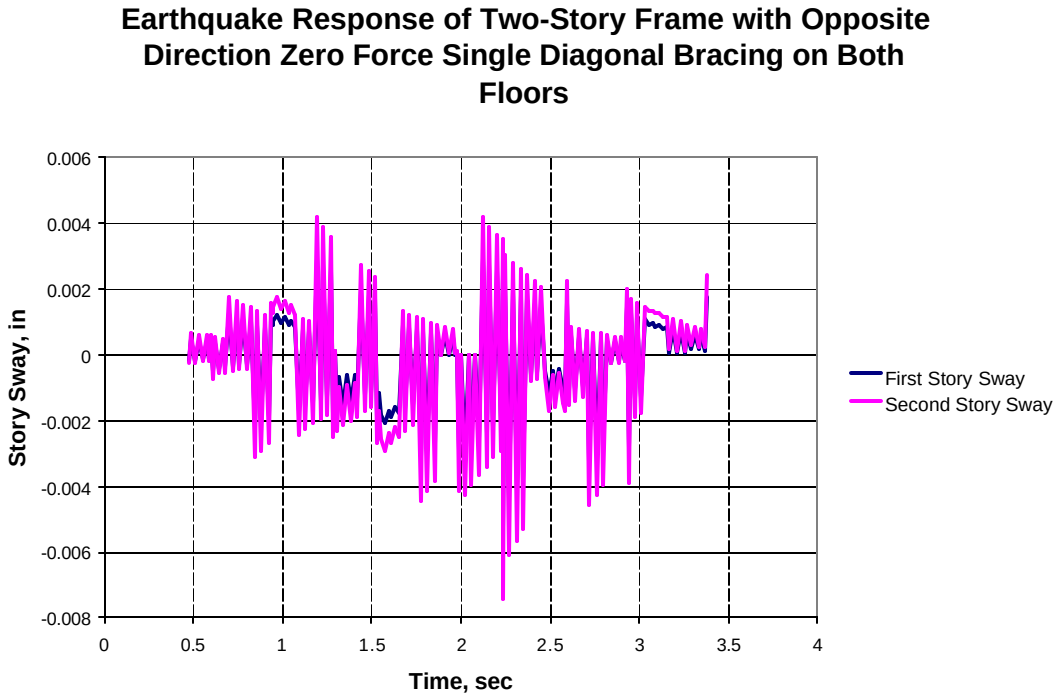

Figure 49: Sway of zero pre-strained TSL1U1 -O frame

Table 44: Maximum sway values

	First Story Sway, in	Time, sec	Second Story Sway, in	Time, sec
Positive Sway	0.002947	1.19	0.004193	1.19
Negative Sway	-0.00522	2.24	-0.00741	2.24

Earthquake Response for TSUL1U1-O (Pre-strain—Compressive): In the case of the both floors singly braced with opposite orientation, a compressive pre-strain of -0.0000141 in/in is induced and response analysis due to El Centro earthquake, as discussed earlier, is undertaken. Table 45 shows the frequency values based on modal analysis, and Figure 50 shows the story sway responses of the frame. The maximum positive and negative sway values are shown in Table 46.

Table 45: Frequency values based on modal analysis

Mode	Frequency
1	28.543
2	29.483
3	33.886
4	34.282
5	50.139
6	58.152
7	66.759
8	98.197
9	116.73
10	127.53
11	128.54
12	141.66
13	226.69
14	247.96
15	389.36

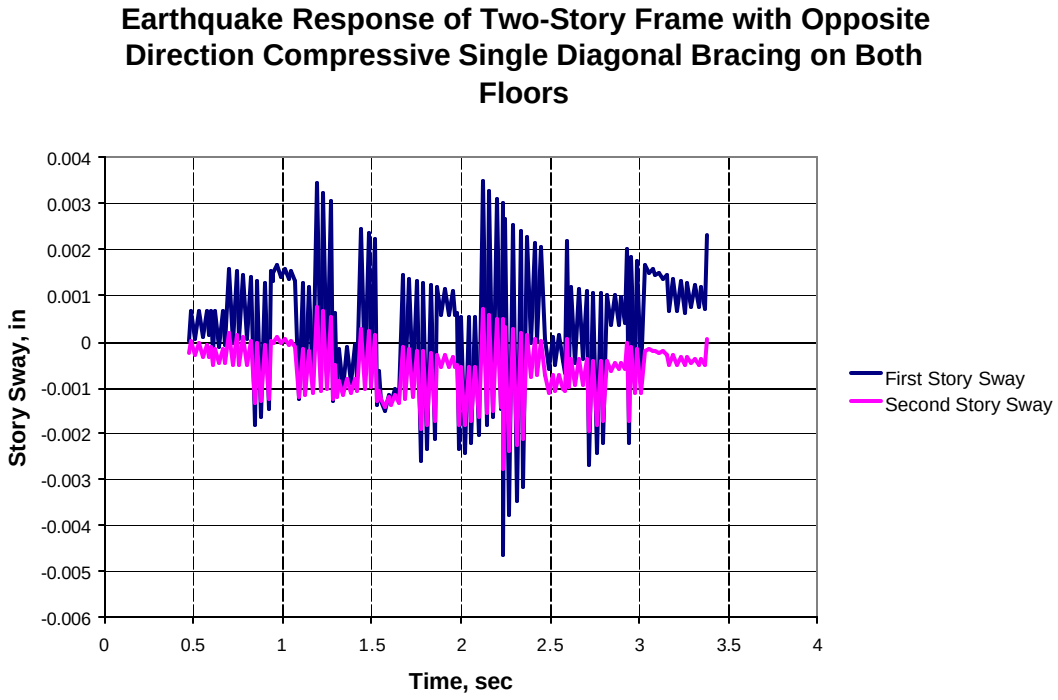

Figure 50: Sway of compressive TSL1U1-O frame

Table 46: Maximum sway values

	First Story Sway, in	Time, sec	Second Story Sway, in	Time, sec
Positive Sway	0.003487	2.12	0.000754	1.19
Negative Sway	-0.00465	2.24	-0.00276	2.24

Earthquake Response for TSLXUX (Pre-strain—Tensile): In the case of the both floors cross-braced, and induced tensile pre-strain of 0.0000141 in/in, the response analysis due to El Centro earthquake, as discussed earlier, is undertaken. Table 47 shows the frequency values based on modal analysis, and Figure 51 shows the story sway responses of the frame. The maximum positive and negative sway values are shown in Table 48.

Table 47: Frequency values based on modal analysis

Mode	Frequency
1	28.429
2	31.760
3	34.172
4	34.217
5	58.093
6	63.743
7	66.691
8	111.39
9	120.88
10	127.42
11	128.41
12	169.55
13	226.68
14	247.94
15	389.29

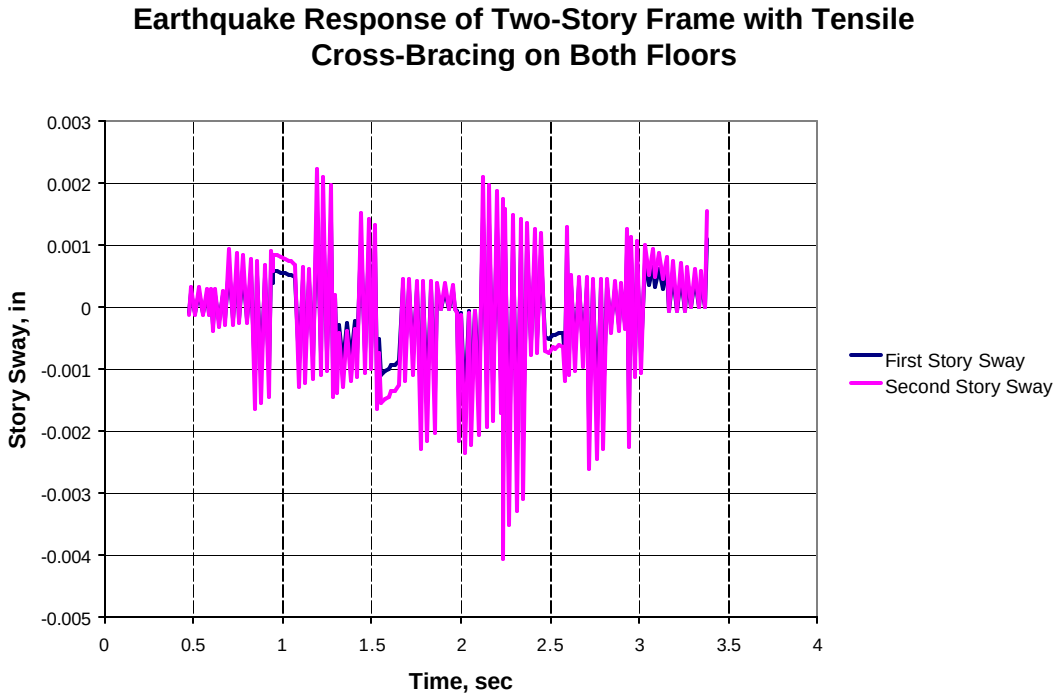

Figure 51: Sway of tensioned TSLXUX frame

Table 48: Maximum sway values

	First Story Sway, in	Time, sec	Second Story Sway, in	Time, sec
Positive Sway	0.001564	1.19	0.002247	1.19
Negative Sway	-0.00282	2.24	-0.00406	2.24

Earthquake Response for TSLXUX (Zero Pre-strain): In the case of the both floors cross-braced, and no pre-strain is induced, response analysis due to El Centro earthquake, as discussed earlier, is undertaken. Table 49 shows the frequency values based on modal analysis, and Figure 52 shows the story sway responses of the frame. The maximum positive and negative sway values are shown in Table 50.

Table 49: Frequency values based on modal analysis

Mode	Frequency
1	28.543
2	31.853
3	34.282
4	34.322
5	58.153
6	63.776
7	66.759
8	111.50
9	121.00
10	127.53
11	128.54
12	169.59
13	226.74
14	248.01
15	389.36

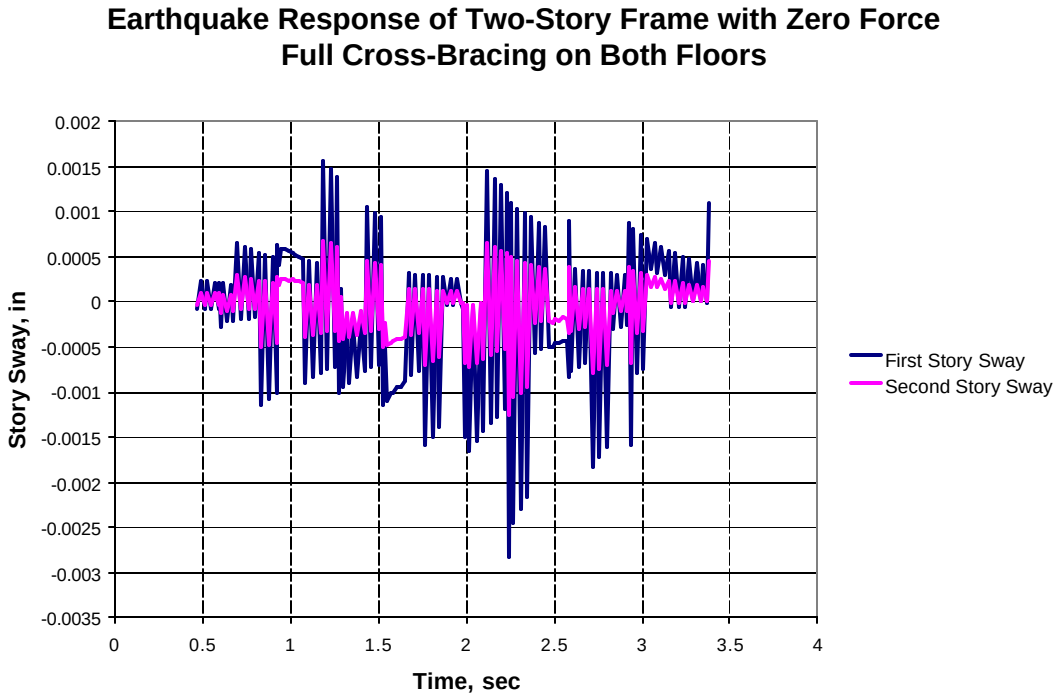

Figure 52: Sway of zero pre-strained TSLXUX frame

Table 50: Maximum sway values

	First Story Sway, in	Time, sec	Second Story Sway, in	Time, sec
Positive Sway	0.001557	1.19	0.000686	1.19
Negative Sway	-0.00283	2.24	-0.00124	2.24

Earthquake Response for TSLXUX (Pre-strain—Compressive): In the case of the both floors cross-braced with an area of 0.009in^2, and induced compressive pre-strain of -0.0000141 in/in, the response analysis due to El Centro earthquake, discussed earlier, is undertaken. Table 51 shows the frequency values based on modal analysis, and Figure 53 shows the story sway responses of the frame. The maximum positive and negative sway values are shown in Table 52.

Table 51: Frequency values based on modal analysis

Mode	Frequency
1	28.656
2	31.945
3	34.391
4	34.427
5	58.212
6	63.810
7	66.827
8	111.61
9	121.11
10	127.65
11	128.67
12	169.63
13	226.81
14	248.07
15	389.44

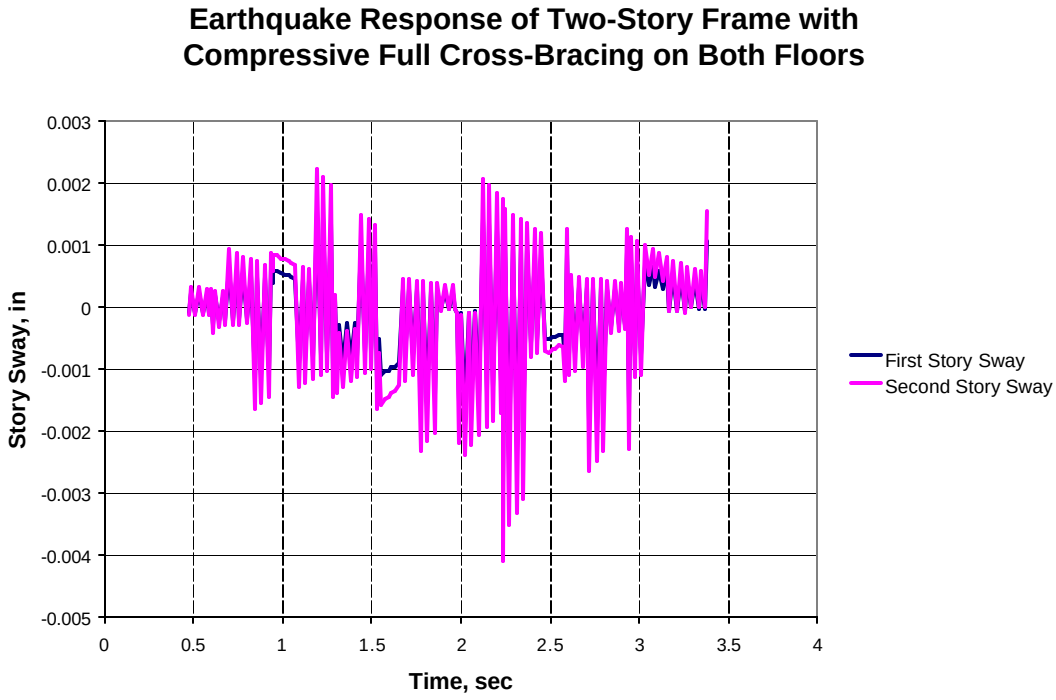

Figure 53: Sway of compressive TSLXUX frame

Table 52: Maximum sway values

	First Story Sway, in	Time, sec	Second Story Sway, in	Time, sec
Positive Sway	0.00155	1.19	0.00224	1.19
Negative Sway	-0.00283	2.24	-0.00407	2.24

CHAPTER IV

EXPERIMENTAL PROCEDURE

To validate the ANSYS predictions and to study the effectiveness of using braces with the preinduced forces for attenuating the of effect dynamic exciting forces like an earthquake, an experimental program was undertaken using a Quanser Shake Table II. The driving and data acquisition computer and shake table set-up is shown in figure 54. Quanser accelerometers were used to measure the floor level motions. The single and double story frames described in Chapter III were used in the experimental study.

Figure 54: Complete testing set-up

Experimental Set-up

The unbraced frames and braced frames with and without pre-strain considered in the tests are shown in figure 55. Thus, the bracing combinations considered in the test were – a one-story bare and cross-braced frame, a two-story frame with only the bottom story cross-braced, and a two-story frame with both stories cross-braced. In the case of braced frames, the structures were tested with no pre-strain and with pre-strain in the bracings.

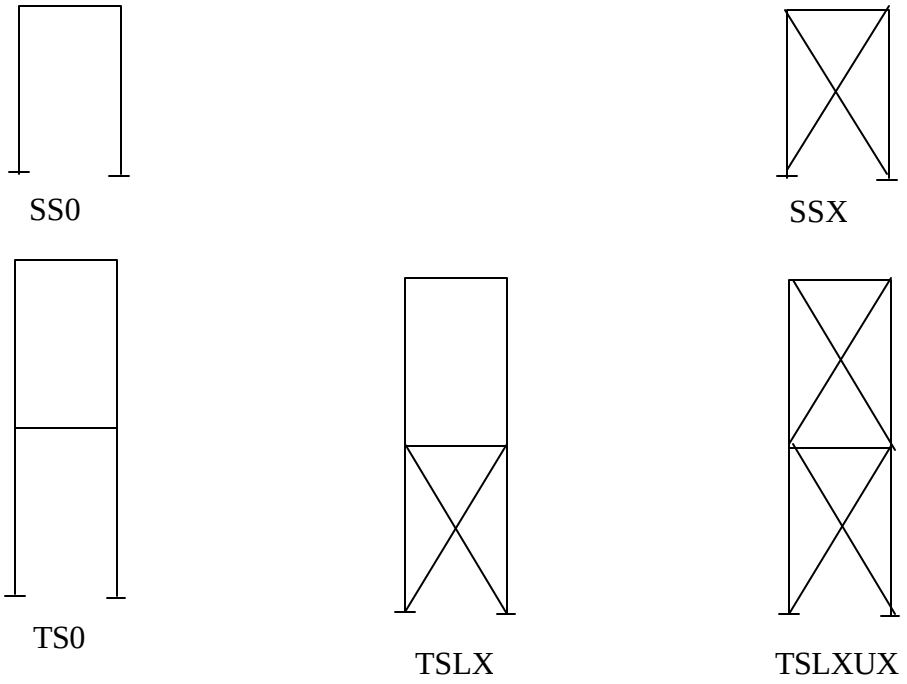

Figure 55: Frame configuration considered for experimental tests

Standard picture hanging wire strand used as bracing were tied and glued to eye-bolts and secured with wing nuts. A view of the connection is shown in figure 56. By turning the wing nuts, the induced tension on the bracing could be varied. The resulting tensile force in the bracing was obtained by determining the fundamental natural frequency of vibration of an individual brace. The procedure used consisted of plucking

the tension bracing and determining its natural frequency with a strobe light source which allowed changing of its flash rate. In the test, the frequency of the strobe light source was set at 50 Hz and the tension in the braces was changed by turning the wing nuts until the plucked brace appeared stationary. At this stage, the natural frequency of the brace was also 50 Hz. A view of the set-up used is shown in figure 57.

Figure 56: Bracing connection

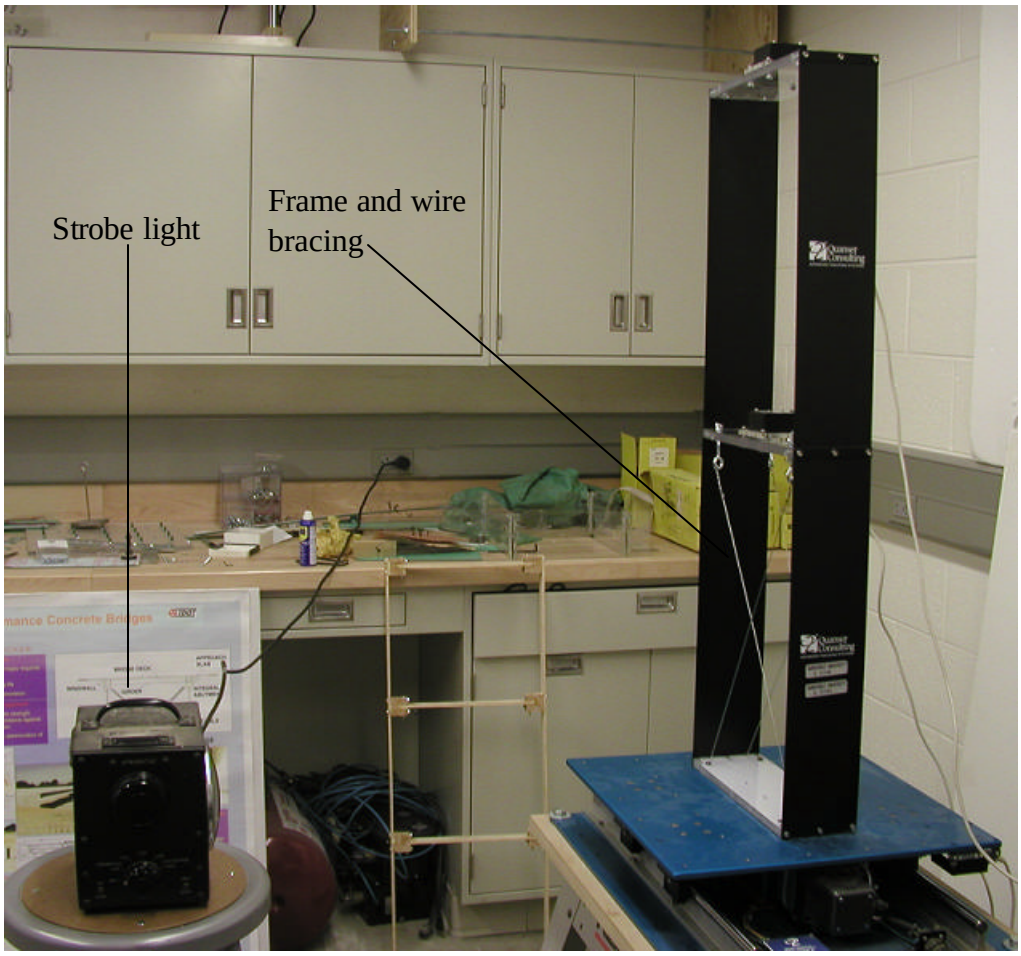

Figure 57: Strobe light set-up

Based on this frequency, the following equation (Serway 1998) can be used to compute the corresponding tension in the bracing.

$$f = \frac{1}{2L}\sqrt{\frac{TL}{m}} \quad ? \quad T = 2mLf^2 \tag{5}$$

With 1.366×10^{-4} lb·sec^2/ft as the unit mass of the brace, the tension in the brace for f = 50 Hz was found to be 1.366 lb. In other words, all pre-strained braces have pre-tensions of the same magnitude.

The details of the test procedure using the shake table are given in Appendix A. The following section contains the data collected from the Shake Table Experiments.

Natural Frequencies

The measured fundamental natural frequency for each frame found by sweeping with sinusoidal base excitation is shown in Table 53.

Table 53: Natural frequencies of experimental frame configurations

	Natural Frequency, Hz
SS0	3.9
SSX—Tensile	9.4
SSX—Zero Force	9.0
TS0	2.2, 6.2
TSLX—Tensile	4.0
TSLX—Zero Force	3.6
TSLXUX—Tensile	>10.0
TSLXUX—Zero Force	6.9

The natural frequency of the frames increased significantly when braced. Inducing tension in the braces increases the frequency further.

Earthquake Response

As mentioned before, the shake table was driven by El Centro earthquake excitation. The excitation induced in the shake table could be measured with an accelerometer mounted on it. In addition, two additional accelerometers were installed at the floor levels to measure acceleration response of the floors. The acceleration versus time plots are shown in figures 58-59 for table accelerations and the corresponding response due to El Centro earthquake input of the one-story frames.

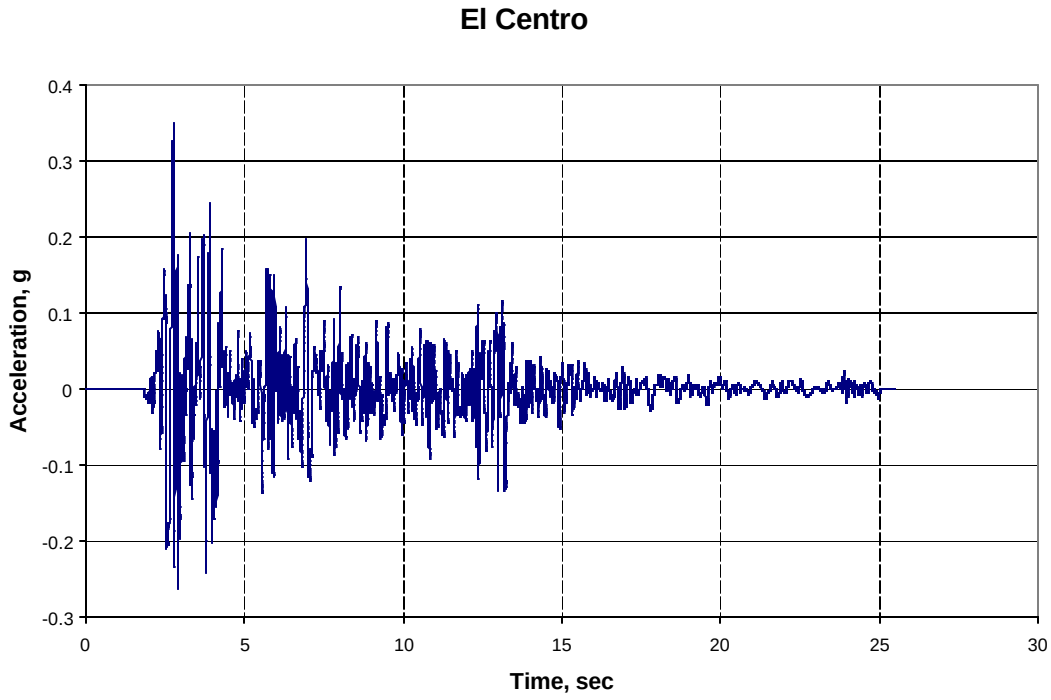

Figure 58: El Centro ground acceleration

The data for El Centro earthquake shown in figure 58 is based on the input data file for the same earthquake available in the shake table driving software WinCon. It is to be noted that this represents only a part of the record. The full El Centro earthquake record is reported in literature for the duration of 54.6 seconds, whereas the plot shown in figure 58 covers the duration of 23.59 seconds, representing the segment which will cause the most damage to the structure.

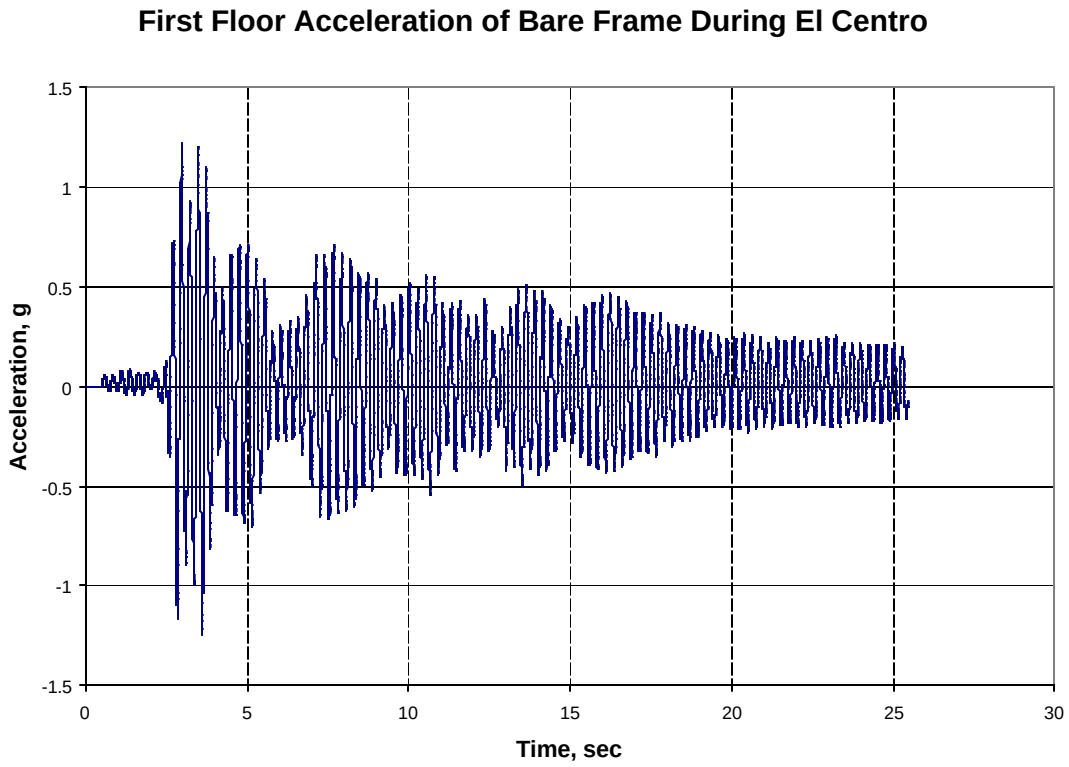

Figure 59: Bare frame first floor acceleration

Figures 60-61 show the acceleration response for the one-story cross-braced frames with zero pre-strain and a tensile pre-strain, respectively. The zero pre-strain has a higher overall acceleration.

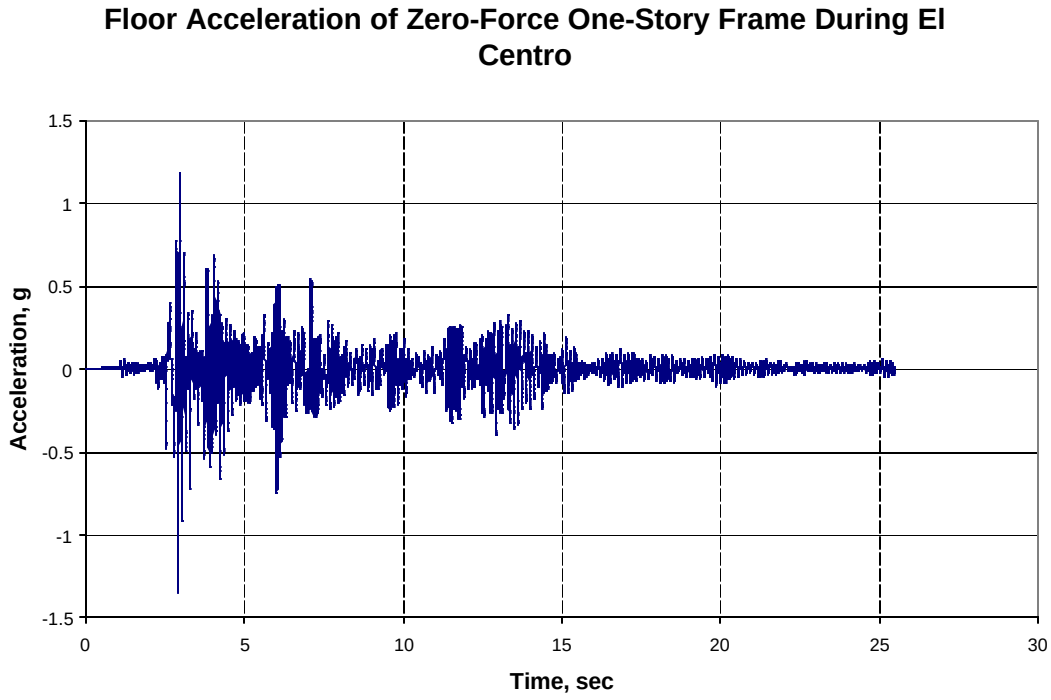

Figure 60: Frame acceleration with zero force bracing

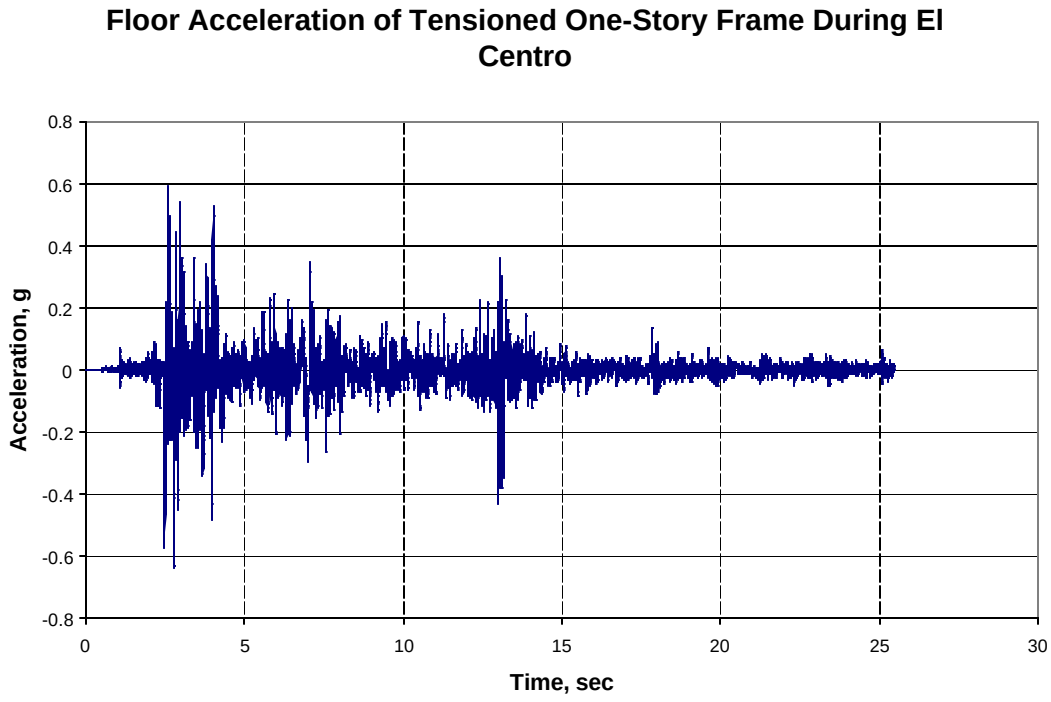

Figure 61: Frame acceleration with tensioned bracing

Maximum acceleration data from the one-story tests and the time it occurred are shown in tables 54 and 55 respectively. The times of occurrence of maximum and minimum acceleration are fairly consistent, but do vary slightly.

Table 54: Maximum accelerations of one-story frame

	Positive Acceleration, g	Negative Acceleration, g
Table	0.348082	-0.261714
No bracing	1.226956	-1.24405
Zero-force bracing	1.186447	-1.34416
Tensioned bracing	0.590892	-0.63729

Table 55: Time of maximum accelerations of one-story frame

	Time of Positive Acceleration, sec	Time of Negative Acceleration, sec
Table	2.763416	2.901437
No bracing	2.964459	3.60956
Zero-force bracing	2.982464	2.923454
Tensioned bracing	2.616405	2.784429

The ensuing figures and tables detail the data collected from the two-story frames.

Earthquake Response for TS0: This case corresponds to the two-story unbraced frame. In response to El Centro excitation, figure 62 shows the data collected from the accelerometer placed on the first floor. Table 56 shows the corresponding maximums and the times these maxima occur. Likewise, Figure 63 shows the data collected from the accelerometer placed on the second floor; and Table 57 shows the corresponding maximums and the time these maxima occur.

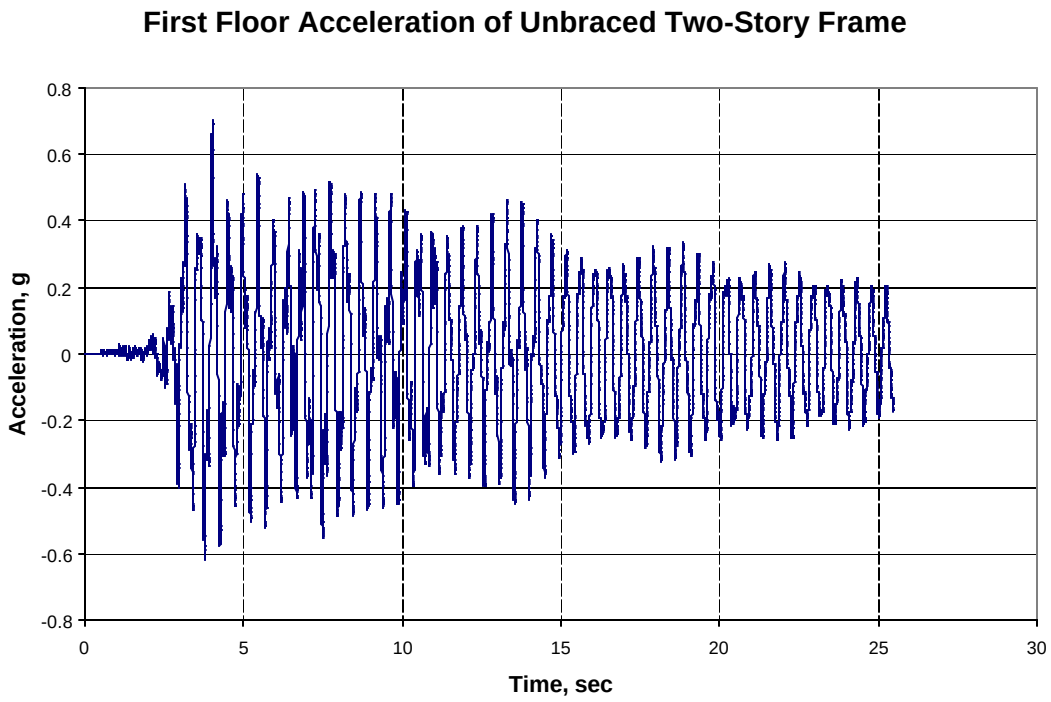

Figure 62: First floor acceleration of TS0 frame

Table 56: Maximum first floor acceleration values

		Time, sec
Positive Acceleration, g	0.703211	4.018619
Negative Acceleration, g	-0.617751	3.780581

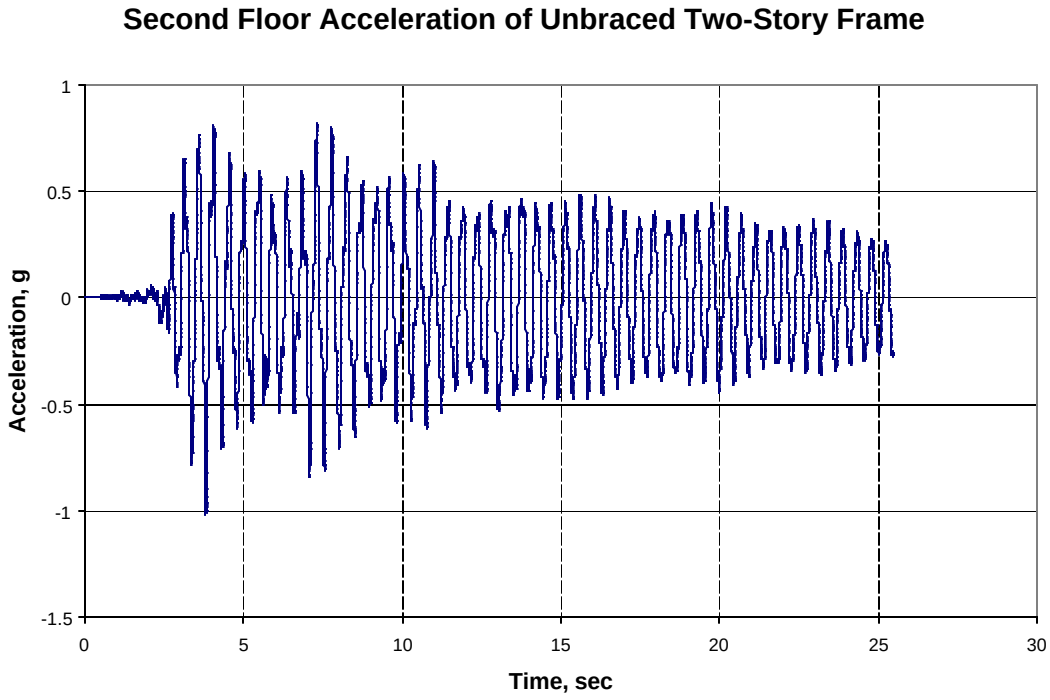

Figure 63: Second floor acceleration of TS0 frame

Table 57: Maximum second floor acceleration values

		Time, sec
Positive Acceleration, g	0.815529	7.31913
Negative Acceleration, g	-1.013307	3.824589

Earthquake Response for TSLX (Zero Pre-strain): In this case the two-story frame with cross bracing in the first floor and zero induced force was subjected to base excitation corresponding to the El Centro earthquake. Figure 64 shows the data collected from the accelerometer placed on the first floor. Table 58 shows the corresponding maximums and the times these maxima occur. Likewise, Figure 65 shows the data collected from the accelerometer placed on the second floor; and Table 59 shows the corresponding maximums and the times these maxima occur.

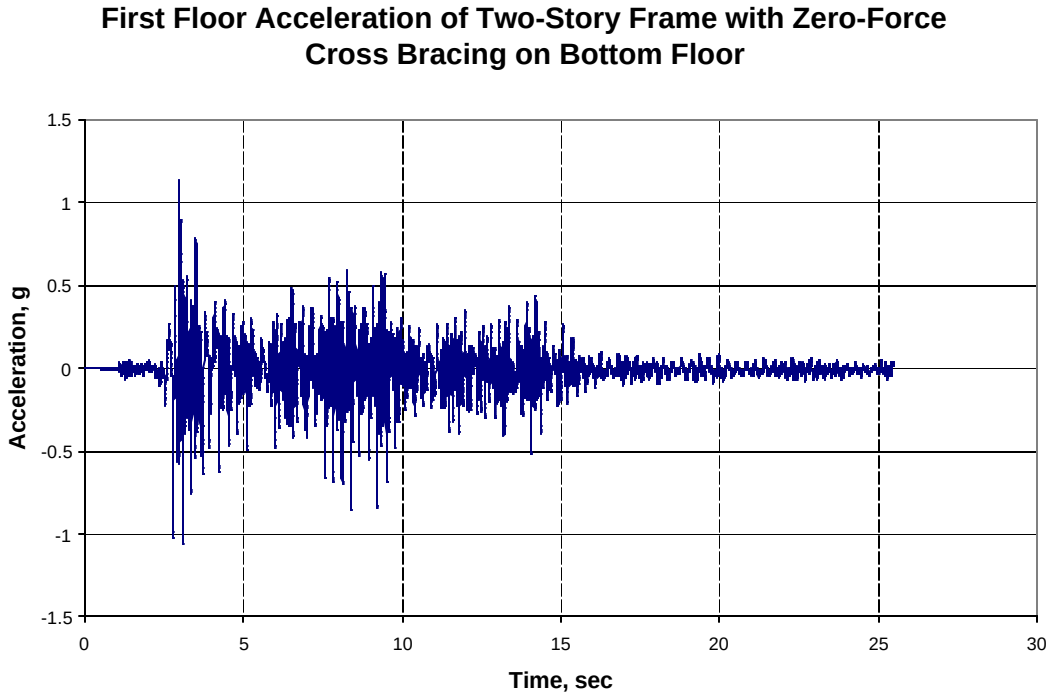

Figure 64: First floor acceleration of zero pre-strained TSLX frame

Table 58: Maximum first floor acceleration values

		Time, sec
Positive Acceleration, g	1.134172	2.961451
Negative Acceleration, g	-1.063362	3.08947

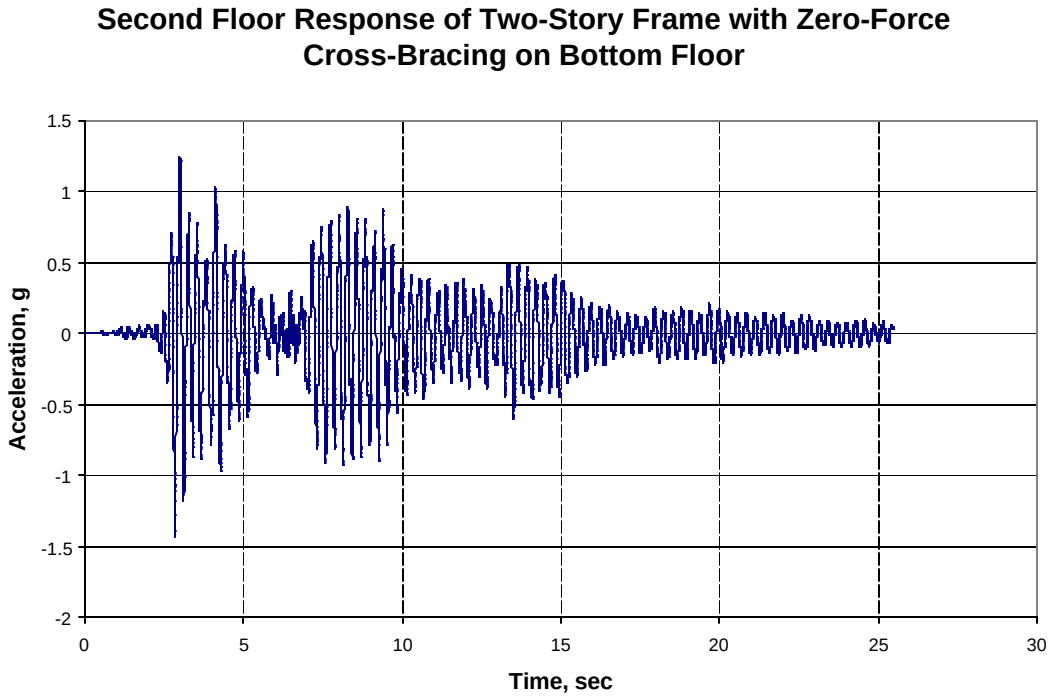

Figure 65: Second floor acceleration of zero pre-strained TSLX frame

Table 59: Maximum second floor acceleration values

		Time, sec
Positive Acceleration, g	1.24649	3.006458
Negative Acceleration, g	-1.423514	2.847434

Earthquake Response for TSLX (Pre-strain—Tensile): This case is similar to the last case, except that tensile forces of 1.366 lbs are induced in the bracings. Figure 66 shows the data collected from the accelerometer placed on the first floor due to El Centro earthquake. Table 60 shows the corresponding maximums and the times these maxima occur. Likewise, Figure 67 shows the data collected from the accelerometer placed on the second floor; and Table 61 shows the corresponding maximums and the times these maxima occur.

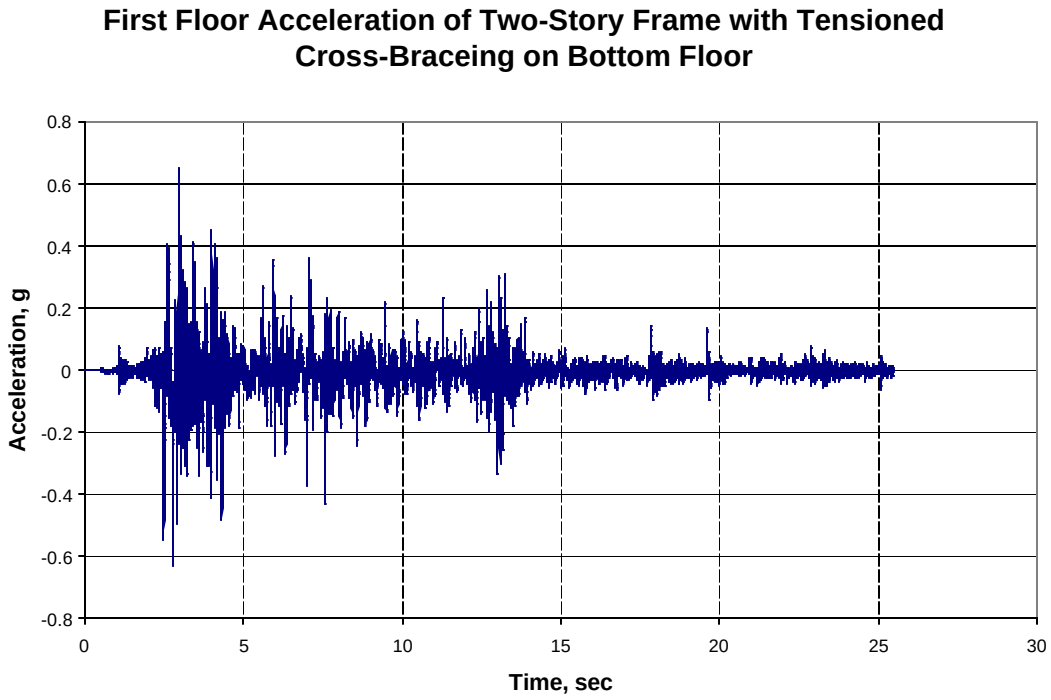

Figure 66: First floor acceleration of tensioned TSLX frame

Table 60: Maximum first floor accelerations

		Time, sec
Positive Acceleration, g	0.650714	2.952459
Negative Acceleration, g	-0.62996	2.78043

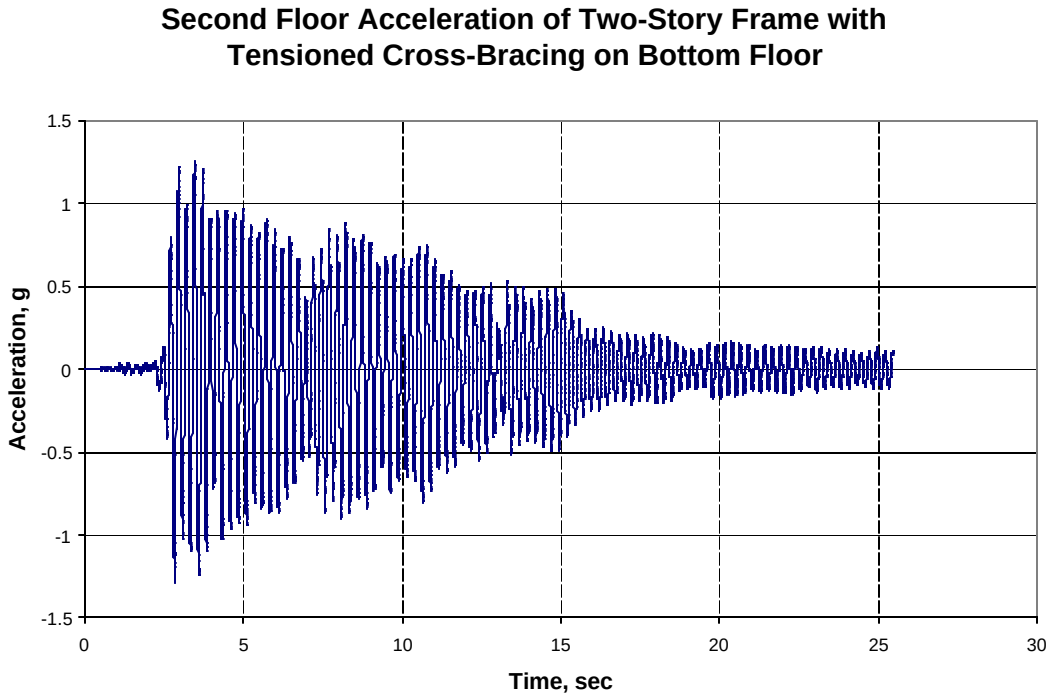

Figure 67: Second floor acceleration of tensioned TSLX frame

Table 61: Maximum second floor accelerations

		Time, sec
Positive Acceleration, g	1.253815	3.452536
Negative Acceleration, g	-1.294103	2.830438

Earthquake Response for TSLXUX (Zero Pre-strain): In this case both the floors of the two-story frame are cross-braced and the response to El Centro excitation is recorded with induced force in the bracings. Figure 68 shows the data collected from the accelerometer placed on the first floor. Table 62 shows the corresponding maximums and the times these maxima occur. Likewise, Figure 69 shows the data collected from the accelerometer placed on the second floor; and Table 63 shows the corresponding maximums and the times these maxima occur.

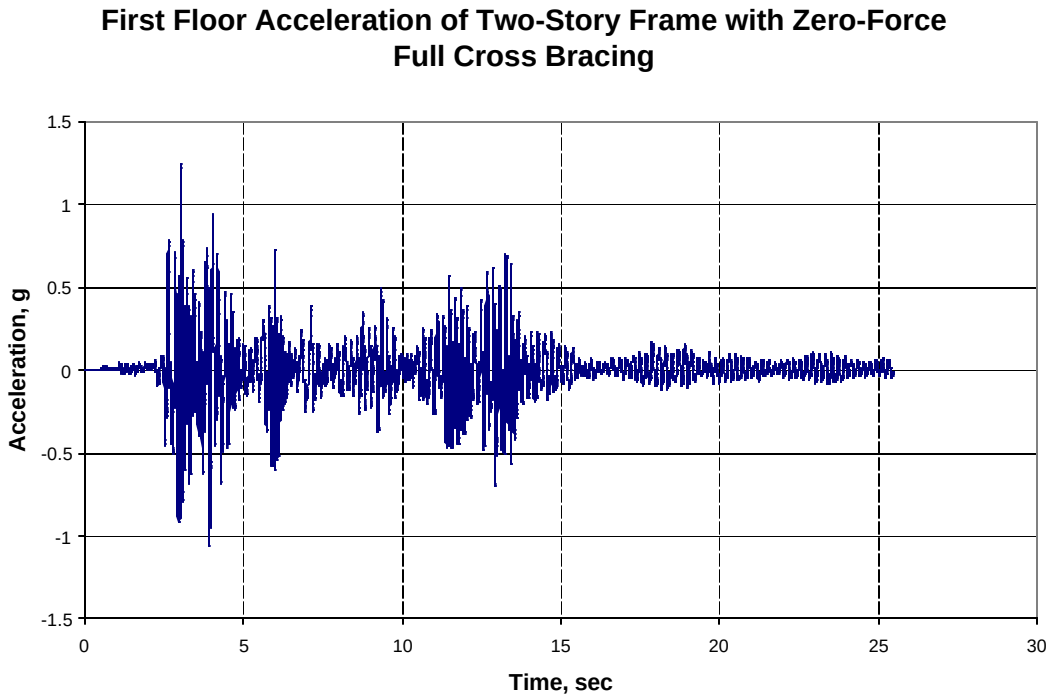

Figure 68: First floor acceleration of zero pre-strained TSLXUX frame

Table 62: Maximum first floor acceleration

		Time, sec
Positive Acceleration, g	1.239165	3.033472
Negative Acceleration, g	-1.063362	3.909609

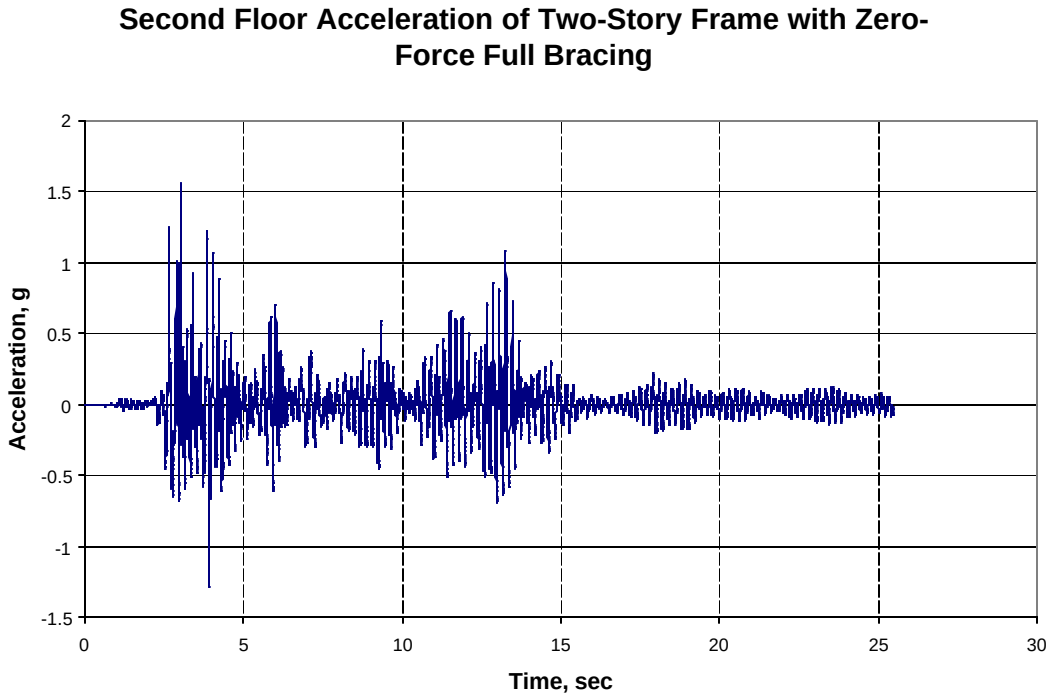

Figure 69: Second floor acceleration response of zero pre-strained TSLXUX frame

Table 63: Maximum second floor acceleration

		Time, sec
Positive Acceleration, g	1.557807	3.054475
Negative Acceleration, g	-1.277011	3.933612

Earthquake Response for TSLXUX (Pre-strain—Tensile): This case is similar to the last case, except that a tensile force of 1.366lbs is induced in the bracings. Figure 70 shows the data collected from the accelerometer placed on the first floor. Table 64 shows the corresponding maximums and the times these maxima occur. Likewise, Figure 71 shows the data collected from the accelerometer placed on the second floor; and Table 65 shows the corresponding maximums and the times these maxima occur.

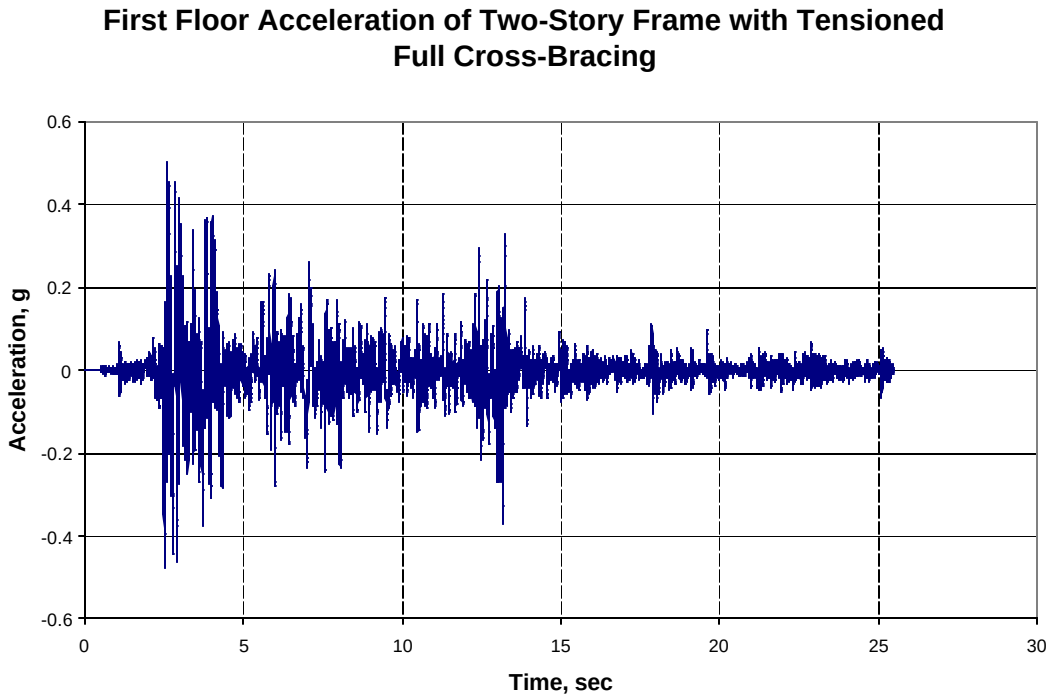

Figure 70: First floor acceleration response of tensioned TSLXUX frame

Table 64: Maximum first floor acceleration

		Time, sec
Positive Acceleration, g	0.500549	2.618405
Negative Acceleration, g	-0.477353	2.510389

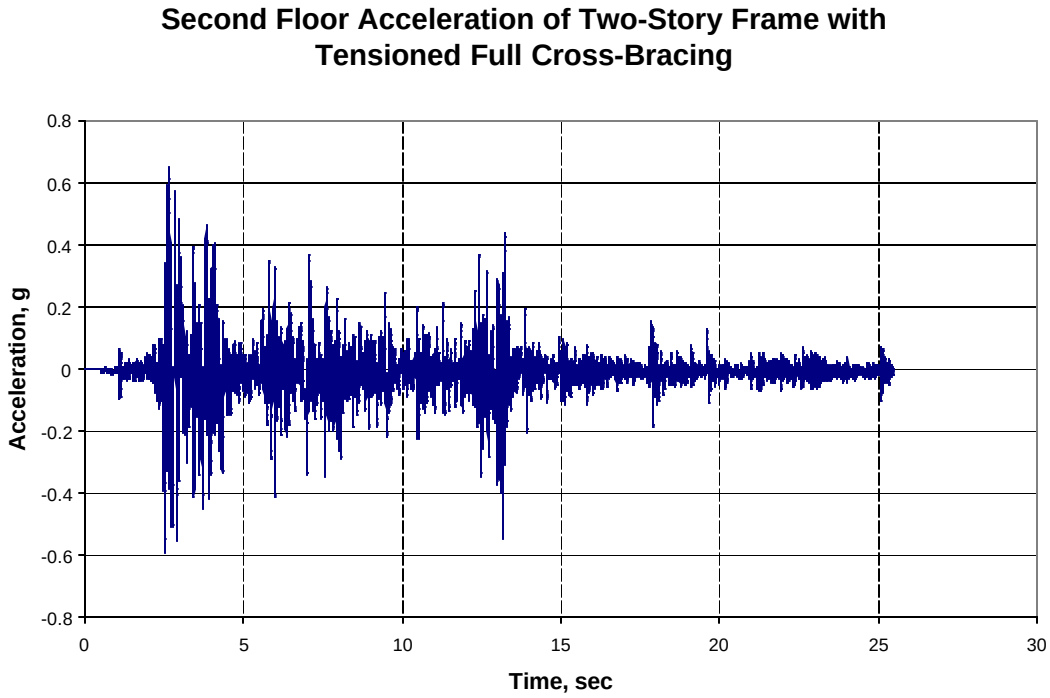

Figure 71: Second floor acceleration response of tensioned TSLXUX frame

Table 65: Maximum second floor acceleration

		Time, sec
Positive Acceleration, g	0.651935	2.684417
Negative Acceleration, g	-0.588451	2.51439

It is interesting to note that although the zero-force bracing provides slight reduction in maximum positive acceleration, the maximum negative acceleration is increased. One reason for this is when the wires were slackened, compression may have been introduced into the columns resulting in the increased maximum accelerations. However when examining the graphs, the overall acceleration is decreased. As expected, the pre-tensioned bracing results in the most acceleration reduction.

CHAPTER V

SUMMARY, CONCLUSIONS, AND RECOMMENDATIONS

Summary

The primary objective of this research effort was to determine the effectiveness of bracing systems with pre-induced stresses in improving the performance of a structure subjected to dynamic excitations like those due to earthquake, wind, and the like. Various passive, semi-active, and active alternatives were evaluated. For the purpose of present study commonly used diagonal bracing system was chosen.

A single and a double-story single bay frame were considered as the basic structures for study. Apart from unbraced systems, different bracing arrangements were investigated. External dynamic excitation at the base of the structures was applied as a segment of the El Centro earthquake. Both analytical and experimental studies were undertaken to ascertain the effectiveness of the bracing system with and without pre-induced stresses. The analytical studies were undertaken using the finite element software ANSYS. The experimental studies were undertaken using a bench top shake table (Quanser Shake Table II).

As part of the analytical study, frequencies and mode shapes were determined and the effect of bracings with and without pre-induced stresses was noted. In addition, the time-history response of the systems was investigated for El Centro excitation.

As part of the experimental study, the base of the structures considered was excited by sine sweep to determine the frequencies and mode shapes. Moreover, the

shake table was subjected to El Centro earthquake input and temporal responses of the structures were recorded.

A major difficulty in experimental study was the inability to completely remove the kinks present in the wire strand used for bracing. The experimental results reflect this fact. However, the analytical results are based on perfectly taut bracing with or without pre-induced strain.

Conclusions

The analytical and ANSYS results are compared and evaluated as below. In table 66 is shown the analytical and experimental fundamental frequency values. In general, the analytical values are larger than the experimental values. The primary reason for this may be attributed to greater base and joint flexibility in the test model as compared to the analytical model, which assumed perfectly fixed base and ideally rigid joints. In addition, the presence of kinks in the test model led to reduced stiffness and hence smaller frequency values. It may be noted from the table that, in general, the discrepancy is more in the case of braced models than the unbraced models. To check this reasoning, the TSLXUX—Tensile case was run again with pinned base condition giving a fundamental frequency which was less than that for fixed base condition by 34%. This further signifies the importance of proper joint modeling in the analytical model. So, the bracings have larger influence on structural stiffness. It is interesting to note that the use of pre-induced strain has very little effect on frequency values predicted by the analytical model. This is expected because of the small magnitude of pre-induced force applied to the bracings. In the experimental study, the pre-induced force was somewhat larger and

hence the larger difference. In the analytical study, a larger pre-induced force could not be used due to numerical difficulties posed by ANSYS. In the case of the test model also, a larger pre-induced force could not be created because it affected the geometry of the structure.

Table 66: Analytical and experimental natural frequencies

	Analytical	Experimental
SS0	4.4795	3.9
SSX—Tensile	32.933	9.4
SSX—Zero Force	32.002	9.0
TS0	2.5026, 6.9539	2.2, 6.2
TSLX—Tensile	4.3704	4.0
TSLX—Zero Force	4.3698	3.6
TSLXUX—Tensile	28.656	>10.0
TSLXUX—Zero Force	28.543	6.9

Analytical studies were undertaken for three single-story cases and six double-story cases as shown in figure 17. In table 66 only those cases are shown for which experimental studies were undertaken.

Table 67: Analytical natural frequencies for all nine cases

Frequency	Unbraced	Braced		
		Tension	Zero Force	Compression
SS0	4.4795	----------	----------	----------
SS1	----------	32.001	32.001	32.002
SSX	----------	31.829	32.002	32.933
TS0	2.5026	---------	---------	----------
TSUX	----------	2.5505	2.5510	2.5515
TSLX	----------	4.3692	4.3698	4.3704
TSL1U1-S	----------	28.543	28.543	28.543
TSL1U1-O	----------	28.543	28.543	28.543
TSLXUX	----------	28.429	28.543	28.656

Table 67 shows the fundamental frequencies for three cases of single-story frame and six cases of double-story frames shown in figure 17. It is clear from the values shown that the bracing system has significant effect on the frequency and hence the stiffness of the structures. It is however not clear what effect will the pre-induced force in the bracings have on the response simply because the magnitude of the pre-induced force happened to be too small and hence of no consequence. It was mentioned earlier that numerical difficulties with ANSYS prevented the use of a larger value. In spite of very small demonstrated effect of the pre-induced force, it may be noticed that, as expected, a tensile pre-induced strain caused lowering of stiffness. On the other hand, a compressive pre-induced strain caused rising of stiffness. It is, however, instructive to actually study the effect of larger pre-induced forces, maybe, using a different software.

In table 68 is shown a summary of the analytical results of time-history analysis due to El Centro earthquake. In the case of single-story frames, it is clear from the table that the use of bracing with or without pre-induced force caused significant drop in the drift index. For instance, in the case of SSX-T the reduced value of the maximum drift index is less than 1% of the value for the unbraced frame. Likewise, in the case of SSX-C the reduced value of the maximum drift index is less than 2% of the value of the unbraced frame.

In the case of two-story frames, for TSUX (-T, -0, -C) in which cross-bracing is used in the top story only, the drift index in the bottom-story is increased by about 38%. On the other hand, in the upper story, the drift index decreases by about 5.7%. As discussed above, no definite conclusions can be drawn about the effect of pre-induced

force because there is hardly any difference in the maximum response between the cases with and without pre-induced forces.

In the case of TSLX (-T, -0, -C), in which cross-bracing is used in the bottom story only, the drift indices for the bottom-story are almost the same for both –T and –C cases. For the same cases, the drift indices are close to 1%. On the other hand, for -0 case it is almost zero. So, the pre-induced strain has no beneficial effect on the lower story drift index. The drift indices for the –T and –C cases were increased by 36%. In the -0 case it is slightly larger. From this study, it is clear that bracing the lower story alone does not have any beneficial effect in controlling the drift index in an earthquake response.

In the case of the two-story frame with single bracing in each story inclined in the same direction, the results are very interesting. For instance, in the case of TSL1U1-S (-T, -0, -C) the drops in lower story drift indices are 97.4%, 97.0%, and 96.4% respectively. It is clear from this result that bracing with pre-induced tension is most effective and that bracing has significant effect on reducing the drift index in the lower story. In the case of the upper story, the drops are 98.5%, 97.6%, and 96.4%. So, the behavior of the upper story is almost identical to the behavior of the lower story.

In the case of the two-story frame with single bracing in each story inclined in opposite directions, the response is similar to that of the previous case.

In the case of the two-story frame with cross-bracings in each story, the drift in the upper story is almost zero, whereas, in the lower story the drift index is about 1.6% of that for the unbraced case.

It may be stated from above that two-story frames with cross-bracing in both the stories is most effective in controlling the drift index during an earthquake. However, the case where a single bracing is used in each story inclined in the same direction the drift response is almost equally good.

In table 69 is shown the experimental results of time-history response for single and double-story frames excited by El Centro earthquake. This table differs from table 68 in that it shows maximum values of negative and positive accelerations and the times of occurrence for three cases of single-story frames and five cases of double-story frames. So, there is no scope for comparison with the analytical solutions. The bracing system, where used, in these frames are of X-type only. It should also be noted that in the experimental set-up only tensile force could be induced in the bracings. The acceleration data shown in the table do not follow a definite pattern and hence definite conclusions cannot be drawn. However, it may be noted that lowest acceleration values are obtained when tensile forces are induced in the bracings both for single-story and double-story frames.

Recommendations

In general, it can be concluded that frames with bracings having pre-induced forces have beneficial effect on the dynamic response of a structure due to earthquake excitation. However, before drawing definitive conclusions more analytical and experimental studies are required to be undertaken in the following lines:

1. Significant improvement in the test model, the bracing system, and the method of inducing and measuring force in the bracing is absolutely essential.

2. To select an analytical tool which can effectively handle the nonlinear behavior of the problem in hand is necessary. Possible use of the full blown version of ANSYS, versus the student version, will handle these problems.
3. A feedback and control system needs to be developed for adaptive application of this structural control scheme.

Table 68: Time-history analytical results summary for El Centro earthquake

	Positive Sway, in	Time, sec	Negative Sway, in	Time, sec	Positive Sway (Second Floor), in	Drift, in	Time, sec	Negative Sway (Second Floor), in	Drift, in	Time, sec
SS0	0.07137	2.11	-0.0726	2.24	----------	-------	---------	----------	-------	----------
SS1-T	0.00319	1.19	-0.0071	2.24	----------	-------	---------	----------	-------	----------
SS1-0	0.00134	1.19	-0.0025	2.24	----------	-------	---------	----------	-------	----------
SS1-C	0.00184	1.19	-0.0019	2.24	----------	-------	---------	----------	-------	----------
SSX-T	0.00068	1.19	-0.0012	2.24	----------	-------	---------	----------	-------	----------
SSX-0	0.00069	1.19	-0.0013	2.24	----------	-------	---------	----------	-------	----------
SSX-C	0.00683	1.19	-0.0013	2.24	----------	-------	---------	----------	-------	----------
TS0	0.09829	1.91	-0.1027	2.25	0.15087	0.05258	1.9	-0.1546	-0.05197	2.27
TSUX-T	0.13492	2.12	-0.1007	2.25	0.13523	0.0003	2.12	-0.1009	-0.00024	2.25
TSUX-0	0.13492	2.12	-0.1007	2.25	0.13522	0.0003	2.12	-0.1009	-0.00025	2.25
TSUX-C	0.13491	2.12	-0.1007	2.25	0.13522	0.0003	2.12	-0.1009	-0.00025	2.25
TSLX-T	0.00117	2.12	-0.0019	2.24	0.08318	0.08202	2.12	-0.0708	-0.06894	2.24
TSLX-0	6.8E-05	1.19	-0.0001	2.24	0.08246	0.08239	2.12	-0.0704	-0.07027	2.24
TSLX-C	0.00116	2.12	-0.0019	2.24	0.08318	0.08202	2.12	-0.0708	-0.06893	2.24
TSL1U1-S-T	0.00247	1.19	-0.0058	2.24	0.00324	0.00077	1.19	-0.0086	-0.00279	2.24
TSL1U1-S-0	0.00296	1.19	-0.0053	2.24	0.00423	0.00127	1.19	-0.0075	-0.00222	2.24
TSL1U1-S-C	0.00351	2.12	-0.0047	2.24	0.00537	0.00187	2.12	-0.0063	-0.00165	2.24
TSL1U1-O-T	0.00245	1.19	-0.0058	2.24	0.00419	0.00174	1.19	-0.0074	-0.00161	2.24
TSL1U1-O-0	0.00295	1.19	-0.0052	2.24	0.00419	0.00125	1.19	-0.0074	-0.00219	2.24
TSL1U1-O-C	0.003487	2.12	-0.00465	2.24	0.000754	-0.00273	1.19	-0.00276	0.00189	2.24
TSUXLX-T	0.001564	1.19	-0.00282	2.24	0.002247	6.83E-4	1.19	-0.00406	-0.00124	2.24
TSUXLX-0	0.001557	1.19	-0.00283	2.24	0.000686	-8.71E-4	1.19	-0.00124	0.00159	2.24
TSUXLX-C	0.00155	1.19	-0.00283	2.24	0.00224	6.9E-4	1.19	-0.00407	-0.00124	2.24

Table 69: Time-history experimental results summary for El Centro earthquake

	Positive Acceleration, g	Time, sec	Negative Acceleration, g	Time, sec	Positive Acceleration (Second Floor), g	Time, sec	Negative Acceleration (Second Floor), g	Time, sec
Table	0.348082	2.763416	-0.261714	2.901437	----------	----------	----------	----------
SS0	1.226956	2.964459	-1.24405	3.60956	----------	----------	----------	----------
SSX-T	0.590892	2.616405	-0.63729	2.784429	----------	----------	----------	----------
SSX-0	1.185447	2.982464	-1.34416	2.923454	----------	----------	----------	----------
TS0	0.703211	4.018619	-0.617751	3.780581	0.815529	7.31913	-1.013307	3.824589
TSLX-T	0.650714	2.952459	-0.62996	2.78043	1.253815	3.452536	-1.294103	2.830438
TSLX-0	1.134172	2.961451	-1.063362	3.08947	1.24646	3.006458	-1.423514	2.847434
TSUXLX-T	0.500549	2.618405	-0.477353	2.510389	0.651935	2.684417	-0.588451	2.51439
TSUXLX-0	1.239165	3.033472	-1.063362	3.909609	1.557807	3.054475	-1.277011	3.933612

APPENDIX A

TEST PROCEDURE

This appendix will detail the procedure followed in the experimental set-up in order to run the shake table through the computer.

1) Make sure the MultiQ is properly connected to the Power Module and the PC as shown in Figure A1.

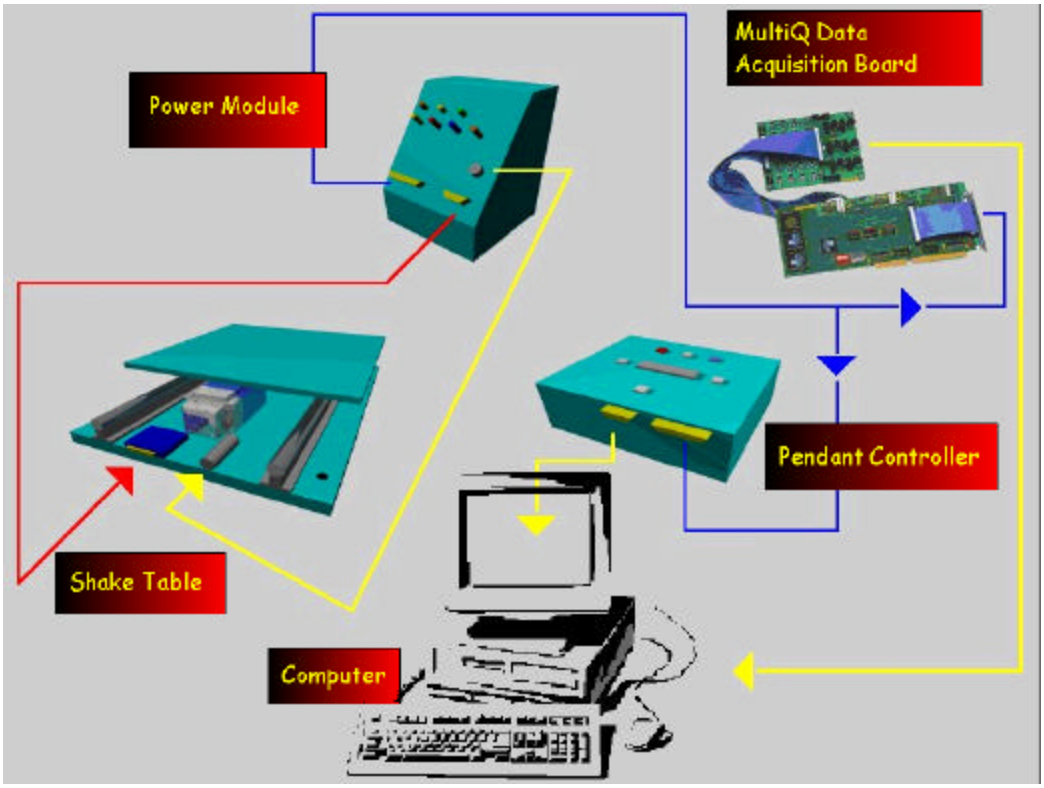

Figure A1: Computer and shake table set-up

2) Make sure that the Power Module is properly connected to the Shake Table.

3) Turn the Power Module switch to the "ON" position. When you turn on the Power Module, the "Left" and "Right" LED's will blink continuously. See figure A2 on the following page.

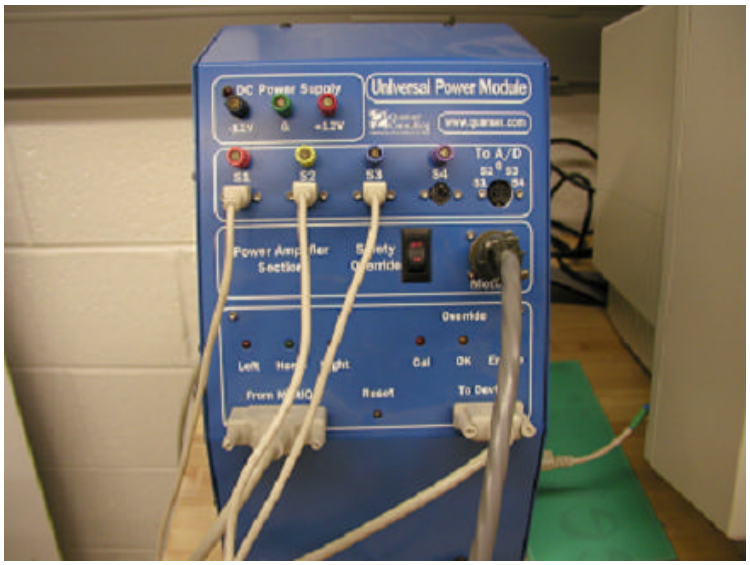

Figure A2: Power Module

4) Before you open the WinCon program, run the "boot.exe" DOS executable one time. This will initialize the power amplifier. Once you run the executable, the LED's will stop flashing.

5) Open the WinCon application. See figure A3.

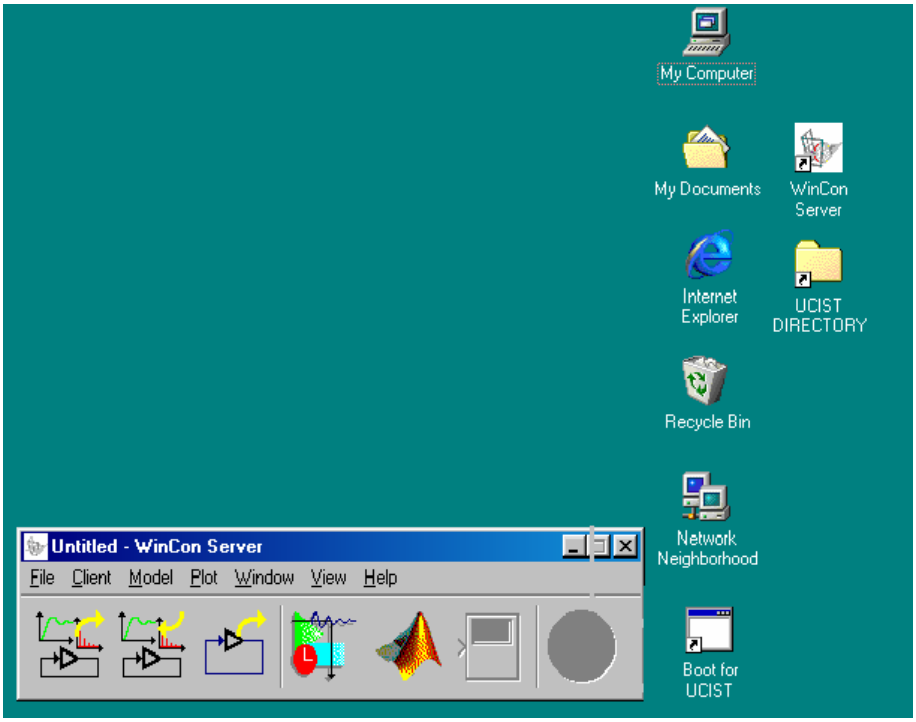

Figure A3: Computer screen and WinCon application

6) Calibrate the shake table by loading the file “cal_x.wcp” using File/Open.

7) Click the “Start” button. This should move the shake table slowly to the central position and stop. The light on the Power Module marked “Cal”, “OK”, and “Enable” will be lit up until the table reaches the home position.

8) Choose a model to run. For example, load the “sine_x.mdl” using Model/Open.

9) Click “Start”. Adjust the frequency and amplitude of the wave by clicking on the respective dials and turning them shown in figure A4.

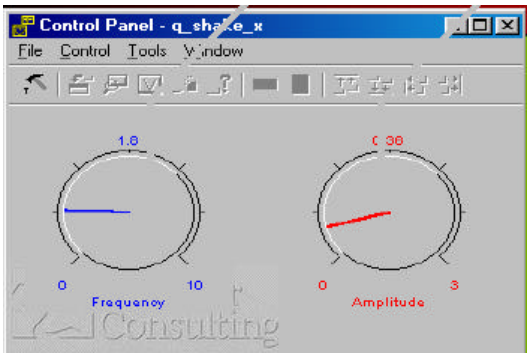

Figure A4: Frequency and amplitude controls

10) This begins the motion of the table and displays plots developing on the graph of displacement vs. time and acceleration vs. time as shown in figure A5.

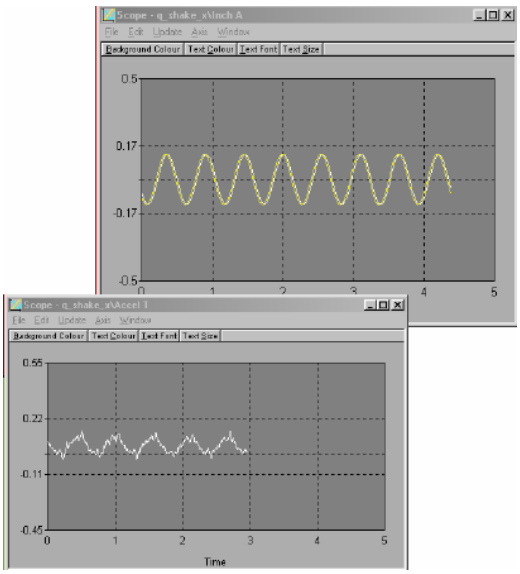

Figure A5: Shake table output plots

BIBLIOGRAPHY

Agrawal, J. N. Y. a A. K. (2002). "Semi-active Hybrid Control Systems for Nonlinear Buildings Against Near-field Earthquakes." Engineering Structures **24**(3): 271-280.

Christenson, R. E. (2002). Semiactive Control of Civil Structures for Natural Hazard Mitigation: Analytical and Experimental Etudies. Department of Civil Engineering and Geological Sciences. Notre Dame, University of Notre Dame**:** 200.

Connor, J. J. (2003). Introduction to Structural Motion Control, Pearson Education, Inc.

Jekabsons, E. (2001). A New Methodology for Adaptive Flutter Control of Aircraft Wings. Civil Engineering. Nashville, Vanderbilt University: 143.

Kwok, K. C. S. a. B. S. (1995). "Performance of Tuned Mass Dampers Under Wind Loads." Engineering Structures **17**(9): 655-667.

Marzbanrad, J., Ahmadi, Goodarz, and Jha, Ratneshwar (2004). "Optimal Preview Active Control of Structures During Earthquakes." Engineering Structures **26**(10): 1463-1471.

Miyamoto, a R. D. H. (2004). Structural Practices, Seismic Dampers: State of the Applications. Structure Magazine: 16-18.

Pnevmatikos G., K. L. F., and Gantes Charis J. (2003). "Feed-forward Control of Active Variable Stiffness Systems for Mitigating Seismic Hazard in Structures." Engineering Structures **26**(4): 471-483.

Serway, R. A. (1998). Principles of Physics. Orlando, Harcourt Brace College Publishers.

Shonkwiler, B. E., and Miller, Thomas H. Small-scale Shake Table Experiments and Comparison to Analytical Results. Corvallis, Oregon State University: 60.

Teng, Y. L. X. a J.(2002). "Optimum Design of Active/Passive Control Devices for Tall Buildings Under Earthquake Excitations." The Structural Design of Tall Buildings **11**(2): 109-127.

Soda, S. (1996). "Role of Viscous Damping in Nonlinear Vibration of Building Exposed to Intense Ground Motion." Journal of Wind Engineering and Industrial Aerodynamics **59** (2-3): 247-264.

Yoshida, I., Kurose, H., Fukui, S., and Iemura, H. (1995). "Parameter Identification on Active Control of a Structural Model." Smart Materials and Structures **4**(1A): p A82-A90.